UNIVERSIDADE DE SÃO PAULO

FACULDADE DE ZOOTECNIA E ENGENHARIA DE ALIMENTOS

GLORIA ESTHER URREA CEFERINO

Carbonatação acelerada: um estudo dos parâmetros, efeito da adição mineral, tipo de polpa celulósica e durabilidade em fibrocimento

Accelerated carbonation: a study of the parameters, mineral additions effect, type cellulosic pulp and durability in fiber-cement

Pirassununga

2016

GLORIA ESTHER URREA CEFERINO

Carbonatação acelerada: um estudo dos parâmetros, efeito da adição mineral, tipo de polpa celulósica e durabilidade em fibrocimento

Accelerated carbonation: a study of the parameters, mineral additions effect, type cellulosic pulp and durability in fiber-cement

(Versão corrigida)

Tese apresentada à Faculdade de Zootecnia e Engenharia de Alimentos da Universidade de São Paulo, como parte dos requisitos para a obtenção do título de Doutora em Ciências.

Área de Concentração: Desenvolvimento, Caracterização e Aplicação de Materiais Voltados à Agroindústria.

Orientador: Prof. Dr. Holmer Savastano Junior

Pirassununga

2016

Ficha catalográfica elaborada pelo
Serviço de Biblioteca e Informação, FZEA/USP,
com os dados fornecidos pelo(a) autor(a)

U387c

Urrea Ceferino, Gloria Esther
Carbonatação acelerada: um estudo dos parâmetros, efeito da adição mineral, tipo de polpa celulósica e durabilidade em fibrocimento / Gloria Esther Urrea Ceferino ; orientador Holmer Savastano Junior. -- Pirassununga, 2016.
147 f.

Tese (Doutorado - Programa de Pós-Graduação em Engenharia e Ciência de Materiais) -- Faculdade de Zootecnia e Engenharia de Alimentos, Universidade de São Paulo.

1. matriz cimentícias. 2. desempenho mecânico. 3. sílica. 4. microestrutura. 5. polpa branqueada. I. Savastano Junior, Holmer , orient. II. Título.

Universidade de São Paulo

ATA DE DEFESA

Ata de defesa pública de Tese do(a) Senhor(a) Gloria Esther Urrea Ceferino no Programa: Engenharia e Ciência de Materiais, do(a) Faculdade de Zootecnia e Engenharia de Alimentos da Universidade de São Paulo.

Aos 03 dias do mês de fevereiro de 2017, no(a) Sala da Congregação realizou-se a Defesa da Tese do(a) Senhor(a) Gloria Esther Urrea Ceferino, apresentada para a obtenção do título de Doutora intitulada:

"Carbonatação acelerada: um estudo dos parâmetros, efeito da adição mineral, tipo de polpa celulósica e durabilidade em fibrocimento"

Após declarada aberta a sessão, o(a) Sr(a) Presidente passa a palavra ao candidato para exposição e a seguir aos examinadores para as devidas arguições que se desenvolvem nos termos regimentais. Em seguida, a Comissão Julgadora proclama o resultado:

Nome dos Participantes da Banca	Função	Sigla da CPG	Resultado
Holmer Savastano Junior	Presidente	FZEA - USP	Não Votante
Carlito Calil Junior	Titular	EESC - USP	APROVADA
João Adriano Rossignolo	Titular	FZEA - USP	Aprovado
Sérgio Francisco dos Santos	Titular	UNESP - Externo	Aprovada
Loïc Barbara Rodier	Titular	Externo	Aprovada
Damanpreet Panesar	Titular	UofT - Externo	APROVADA

Resultado Final: APROVADA

Parecer da Comissão Julgadora *

Eu, Erica Cristina Mello Ferraz _____, lavrei a presente ata, que assino juntamente com os(as) Senhores(as). Pirassununga, aos 03 dias do mês de fevereiro de 2017.

Carlito Calil Junior

João Adriano Rossignolo

Sérgio Francisco dos Santos

Loïc Barbara Rodier

Damanpreet Panesar

Holmer Savastano Junior
Presidente da Comissão Julgadora

* Obs: Se o candidato for reprovado por algum dos membros, o preenchimento do parecer é obrigatório.

A defesa foi homologada pela Comissão de Pós-Graduação em 06.02.2017 e, portanto, o(a) aluno(a) faz jus ao título de Doutora em Ciências obtido no Programa Engenharia e Ciência de Materiais - Área de concentração: Desenvolvimento, Caracterização e Aplicação de Materiais Voltados à Agroindústria.

Presidente da Comissão de Pós-Graduação

Prof. Dr. Saulo da Luz e Silva
Comissão de Pós-Graduação
Suplente de Presidente

Dedication

To my inspiring Father, Mother (in memoriam), Sister, Godfather and Godmother, for showing me the true love, being the pillows, role models, support me and cheerleading.

ACKNOWLEDGMENTS

The realization of this work was only possible due to the collaboration of several people, to which I desire to express my gratefulness, to all of them I will like to say: God speaks through them and show me how wonderful life is.

I would like to thank to my family, for being there in any moment and any time supporting me.

To Professor Holmer Savastano Junior, my supervisor, I am grateful for believing in me, for being patient and guiding me through this project. Thank you for seeing in my research spirit that I have inside.

I would like to thank from a special way to Professor Daman Panesar, my co-supervisor, I am grateful for the wonderful opportunity that she gave me to develop part of my research at University of Toronto, the scholarship for two months and the proper guidance for the data analysis.

Thank you to Coordenação de Aperfeiçoamento de Pessoal de Nível Superior (CAPES) and the National Science and Engineering Research Council of Canada (NSERC) for the research scholarship.

To all technical and laboratory assistance from Mr. Nelson Ferreira (USP), Mr. Rodrigo Lourenço (USP), Mrs. Mariana Pavesi (USP), Mr. George Kretshmann (U of T), Dr. Pei-yu kuo (U of T), and Dr. Olga Perebatova (U of T).

To Sergio a great friend who helped me at the beginning of this research process and introduced me to fibrocement world.

To Zaqueu for his friendship and great willingness to help.

To Constrambi laboratory Family Vivi, Debora, Carol, Julian, Valdemir, Gonzalo, Rafael, Loic, Valderie, Liza, Cristian, Ana, Erika, Mateus, Patricia, Ronaldo and Diego.

I would like to thank to my colleagues at University of Toronto Amy, Deepak, Rodrigo, Hari, Madeh, Deepak, kanraj, Bjshou, Mohammad and specially to Sandeep, Runxiao and Nolan.

I would like to give a special thanks to Professor Tatiana Chaparro, Professor Beth Morais, Hilda Canato Gonçalves (in memoriam) and Professor Maria G Marques, for the guidance and advice in a proper time of my life.

To all the people that I lived with Pirassununga and in Toronto: Katia, Ryan, Raphael, and especially to Nubia and Sal, for encouraging me to keep going and for the long talks with tea.

To Beth Zillioto, Carmen de Fatima and Leila for be wonderful human been with me here in Pirassununga.

Finally, I would also to express my appreciation to all my friends, from many parts of the world (Brazil, Canada, China, Colombia, Guadalupe, Iran, India, Italy, Madagascar, Mozambique, Pakistan, Peru, etc.) they giving to me new good visions, teach me and allow me to learn about general culture knowledge, show me the kindness and the value of the friendship along my PhD studies.

EPIGRAPH

“Perder tempo em aprender coisas que não interessam, priva-nos de descobrir coisas interessantes”

Carlos Drummond de Andrade

RESUMO

CEFERINO, G.E.U. **Carbonatação acelerada: um estudo dos parâmetros, efeito da adição mineral, tipo de polpa celulósica e durabilidade em fibrocimento.** 2016. 147 f. Tese (Doutorado) – Faculdade de Zootecnia e Engenharia de Alimentos, Universidade de São Paulo, Pirassununga, 2016.

O processo de cura de carbonatação acelerada em matrizes cimentícias reforçadas com fibras naturais é um avanço no caminho para a inovação dos materiais compósitos adequados para aplicação nas regiões em desenvolvimento. No entanto, estudos adicionais, sobre o mecanismo da carbonatação em compósitos cimentícios reforçados com fibras naturais, conhecimento para a escolha do tipo de fibra celulósica, os parâmetros da câmara de carbonatação, a idade para começar o processo de cura com carbonatação, a influência da adição mineral e quantificar as fases hidratadas do cimento antes e depois do ensaio de envelhecimento acelerado, e o teste de durabilidade são ainda necessários. O objetivo deste trabalho foi avaliar a definição de parâmetros opcionais para o processo de cura com carbonatação acelerada, identificar as principais fases hidratadas da matriz de cimento e a durabilidade do fibrocimento reforçado com polpa celulosica. As matérias-primas utilizadas para as formulações dos compósitos cimentícios usados nesta investigação incluem: cimento Portland, adição mineral (calcário ou sílica) e reforço de fibra natural (Eucalipto ou Pinus). Os compósitos cimentícios foram produzidas por um processo de sucção a vácuo da mistura e posterior prensagem em pequena escala em laboratório. As condições de cura foram conduzidas em vários conjuntos de amostras, que estudaram o efeito da concentração da carbonatação acelerada (0%, 20% e aproximadamente de 100% de CO_2); o efeito de polpa celulósica (não branqueada e branqueada); o efeito da adição mineral (Calcário e Sílica) e, o efeito da durabilidade com o ensaio de envelhecimento acelerado (200 ciclos de imersão e secagem). Utilizou-se uma variedade de métodos de análise para avaliar a cinética de hidratação, as propriedades mecânicas e físicas e as implicações químicas nos compósitos; entre eles: difração de raios-X (DRX), análise termogravimétrica (TG e DTG), espectroscopia de infravermelho (FTIR), microscopia electrônica de varredura (MEV) e área superficial específica B.E.T. Nos compósitos sob concentrações perto do 100% de CO_2, os resultados indicam que os compósitos reforçada com polpa branqueada apresentam nos ensaios de flexão valores médios estatisticamente significativos maiores do modulo de ruptura (MOR) e energia especifica ao redor do 24% comparados com os reforçados com polpa não branqueada. Nos compósitos sob concentrações 20% de CO_2 os compósitos de sílica resultarem nos ensaios de flexão em valores

médios estatisticamente significativos maiores no limite de proporcionalidade ao redor do 46% comparando com os compostos de calcário; O composto que utiliza sílica como adição mineral tem menor quantidade de hidróxido de cálcio (CH) em comparação com o composto com adição de calcário, com base no resíduo de CH detectado na análise de DRX: 3% e 11,5%, respectivamente. Após o envelhecimento acelerado, os compósitos com sílica sujeitos a dois regimes de cura diferentes (carbonatados e não carbonatados) não apresentam redução estatística do desempenho mecânico, com exceção da energia especifica; também há ausência de ettringite (AFt) no padrão XRD. Entretanto, os compósitos que foram sujeitos ao processo de carbonatação apresentam valores médios de MOR estatisticamente significativos mais elevados. Esta assim concluísse em este estudo que para compósitos cimentícios curados com carbonatação acelerada é indicado o uso de polpa branqueada com a sílica como adição mineral.

Palavras-chave: polpa branqueada, polpa não branqueada, sílica, matrizes cimentícias, ciclos de envelhecimento, desempenho mecânico, microestrutura.

ABSTRACT

CEFERINO, G.E.U. **Accelerated carbonation: a study of the parameters, mineral addition effect, type cellulosic pulp and durability in fiber-cement.** 2016. 147 p. Thesis (Doctorate) – Faculdade de Zootecnia e Engenharia de Alimentos, Universidade de São Paulo, Pirassununga, 2016.

Carbonation accelerated curing process on cementitious matrices reinforced with vegetal fiber is an advance on the way for innovative composite materials suitable for application in developing regions. However, further studies on the carbonation mechanism in natural fiber reinforced cement composite, knowledge about the choice of cellulose fiber, carbonation chamber parameters, the age at which to begin the carbonation curing, the influence of mineral addition and the amount of the main hydrated clinker phases before and after of accelerated aging cycles, and durability test are still needed. The aim of this work was to evaluate the definition of optional parameters for accelerated carbonation curing process, the main hydrated phases of the cement matrix and the durability of fiber-cement reinforced with cellulose pulp. The raw materials used for the cementitious composite mix designs used in this investigation include: Portland cement, filler (limestone or silica) and natural fiber reinforcement (eucalyptus or pines). The cementitious composites were produced by a slurry vacuum dewatering process followed by pressing in laboratory small scale. The curing conditions were conducted on various sets of samples which were studied the effect of accelerated carbonation concentration (0%, 20% and close of 100% of CO_2); the effect of cellulosic pulp (unbleached or bleached); the filler effect (limestone and silica); and, the effect of accelerated ageing test (200 soak & dry cycles). A variety of analytical test methods were used to assess the hydration kinetics, the mechanical and the physical properties, and chemical implications in the composites; between them: (X-ray diffraction (XRD), thermogravimetric analysis (TG and DTG), Infrared spectrometer (FTIR), scanning electron microscopy (SEM) and B.E.T. surface area analyzer. On the samples subject to close 100% of CO_2 the results indicate that the bleached pulp reinforcement composites show in flexural test average statistically significant higher values of modulus rupture and specific energy around 24 % relating with unbleached pulp. On the samples subject to 20% CO_2 the silica composite resulted in flexural test average statistically significant higher values of Limit of proportionality around 46% comparing with the limestone composite; the composite with silica addition presents less amount of calcium hydroxide (CH) in comparison with the composite with limestone addition, based on the CH residue detected in the XRD analysis: 3% and 11.5% respectively. After accelerated aging, the silica composites

subject to two different curing regimes (carbonated and uncarbonated) presents no statistical reduction of mechanical performance, also there is an absence of ettringite (AFt) at XRD pattern; nevertheless, the carbonated composites present a significantly higher average MOR values. Thus, it is concluded in this study that for cementitious composites cured with accelerated carbonation the use of bleached pulp with silica as mineral addition is indicated.

Keywords: bleached pulp, unbleached pulp, silica, cement matrix, aging cycles, mechanical behavior, microstructure.

ABBREVIATIONS LIST

Aft	Ettringite
ASTM	American Society for Testing and Materials
B.E.T.	Brunauer Emmett Teller
CP V-ARI	Portland cement type (high initial strength),
$CaCO_3$	Calcium Carbonated
CH	Calcium Hydroxide
CO_2	Carbon dioxide
C–S–H	Calcium silicate hydrate
C_3S	Alita
C_2S	Belite
DTA	Differential thermal Analysis
EN	European Committee for Standardization.
FAO	Food and Agriculture Organization of the United Nations
FTIR	Infrared spectrometer
H_2CO_3	Carbonic acid
LOP	Limit of proportionality
MgO	Magnesium oxide
MOE	Modulus of elasticity
MOR	Modulus of rupture
MPTS	Methacryloxypropyltri-methoxysilane
PVA	Polyvinyl alcohol fibers
SCM	Supplementary Cementitious Materials
SEM	Scanning electron microscopy
SiO_2	Silica
TG	Thermogravimetric analysis
VF	Vegetal Fibers
XRD	X-ray diffraction

SUMMARY

1. INTRODUCTION

Presently, the building materials industry is looking for eco-friendly alternatives to supply the increasing construction demand, not only in developing regions but all around the world (SAVASTANO et al., 2005). These studies indicate that natural resource based alternative materials should have a low production cost and minimal pollutant emissions, they should also be durable while having the lowest possible impact on the environment (SAVASTANO et al., 2005; TONOLI et al., 2010; ARDANUY et al., 2015). Significant advances have already made, but more research and innovation are needed to find an ideal material that fits actual market requirements including environmental and accessibility concerns.

The fiber-cement industry is particularly interested in the use of Natural waste fibers, including wood fibers. These are intriguing potential alternative materials, especially due to the extensive presence of plantations for these natural fibers (i.e. eucalyptus) reported in Brazil (ARDANUY et al., 2015); these materials exhibit a set of important advantages, such as wide availability at relatively low cost, biodegradability, and interesting physical and mechanical properties (low density and well-balanced stiffness). However, the low durability caused by degradation when exposed to an alkaline-mineral environment, has been an issue for fibers being used as reinforcement in various composites, like cementitious ones (ARDANUY et al., 2015; PICANÇO et al., 2008).

The literature indicates that the process of carbonation can result in a number of benefits, such as improved durability, reduced alkalinity of the cement matrix, reduced open porosity percent, volume stabilization of the composite when exposed to humidity oscillation and strain gain. There are two categorized groups of carbonation processes: carbonation of mature cementitious matrices and carbonation of fresh cementitious composites. The first one is a phenomenon in which well-developed hydration products react with atmospheric CO_2 through prolonged exposure, whereas in the second case carbonation is intentionally applied to fresh cement paste wherein CO_2 reacts with the anhydrous phases and hydration products to form carbonates (FERNANDEZ-BERTOS et al., 2004; ROSTAMI et al., 2012). The accelerated curing process, when applied to the cementitious matrix, results in an initial reaction between hydration products (e.g. calcium hydroxide and C-S-H), anhydrous phases (e.g. C_3S and C_2S) and carbon dioxide in order to produce stronger composites (e.g. calcium carbonate) (FERNANDEZ-BERTOS et al., 2004; SANTOS et al., 2015).

In natural fiber-cement, the curing process by accelerated carbonation has been identified as an effective procedure to mitigate the degradation of cellulose fibers, by improving mechanical behavior and volumetric stabilization of these composites. Furthermore, the carbonation process on cementitious composites leads to: decreased alkalinity of the cement matrix due to a lower content of $Ca(OH)_2$, pore refinement, associated with the densification of the matrix through precipitation of $CaCO_3$, which is a denser and more stable product than $Ca(OH)_2$ (PIZZOL et al., 2014; ALMEIDA et al., 2013, TONOLI et al., 2010). Previous studies on carbonation curing process in fiber-cement have highlighted that the relative humidity inside the CO_2 chamber must be high and in proximity to 90% to allow the diffusivity of CO_2 in the bulk (HOUST, 1996). The effectiveness of the accelerated carbonation curing process in natural fiber-cement composites is affected by factors like the selection of the cellulosic pulp, the chamber parameters, and the mineral addition.

A variety of carbonation curing conditions for cementing materials and also fiber composites have been reported in the literature, but typically ranging from 2 to 20% CO_2 concentration with a wide range of combinations of pressure and temperature (LIWU et al., 2012). For example, Almeida et al. (2013) have studied carbonated cement based specimens reinforced with bleached eucalyptus pulp, the settings of climate chamber were 60°C temperature, 90% relative humidity (RH) and atmospheric CO_2 concentration (15 vol%) for two days. Pizzol et al. (2014) have studied the accelerated carbonation process in cement based specimens reinforced with bleached cellulosic pulp and synthetic fibers, the settings of climate chamber were 60°C temperature, 90% relative humidity (RH) and atmospheric CO_2 concentration (15 vol%) for ten hours. Santos et al., (2015) have studied the supercritical carbonation on extruded fibre-cement reinforced with bleached eucalyptus pulp and residual sisal chopped fibres, the specimens were placed into the chamber with total saturation (close of 100% concentration) of supercritical CO_2 at 20 MPa and at 45°C in the chamber.

Limestone is normally used in the industry as a mineral addition in cementitious matrices in order to reduce costs concerning the production of fiber-cement (BENTUR et al., 2007). Also, limestone was selected as mineral addition in the carbonated composites studied by Almeida et al. (2013), Pizzol et al. (2014) and Santos et al. (2015). Calcium carbonate filler (limestone), which even if inert materials blended with cement may have a significant effect on the hydration of the clinker phases (GUTTERIDGE et al., 1990), one those effects is the precipitation of CaCO3 (LOTHENBACH et al., 2008). In addition, calcium carbonate is the principal reaction product of accelerated carbonation curing process at freshly cast cement, which could make

difficult analyze the quantification calcium carbonate formed along the accelerated carbonation curing process.

Silica quartz is a neutral material, chemically and thermodynamically very stable at low temperatures (e.g. 45°C) and atmospheric pressure (FOURNIER AND ROWE, 1977; SINGH et al., 2013). Furthermore, the quartz used as filler does not react significantly and is nominally inert material, and gives more space for hydration product of the PC so the acceleration period is prolonged (LOPEZ, 2009; THOMAS et al., 2011). The use of quartz as the mineral addition in carbonated cementitious composites could be a strategy for isolating the carbonation process, in order to identify and estimate the amount of the main crystalline phases before and after of accelerated aging cycles.

This introduction leaves clear that further studies on the carbonation mechanism in natural fiber reinforced cement composite, the choice of cellulose fiber, the mineral addition effect, the kinetic of hydration, the age at which to begin the carbonation curing, carbonation chamber parameters, and durability test are still needed.

1.2. General objective

The aim of this work was to evaluate curing parameters for accelerated carbonation process, the mineral addition effect, the main hydrated phases of the cement matrix and durability of fiber-cement reinforced with cellulose pulp, in order to apply this technology to building materials industry.

1.3. Specifics objectives

1. Study of the definition of optimal parameters for supercritical carbonation process of vegetable fiber-cement composites at a very early age
2. Comparative study of two kinds of mineral addition in cellulose pulp fiber-cement composites subjected to accelerated carbonation at early age.
3. Durability and hydration kinetics study in carbonated fiber-cement composites using silica as a mineral addition.
4. Evolution of the hydration kinetics on unbleached cellulose pulp fiber-cement composites subjected to accelerated carbonation at very early age.

1.4. Description of the thesis

This study was development along five stages, follow describe:

Stage 1: Literature review

This stage describes the natural fiber-cement reinforcement, the structure of vegetable fibers, the cellulosic fibers, the fiber-cement production, the properties of cementitious materials reinforced with natural fibers, the durability, and finally introduces the fiber-cement curing with two processes: CO_2 atmospheric curing process and atmospheric curing process.

Stage 2: Definition of optimal parameters for supercritical carbonation process of vegetable fiber-cement composites at a very early age

In vegetal fiber-cement, the curing process by accelerated carbonation has been identified as an effective procedure to mitigate the degradation of cellulose fibers, by reducing the pH of the bulk matrix and improving mechanical behavior and volumetric stabilization of these composites. Furthermore, the carbonation process on cementitious composites leads to: a decreased alkalinity of the cement matrix due to a lower content of $Ca(OH)_2$, pore refinement, reduction to the average pore size, associated with the increased densification of the matrix through precipitation of $CaCO_3$, which is a denser and more stable product than $Ca(OH)_2$ (PIZZOL et al., 2014; ALMEIDA et al., 2013, TONOLI et al., 2010). Previous studies on carbonation curing process in fiber-cements have highlighted that the relative humidity inside the CO_2 chamber must be high and in proximity to 90% to allow the diffusivity of CO_2 in the bulk (HOUST, 1996).

The concentrations of CO_2 influence the carbonation rate of cement composites. Carbonation reaction could be slow with atmospheric CO_2 concentration levels (0.03%– 0.04%), while in accelerated curing, the concentration of CO_2 in a chamber is typically 2%–20% and if supercritical CO_2 methods are used there is a greatly accelerated curing process with concentrations close to 100%. In natural conditions, complete carbonation of engineering-sized components takes years instead of hours in laboratory conditions. In general, increasing CO_2 concentration and pressure facilitates diffusion processes and the dissolution of CO_2, thus high-density $scCO_2$ eases the penetration into the cement paste pore network or complex pores typical for fiber–cement matrices (SANTOS et al., 2015; GARCÍA et al., 2006; CHANG et al., 2006; FARAHI et al., 2013; LIWU et al., 2012).

The aim of the aim of the stage 2 is to study the influence of: the bleaching of eucalyptus cellulose pulp, the initial curing duration, the CO_2 exposure time and accelerated aging cycles, on natural fiber-cement composites subjected to supercritical carbonation at a very early age. All samples of the composites were subjected to mechanical, physical, and microstructural tests.

Stage 3: Comparative study of two kinds of mineral addition in cellulose pulp fiber-cement composites subjected to accelerated carbonation at early age.

Limestone is normally used in the industry as a mineral addition in cementitious matrices in order to reduce costs concerning the production of fiber-cement (BENTUR et al., 2007). Also, limestone was selected as mineral addition in the carbonated cementitious composites studied by Almeida et al., (2013); Pizzol et al., (2014) and Santos et al., (2015). The use of limestone with Portland Cement PC, it is being reported the high affinity between calcium aluminate and carbonate phases to form monocarbonate. Also, at the initial hydration heat evolution indicating a slight acceleration of the cement hydration in the presence of finely ground calcite (FELDMAN et al., 1965; BENSTED, 1980; LOTHENBACH et al., 2008). Silica quartz type is a neutral material, chemically and thermodynamically stable at low temperatures (e.g. 45°C) and atmospheric pressure (FOURNIER AND ROWE, 1977; SINGH et al., 2013). Additionally, the quartz used as filler in a mix design with PC, it does not react significantly, is an inert material due the crystalline characteristic and gives more space to the particle distribution for hydration product of the PC so the acceleration period is prolonged, compare with 100% PC after mixing (LOPEZ, 2009; THOMAS et al., 2011). The use of quartz as mineral addition in carbonated cementitious composites could be a strategy for isolating the carbonation process, in order to identify and estimate the amount of the main crystalline phases. In addition, calcium carbonate is the principal reaction product of accelerated carbonation curing process at freshly cast cement, which could make difficult to analyze and quantify the calcium carbonate formed along the accelerated carbonation curing process.

Carbonated natural fiber-cement composites using two kinds of mineral addition could have different: (i) mechanical behaviour, (ii) microstructure and (iii) amount of phases. The aim of the stage 3 is compare two kind of mineral addition (limestone v. ground silica) and the initial curing duration (10 h v. 24 h), on natural fiber-cement composites subjected to accelerated carbonation curing process at a very early age. All samples of the composites were subjected to mechanical, physical, and microstructural tests.

Stage 4: Durability and hydration kinetics study in carbonated fiber-cement composites using silica as a mineral addition.

Worldwide cellulose fibers are extensively available, have many varieties and also are a renewable source, which makes for an attractive concept to be used in composite building materials. The mechanical performance of these composites at early ages was deemed to be satisfactory, however, in the presence of moisture and alkalinity above (pH 8.5), the wood fibres swell, and chemically degrade as a result of mineralization processes which in turn adversely affects the mechanical properties, namely strength and stiffness of the composite matrix. As well it is affected the long-term performance after natural or accelerated ageing (e.g. wet/ dry cycling); it is adverse for the strength and toughness of the composite (MOHR et al., 2005; MOHR et al., 2007; BENTUR et al., 2007; TONOLI et al., 2009; DAI et al., 2014).

In Natural Fiber-cement, the curing process by accelerated carbonation has been identified as an effective procedure to mitigate the long-term degradation of cellulose fibers, by reducing the pH of the bulk matrix and improving mechanical behavior and volumetric stabilization of these composites. Furthermore, the carbonation process on cementitious composites leads to a decreased alkalinity of the cement matrix due to a lower content of $Ca(OH)_2$, pore refinement, reduction to the average pore size, associated with the increased densification of the matrix through precipitation of CaCO3, which is a denser and more stable product than Ca(OH)2 (PIZZOL et al., 2014; ALMEIDA et al., 2013, TONOLI et al., 2010).

Fast carbonation curing is beneficial for accelerating the plastic shrinkage of the composite, and avoiding dimensional instability of the composite in the initial ages and during the lifetime. These studies also show the improvement of mechanical properties after the Accelerated Aging Cycles, as an evidence that the cement matrix improves its performance with the carbonation curing process at early ages and with the progress of the cement hydration process (ALMEIDA et al., 2013).

As was previously mentioned at stage three silica quartz type is a neutral material, chemically and thermodynamically stable at low temperatures (e.g. 45°C) and atmospheric pressure (FOURNIER AND ROWE, 1977; SINGH et al., 2013). Additionally, the quartz used as filler in a mix design with OPC, it does not react significantly, is an inert material; due the crystalline characteristic of the quartz, so gives more space to the particle distribution for hydration product of the OPC so the acceleration period is prolonged, if it is compared with a mix with 100%

Portland cement (LOPEZ, 2009; THOMAS et al., 2011). The use of quartz as a mineral addition in carbonated cementitious composites could be a strategy for isolating the carbonation process, in order to identify and estimate the amount of the main crystalline phases before and after of accelerated aging cycles. Also, for know about the mechanical properties after the Accelerated Aging Cycles.

The use of quartz as a mineral addition in carbonated cementitious composites could be a strategy for isolating the carbonation process, in order to identify and estimate the amount of the main crystalline phases before and after of accelerated aging cycles. Also, the use of silica as a mineral addition in carbonate fiber-cement composite there is not knowledge about the mechanical properties behaviour after the Accelerated Aging Cycles.

The use of silica as a mineral addition in carbonated composites could allow discussing in this stage: (i) the effect of initial hydration; (ii) the identification of the main phases; (iii) the carbonation effect and (iv) the durability. The aim of stage four is to study the durability and the hydration kinetics in carbonated composites reinforced with unbleached pines cellulose pulp fiber and use silica as a mineral addition. Composites were subjected to mechanical, physical, and microstructural tests.

Stage 5: Evolution of the hydration kinetics on unbleached cellulose pulp fiber-cement composites subjected to accelerated carbonation at early age

As was mentioned in stage 3 and stage 4, Limestone is normally used in the industry as a mineral addition in cementitious matrices in order to reduce costs concerning the production of fiber-cement (BENTUR et al., 2007). Also, limestone was selected as the mineral addition in the carbonated cementitious composites studied by Almeida et al. (2013), Pizzol et al. (2014) and Santos et al. (2015). According with Tonoli et al. (2016), the main phases identified in the X-ray diffraction patterns of the control uncarbonated and carbonated cementitious composites are: calcite ($CaCO_3$); vaterite (Va); aragonite (Ar); monosulfoaluminate (AFm); ettringite (Aft); portlandite (P); monocarboaluminate (Mc); tricalcium aluminate (C3A); tetracalcium aluminoferrite (C4AF); belite (C_2S) and alite (C_3S).

Previously mentioned, silica quartz type is a neutral material, chemically and thermodynamically very stable at low temperatures (e.g. 45°C) and at atmospheric pressure (FOURNIER AND ROWE, 1977; SINGH et al., 2013). The use of silica type quartz as a mineral addition in carbonated cementitious composites could be a strategy for isolating the

carbonation process, in order to identify the main crystalline phases along the 10 h carbonation process and to study the carbonation kinetic hydration at early edge.

The use of silica as a mineral addition in carbonated composites could allow discussing following subjects: (i) the carbonation kinetic hydration along 10 h; (ii) the identification of the main phases and (iii) the microstructure at early edges. The aim of stage 5 is to study the kinetic hydration in carbonated at early edge unbleached pines cellulose pulp fiber-cement composites that use silica as a mineral addition. For looking into the kinetic hydration, for each condition two samples were removed from the chamber each hour running the carbonation curing process. Then the samples were immersed in acetone, in order to interrupt the hydration of the cementitious matrix. Also, a small piece of the sample was cut for adding the phenolphthalein indicator and checking the status of the internal surface, according to the intensity of the color displayed by the indicator. All samples of the composites were subjected to microstructural tests.

2. LITERATURE REVIEW

As previously mentioned in section 1.4. this stage makes an introduction of the natural fiber-cement reinforcement, the structure of vegetable fibers, the cellulosic fibers, the fiber-cement production, the properties of cementitious materials reinforced with natural fibers and the durability, finally introduce the fiber-cement curing process with two processes: CO_2 atmospheric curing process and atmospheric curing process. The first one curing process mentioned was considered a treatment to improve the mechanical properties of this kind of composites, even through many variables or factors could be affected the effectiveness of this treatment.

2.2. Natural Fiber-cement reinforcement

Since the early 1940s, many studies have investigated the concept of vegetal fiber reinforcement in cement-based materials as a potential substitute for asbestos fibers. Since then, the potential applications of VF cement composites have grown, especially with regards to thin walled materials: mainly thin-sheet products for partitions, building envelopes or ceiling flat sheets; roofing tiles and premanufactured components in general (ROMA et al., 2008). Other reasons for the increased interest in vegetable fiber integration with building materials, include their decreasing pressures for the dependence on the building materials industry to use petroleum based products (e.g. synthetic fibers), with increasing interest in the use of renewable resources (e.g. cellulosic fibers), and variety of morphologies and aspect ratios (PICANÇO et al., 2008; SATYANARAYANA et al., 2009; TONOLI et al., 2009).

According to regional statistical yearbooks of 2014 from the Food and Agriculture Organization of the United Nations (FAO) (FAO Statistical Yearbooks – World food and agriculture 2014), the land and forestry report in 2011 estimates forest and fibers areas to be 517.3 million ha and 1.7 ha, respectively. Table 1 shows the classification of tropical region vegetal fibers:

Table 1 – Classification of tropical vegetal fibers.

Classification	Example
Bast fibers	hemp, jute, kenaf, flax, ramie
Leaf fibers	sisal, henequen, pineapple, oil palm leaf fibers, banana,
Stalk fibers	straws – rice, wheat and barley; reeds – bamboo grass – esparto and elephant grass
Seed fibers	cotton, coir,

Source: (BIAGIOTTI et al., 2008; JAWAID et al., 2011).

2.2.1. Structure of vegetable fibers

Cellulose is the most abundant and biodegradable natural polymer that exists on planet earth, it is the principal fiber reinforcement of wood, non-wood plants, seaweeds and some bacteria (LAVOINE et al., 2012). The structure of an individual wood cell is composed mainly of long, oriented cellulose molecules, with a degree of polymerization of ~25,000. The cellulose molecule chains are grouped in long, oriented microfibril units having a thickness of about 0.7 mm and a length of a few μm. The other components of the cell wall, hemicellulose, and lignin, have much lower degrees of polymerization and are located mainly in the middle lamellae which connects the individual fiber cells together (BENTUR AND MINDESS, 2007; CORREIA, 2015).

Four different polymorphs of cellulose are known, named cellulose I, II, III, and IV. Cellulose I is the form found in nature and it occurs in two allomorphs Iα and Iβ. Cellulose II is the crystalline form more stable and also emerges after re-crystallization with aqueous sodium hydroxide, and it is the thermodynamically most stable crystalline form. Cellulose II and cellulose I have antiparallel and parallel packing, respectively. Cellulose III is obtained by a liquid ammonia treatment of cellulose I, and cellulose IV is a result of heating cellulose III, the transformation usually being only partial (AULIN, 2009; CORREIA, 2015). Figure 1 shows how cellulose is present in nature. Inattentive of its source, cellulose is a white fiber-like structure with no smell and has a density of around 1.5 g/cm³ (LAVOINE et al., 2012).

Figure 1 - Details of the cellulosic fiber structure with emphasis on the cellulose microfibrils (in color).

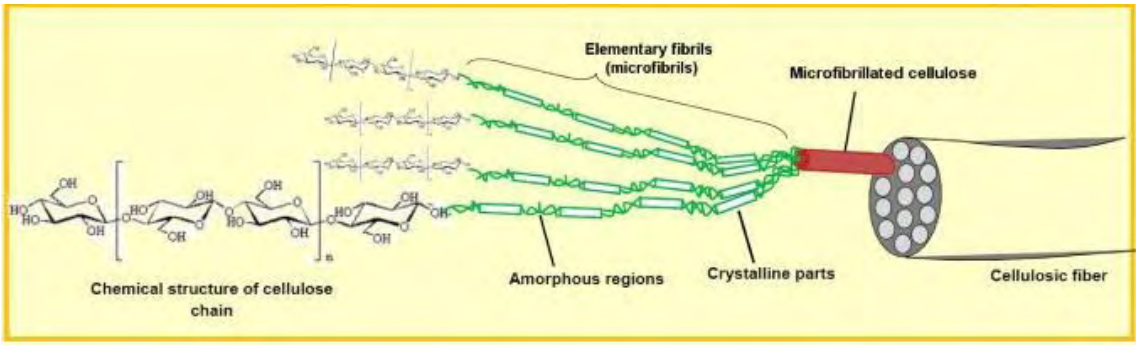

Source: (LAVOINE et al., 2012).

The sorption isotherm of cellulosic material depends on the purity of cellulose and the degree of crystallinity. There are many hydroxyl (OH) groups in cellulose, which in amorphous phase are accessible to water and available for interaction. They interact with water not only at the surface but also in the bulk. But, there are significant problems of compatibility between the fiber and cementitious composite, which weakens interface areas between natural fibers and matrices (THOMAS et al., 2011; SHALWAN et al., 2013). TONOLI et al., 2009 reported that with a proper alkaline treatment, cement composites with vegetable fibers previously submitted to surface modification with methacryloxypropyltri-methoxysilane (MPTS) show fibers free from cement hydration products, reducing their hydrophilic character and improving their adhesion.

The diminution of the moisture absorption and the surface modification of fibers may also increase tensile properties of the fibers and also the strength properties of biodegradable composites, keeping in mind the composition and structure of lignocellulosic fibers. In considering the applicability of cellulose fibers to cement reinforcement, lignin is an amorphous chemical species susceptible to dissolution in an alkaline medium such as a cement matrix (COUTTS et al., 2005; AGOPYAN et al., 2005; TONOLI et al., 2009; SATYANARAYANA et al., 2009).

Lignin and hemicellulose have one characteristic in common: sensitivity to the alkaline environment, which means that they easily undergo the alkaline hydrolysis of cellulose molecules in the highly alkaline cementitious matrix due to the high calcium hydroxide content. For increasing the durability of vegetable fibers, it is research through modifying the fibers with impregnation, treatments, and fibrillation; to minimize the degradation at fiber-cement composites during wetting and drying cycles. (BENTUR AND MINDESS, 2007; MOHR et al.,

2007; PACHECO-TORGAL et al., 2011; ALMEIDA et al., 2013; ARDANUY et al., 2015; WEI et al., 2015).

2.2.1.1. Cellulosic fibers

Cellulosic fibers can be obtained from timber, by chemical, mechanical, biological processes, and many combined processes. They are classified by their length and form: macroscopic level (normally 0.1–1 m), mesoscopic level (normally 1–10 mm), microscopic level (normally 0.01–6 mm) and ultrastructural level (normally 1–25 μm) (ARDANUY et al., 2015; DAI et al., 2014).

At the microscopic level, two kinds of wood cells have different hierarchical structures: softwood fibers (pines, firs, etc.) and hardwood fibers (the birch tree, eucalyptus, beech, etc.). Both kinds of fibers are non-hazardous, renewable and widely available. The differences between softwood and hardwood fibers are the high price of the former and the faster growing plantations of the latter in tropical countries. The VF in previous decades received the attention to be used as replacement for hazardous asbestos fibers. The VF is a reinforcing material that today is found in products such as extruded non-pressure pipes and non-structural building materials, mainly thin-sheet products (MOHR et al., 2005; PIZZOL, 2013; DAI et al., 2014; ARDANUY et al., 2015).

At the ultrastructural level, the wood fibers are built up of four layers. These are M (middle lamella), the P (primary cell wall) containing cellulose microfibrils, the S (secondary wall) and W (warty layer). The secondary wall is composed of three separate and distant layers – S_1 (outer layer of the secondary wall), S_2 (middle layer of the secondary wall) and S_3 (inner layer of the secondary wall). S_2 layer is the thickest and the most important in determining mechanical properties (THOMAS et al., 2011; DAI et al., 2014). Inside microfibril containing regions, networks contain organized structure (crystalline) and loose structure (amorphous). At crystalline regions, the network interactions and molecular orientations could change, given origin to polymorph and allomorph (CORREIA, 2015).

Cellulosic fibers provide adequate stiffness, strength and bonding capacity to cement-based matrices, so they have been extensively applied as the sole reinforcing element in commercial autoclaved and air-cured Portland cement products, because of the retention of cellulose fibers particles on the Hatschek process (CORREIA et al., 2014; WEI et al., 2015).

2.2.2. Fiber-cement production

The current worldwide production cellulosic Fiber-cement, in conjunction with polyvinyl alcohol (PVA) fibers for air-cured (non-autoclaved) products, is located in United States of America, Europe, Oceania and Asia. Brazil has 17 cement plants in ten Brazilian states, offering five thousand jobs and producing 1.3 million tons per year (PIZZOL, 2013).

The Hatschek process was patented by Hatschek in 1900. It consists of producing fiber cement sheets by stacking thin laminas made from a suspension of cement, fibers, mineral admixtures and water, in a process that resembles the production of paper. The first step of the process is preparing the slurry, the mixture of adequate proportions of solid materials (i.e. water, cement, cellulose fibers, and limestone filler) by a roller from a tank under continuous agitation. The slurry is then transported to the vats with sieve cylinders where wet solid material is deposited and then removing, thus, forming a green lamina. Using a vacuum system, a significant portion of the mixing water is removed from the slurry, forming a very thin sheet (about 1 mm). Finally, the fresh sheet is cut, shaped (corrugated sheets and accessories) and submitted to curing under air or steam conditions -autoclave-. Hatschek machines were designed to produce homogeneous materials, so these processes produce composites with an adequate percentage of fibers well dispersed into the matrix (DIAS et al., 2010; ARDANUY et al., 2015).

Figure 2 - Schematic drawing of a typical Hatschek process. In this figure F is the green sheet fiber cement and P is a final product.

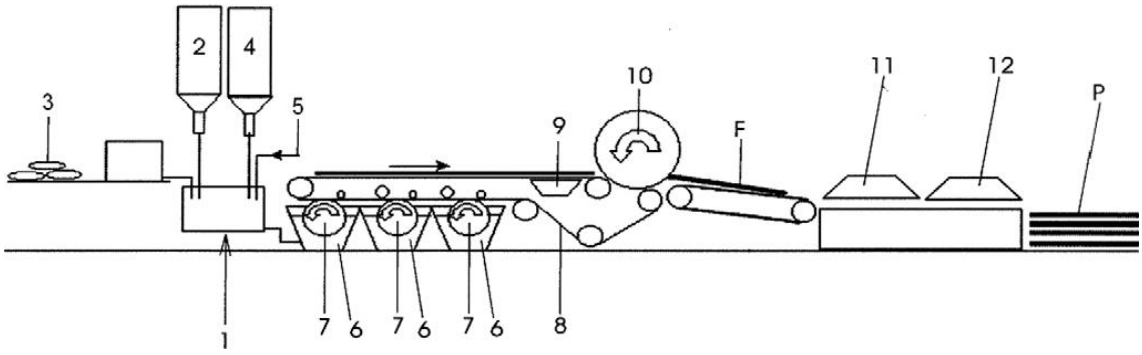

Source: (DIAS et al., 2010)

At laboratory scale, the specimens are made using a slurry-dewatering process followed by a pressing technique, as a similar reproduction of the Hatschek process used in the industrial production of fiber cement (SAVASTANO et al., 2000). Figure 3 shows the Schematic drawing with the respective stages.

Figure 3 – Schematic drawing of slurry-dewatering process follow: a) Mix, b) slurry-dewatering c) pressing manual d) slurry-dewatering e) Pressing.

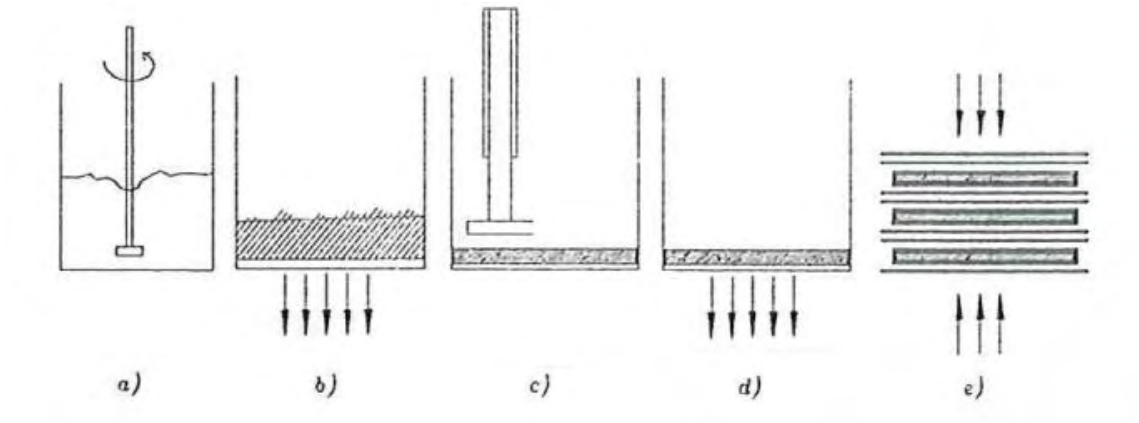

Source: (DEVITO, 2003)

2.2.3. Properties of cementitious materials reinforced with vegetal fibers

The majority of studies about the mechanical behavior of specimens of cement composites prepared at laboratory analyze their mechanical properties using both the three-point and four-point bending configurations. Those are employed to evaluate the limit of proportionality (LOP), modulus of rupture (MOR), modulus of elasticity (MOE) and specific energy (SE). The standard TFR1 of RILEM recommends a proportion between the maximum distance between supports and the thickness of the specimen higher than 20 (TONOLI et al., 2013; ARDANUY et al., 2015).

The tensile strength, void content and interfacial adhesion of the composite is influence by optimum fiber volume fraction of natural fibers and type of fiber. The effects of fiber content on strength show a maximum in the range of 8–12% by mass. Comparing a composite with fiber compare without fibers, both subjected to mechanical stress, the crack is going to be greater magnitude through is not reinforced by fibers. In Figure 4 shows schematic representation composite flexural behavior: (a) without fibers, (b) with fiber reinforced (c) crack detail through the reinforced composite fibers: (1) and (2) bridging and detachment of the fiber; (3) pullout fiber; (4) disruption of fiber (BENTUR AND MINDESS, 2007; PIZZOL, 2013; SHALWAN et al., 2013).

Figure 4 – Schematic representation composite flexural behavior

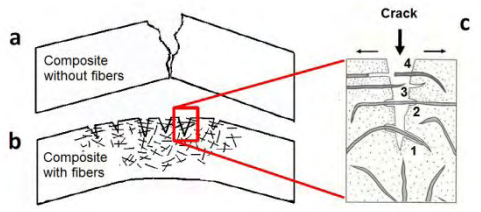

Source: (TONOLI et al., 2009).

Beyond the optimum fiber content, the detrimental effect due to the porosity increase is greater than the reinforcing influence of the added fiber. Porosity inside cement composite is influenced at the early edge by the curing process and by climatic conditions. The total initial porosity of cement paste depends on by relations between temperature, paste composition and mineralogy. The amount of porosity could be increased by rising cure temperatures, the alteration, and solubility of AFt, the evaporation of water excess and gasses from the outside into the inside of the cement material. Furthermore, depending on weather, the pore network may be dry, semi-saturated and saturated. This porosity is one of the causes of the lack of durability of the cement pastes (BENTUR AND MINDESS, 2007; MATSCHEI et al., 2010; ARDANUY et al., 2015).

Cellulosic fiber-cement reinforcement presents a satisfactory mechanical performance at early ages, but the wood fibers swell in the presence of moisture or water and high alkalinity of the cementitious matrix cause a chemical degradation and negatively influenced of stiffness and strength (ARDANUY et al., 2015).

Attempts have been made to optimize the properties of the composites by changing the fiber content and their quality, through modifications in the pulping process as well as by surface treatments to enhance fiber–matrix interactions. The evaluation of the reinforcing effects is usually determined by testing composites made in a full-scale Hatschek process or used a variation of the process (the slurry vacuum de-watering technique) (BENTUR AND MINDESS, 2007; CORREIA et al., 2014; DAI et al., 2014).

2.2.4. Durability

The industrial production of cement-based composites reinforced with VF is currently limited by the long-term durability of these air-cured composites due to the deterioration caused by several mechanisms associated with the environment (i.e. natural weathering, sulphate or chloride attack, etc.) and inside the composite (i.e. alkali attack, fiber mineralization, and volume variation). The following sequence of degradation occurs in the vegetable fibers when

the composite is subjected to various wet/dry cycles: (a) loss of adherence between the fiber and the matrix; (b) reprecipitation of the hydrated compounds within the void space at the former fiber–cement interface; (c) full mineralization, and thus the embrittlement of the vegetable fibers. After the post-cracking, this causes the material to have a reduction in strength and toughness (BENTUR AND MINDESS, 2007; PACHECO-TORGAL et al., 2011; ALMEIDA et al., 2013; ARDANUY et al., 2015; WEI et al., 2015).

The swelling and shrinking of the fibers during wetting and drying, with strains greater than those of the matrix, may lead to changes in the contact pressure across the interface, thus causing variations in the actual bond. A proper fibre–matrix interaction depends on the availability of hydroxyl groups on the surface of the cellulose are the prime means by which fibers and cement bond together, also influence the cellulose-pulp fiber failure. Improving the fibre-matrix bond too much will lead to the composite becoming too brittle and susceptible to movement cracking in service (COUTTS AND KIGHTLY, 1984; COUTTS, 2005; BENTUR AND MINDESS, 2007).

In a highly alkaline cementitious matrix, the harsh hydrolysis of the hemicellulose and lignin causes molecular chains to divide and decreases the degree of polymerization due to the greater amount of calcium hydroxide, that reprecipitation is a dominant step in kraft pulp fiber-cement composite degradation during wet-dry cycling. The migration of alkaline hydration products to lumens and to the middle lamella, caused a volume variation in these fibers due their high-water absorption, also produce fiber mineralization by be sensitive to the amount of CH in the matrix (BENTUR AND MINDESS, 2007; MOHR et al., 2007; WEI et al., 2015).

Many authors have reported fiber mineralization as a source of degradation which leads to fiber embrittlement and the reduction of strength and strain capacity. The CH-mineralization is a mechanism of degradation of the fiber due to the CH content of the matrix and deleterious effect of Ca^{2+} elements. The degradation of cellulose can be simply generalized as the disconnection of discrete cellulose nanocrystals caused by decomposition of reducing ends (feature original C^{4-} OH) in amorphous regions. The accelerated carbonation curing process is projected to decrease the amount of calcium hydroxide in cement-based composites, as well as lower the pH and porosity, and minimize the degradation of the fiber (SILVA, 2002; PACHECO-TORGAL et al., 2011; MOHR et al., 2007; WEI et al., 2015).

Some researchers have revealed that the long term integrity of the vegetable fibre–cement composite matrix may be compromised upon exposure to environmental conditions such as

moisture (SAVASTANO et al., 1999; MOHR et al., 2007; TONOLI et al., 2009). One potential strategy to reduce the vulnerability of vegetable fibre-cement composites to degradation over the long term is to use fibre–cement composed of Portland cement, finely ground crystalline silica, and cellulose fibre which are autoclaved to a specified strength, durability and dimensional stability (COUTTS et al., 1995; COOKE et al., 2000). In addition to the autoclave process, carbonation curing of fresh cementitious composites is reported to also reduce the vulnerability of the degradation of cellulose fibres since carbonation reduces the pH of the bulk matrix leading to less fibre degradation which is beneficial for the mechanical behaviour, microstructure and improves the plastic shrinkage (ALMEIDA et al., 2010; TONOLI et al., 2010; PIZZOL et al., 2014; BERTOS et al., 2004; SANTOS et al., 2015).

2.3. Fiber-cement composites curing process

2.3.1. CO_2 atmospheric curing process

Cementitious composites are well known to be reactive with carbon dioxide. There are two ways this carbonation reaction occurs: carbonation of mature cementitious matrices and carbonation of fresh cementitious composites. The first one is a phenomenon in which well-developed hydration products react with atmospheric CO_2 through prolonged exposure and the second case carbonation is intentionally applied to freshly cement paste where in CO_2 reacts with the anhydrous phases to form strength contributing hydrates and carbonate (ALMEIDA et al., 2013; ROSTAMI et al., 2012).

Complete carbonation of engineering-sized components in natural conditions can take years instead hours like a laboratory conditions, due concentrations of CO_2 influence the carbonation rate of cement composites. Carbonation reaction could be slow with atmospheric CO_2 concentration (0.03%–0.04%), while in accelerated curing carbonation in a chamber is typically used 2%–20% concentration of CO_2 and with supercritical CO_2 is greatly accelerated curing process with rate close 100%. In general, increasing CO_2 concentration and pressure ease diffusion processes and the dissolution of CO_2 (GARCIA-GONZALEZ et al., 2006; CHANG et al., 2006; LIWU et al., 2012; FARAHI et al., 2013).

Reinforced concrete has a highly alkaline medium (pH 13), to cement present; giving to steel a passive protection oxide film. On service is exposed to atmospheric carbon dioxide, CO_2 diffuses through the unsaturated pores. This reaction generates shrinkage, reduced sorptivity, decreased water permeability and reduces the pH value in the environment of the reinforcement, induced steel corrosion of steel reinforcing bars. Consequently, the oxidizing affected the

durability of the structure (FERNÁNDEZ-BERTOS et al., 2004; PETER et al., 2008; ROSTAMI et al., 2011; ROSTAMI et al., 2012).

Carbonation accelerated curing process at freshly cast cement paste, cured concrete and fiber composites, is extensive reported that shown to offer improved mechanical and durability properties (PETER et al., 2008; ROSTAMI et al., 2012). Furthermore, in vegetal Fiber-cement composites submitted to an accelerated carbonation test has been identified as effective procedure to mitigate the degradation of cellulose fibers and to improve mechanical behaviour and volumetric stabilization of these composites (ALMEIDA et al., 2013; SANTOS et al., 2015).

Therefore, a minimum content of water is essential for the ionization of compounds to promote the reaction of carbonation, but a large amount of water (i.e. saturated pores) limits the reaction due to the blockage of the pores (ALMEIDA et al., 2013). Independent of the concentration of CO_2 the chemical reaction is similar in that the carbon dioxide diffuses into the capillary pores of the cementitious composites and combines with aqueous phase in the pores, forming carbonic acid (H_2CO_3) that dissociates into carbonate (HCO_3 and CO_3). Once carbon dioxide dissolves reacts with hydration products, such as calcium hydroxide (CH) and calcium silicate hydrate (C–S–H), forming $CaCO_3$ by the combination of moist CO_2 with Ca^{2+} and silica gel, the follow equations shows the process (Eqs. (1)–(2)) (FERNÁNDEZ-BERTOS et al., 2004; ROSTAMI et al., 2012; ALMEIDA et al., 2013; FARAHI et al., 2013):

$$Ca(OH)_2 + CO_2 \rightarrow CaCO_3 + H_2O \quad \text{(Eq. 1)}$$

$$C\text{-}S\text{-}H + 2CO_2 \rightarrow SiO_2 + 2CaCO_3 + H_2O \quad \text{(Eq. 2)}$$

Another way to explain the interaction between carbon dioxide and hydrated Portland cement at atmospheric pressure and ambient temperature conditions is through the Figure 5.

Figure 5 - Diagram with principal mechanisms for accelerated carbonation in Portland cement.

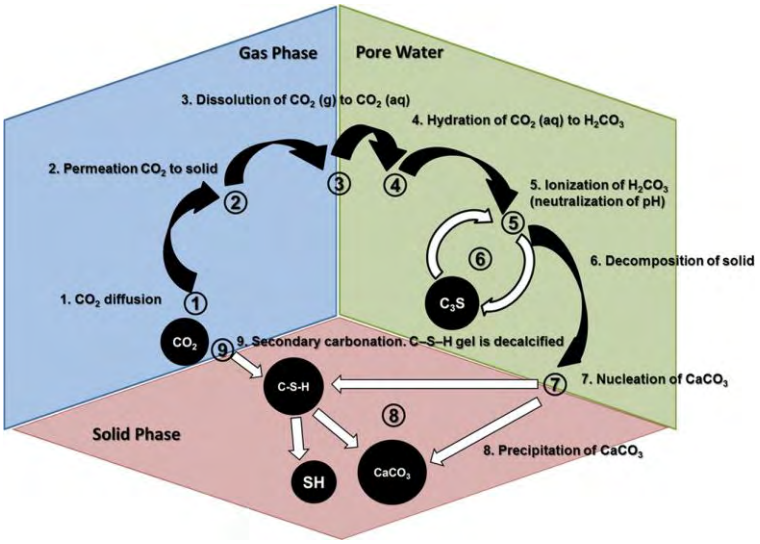

Source: SANTOS et al. 2015 and FERNÁNDEZ-BERTOS et al. 2004.

Carbonation of $Ca(OH)_2$ into $CaCO_3$ causes an increase of volume, depending on the crystal form, which is 3% for aragonite, 12% for calcite and 19% for vaterite. Calcite is the stable form under normal temperature and pressure and is the principal kind of calcium carbonate formed by carbonation (HOUST, 1996).

Accelerated carbonation curing process model must consider the kinetic and thermodynamic parameters that influence the equilibrium of each phase and the interaction thereof. Consequently, the dissolution and precipitation of chemical compounds or ionic equilibrium with carbonation process vary with the temperature, ionic strength and pH solution (TONOLI et al., 2010; MATSUSHITA et al., 2004; CHEN et al., 2007; BULLARD et al., 2011).

2.3.1.1. Influenced by the relative humidity on Carbonation reaction

The diffusivity of gases in cementitious composites is influenced by the porosity, the cement content, the kinetic hydration, the water to cement ratio, etc. It was found that the effective diffusivity of CO_2 does not depend on the CO_2 concentration. The effective diffusivity of carbon dioxide is a function of the relative humidity, this is due to the large reduction of the equilibrium water content caused by carbonation. At the cementitious composite the porosity needs to consists of micro- and meso-pores where water can adsorb and condense. Consequently, the porous volume allowing gas diffusion is reduced. In non-carbonated materials the influence of humidity is much lower (HOUST, 1996).

According to Fernandez-Bertos et al. 2004, the water content affects the reaction of CO_2, because it is essential for the solvation and hydration of the carbon dioxide. It dissolves the Ca^{2+} ions from the solid that will in turn react to form the $CaCO_3$. Subsequently, it influences the amount of product generated, which is also related to the development of strength.

For conventional concrete, it has been well reported that the occurrence of carbonation reactions is most likely between 40% and 80% relative humidity. Various researchers have used a range of 65% to 70% relative humidity in accelerated laboratory carbonation chambers for tests on conventional cement (CHANG et al., 2006; SISOMPHON et al., 2007; SULAPHA et al., 2003). However, accelerated carbonation chambers for cement-based materials containing reactive MgO are more effective at a higher relative humidity (i.e. 98%) (LIWU et al., 2012). On cement pastes samples exposed to a highly carbonating environment with pure carbon dioxide at 90 % relative humidity, was chosen as it has been observed that the hydration of the cement is very slow, but the carbonation rate is high at this humidity (HOUST, 1996; YLMÉN et al., 2013; ALMEIDA et al., 2013; PIZZOL et al., 2014).

2.3.2. Hydration of Portland cement curing process

The hydration of Portland cement consists of the reaction of its phases with water, through an exothermic reaction, which transform the cement fluid mix and water into a solid phase (PEREIRA, 2012). Chemical processes, the effect of curing conditions, equilibrium solubility, rate of dissolution, and other aspects involve understanding hydration process during the different periods. A way to simplify the explanation, is to isolate and study the individual rate processes that govern cement hydration (BULLARD et al., 2011).

C_3S/alite constitutes between 50% and 80% of Portland cement and dominates the development of properties (SCRIVENER et al., 2011). So it is clear why many studies discuss the hydration of the Portland cement clinker, focusing on the three main periods of reaction of alite/C_3S:

- Up to the end of the induction period (about 3 h)
- Main heat evolution peak (approx. 3–24 h), including impact of mineral additions
- Continuing reaction after 1 day (particularly from 1 to 28 days)

The induction period is characterized by fast reactions between C_3S and water that starts immediately upon wetting, characterized by a large exothermic signal in isothermal calorimetry experiments (COSTOYA, 2008). There are many reasons why there is little growth of C-S-H through the induction period, like the degree of hydration at the end of the induction period is only around 2–4%. As soon as the precipitation of product happens, the concentration of Ca in solution increases, eventually up to around 35 to 40 μmol, at the end of the induction period (BROWN et al., 1984). In parallel the concentration of silicate drops dramatically to the μmol range. Thus, the rate of dissolution of C_3S becomes very slow as the solution is supersaturated with respect to calcium hydroxide (SCRIVENER et al., 2015).

At the end of the induction period C–S–H and Portlandite begin to grow rapidily. Bazzoni et al. 2014, propose that the kinetics along the principal heat evolution peak are controlled by the growth of C−S−H "needles". The needles nucleate on the surface of particles and, those properly oriented, grow outwards. Thus, calcium hydroxide does not precipitate during the induction period, there are two possible mechanisms (BULLARD et al., 2010): either the presence of an inhibiting layer, or the "geochemical" approach. In addition, a modeling program HydratiCA showed that in the second case an inhibition of the nucleation or growth of Portlandite (without impacting the other reactions) would produce retardation (SCRIVENER et al., 2015).

The hydration kinetics beyond one day include two relevant processes: first, from 1 to 6 days the quantity of hydration seems to be principally determined by the water to cement ratio or the space available for the cement hydrates. After about 6 days all the systems seem to have very similar kinetics. Second, the period 1−28 days is of great practical importance as 75% of the design strength may develop during this period. The heat evolution rate is very low after 28 days of hydration process (SCRIVENER et al., 2011; SCRIVENER et al., 2015).

Isothermal conduction calorimetry (Figure 6) indicates the onset of the acceleration period at approx. 3h in PC (Portland cement without limestone addition) and PC4 (Portland cement with limestone addition). The maximal heat evolution of the cement hydration was slight accelerated in the presence of finely ground calcite (PC4). Due to the nucleation and growth of hydration products (STARK, 2004; PERA et al., 1999).

Figure 6 - Isothermal calorimetry of Portland cement without additional limestone PC (black lines) and blended with 4 wt.% limestone PC4 (grey lines) expressed as J/h/g unhydrated cement.

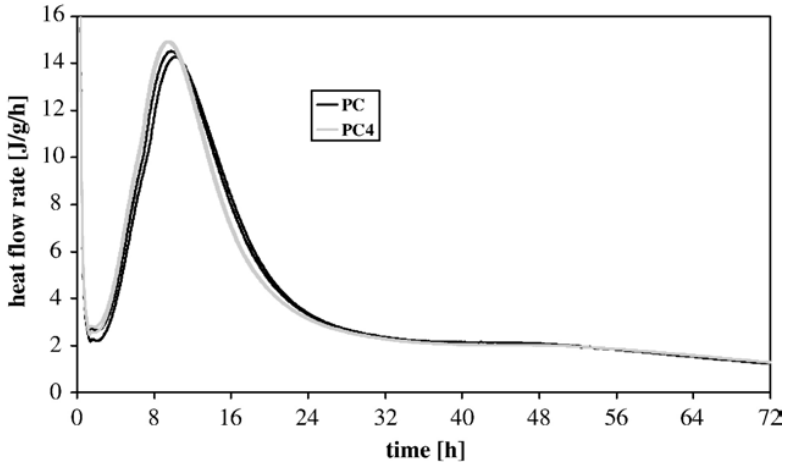

Source: (LOTHENBACH et al., 2008).

Figure 7 shows the rate of heat evolution as a function of the clinker phases for 3 systems: a pure Portland system, a blend of the same Portland with 40% quartz (inert) and a blend with 40% slag. For the first 28 h the curves for the blends with quartz and slag are essentially the same, confirming that the reaction of slag itself is not occurring in this period. Nevertheless, when the rate of heat evolution is normalized relative to the clinker component (in this case) it is clear that the slag and quartz enhance the reaction of the clinker component due to their physical presence; this is named the mineral addition effect (SCRIVENER et al., 2015).

Figure 7 - Rate of heat evolution normalized to clinker content for a Portland cement and the same cement substituted 40% by quartz or by slag.

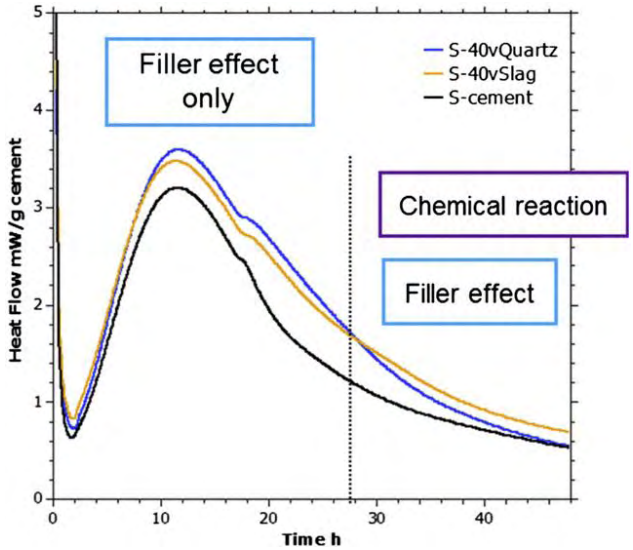

Source: (SCRIVENER et al., 2015).

2.4. Mineral addition effect

The mineral addition effect can be attributed to two main aspects. First, when supplementary cementitious material particles substitute Portland Cement particles, as illustrated in Figure 8, there is comparatively more space available for the hydrates of the clinker phases to form in. Secondly, the surface of the SCM particles act as sites for the heterogeneous precipitation and growth of hydrates (SCRIVENER et al., 2015)..

Figure 8 - Schematic of the particle distribution after mixing for a 100% Portland cement system at a water to cement ratio of 0.4 (left) and for the same system but with 40% of the clinker particles replaced by a mineral addition (right).

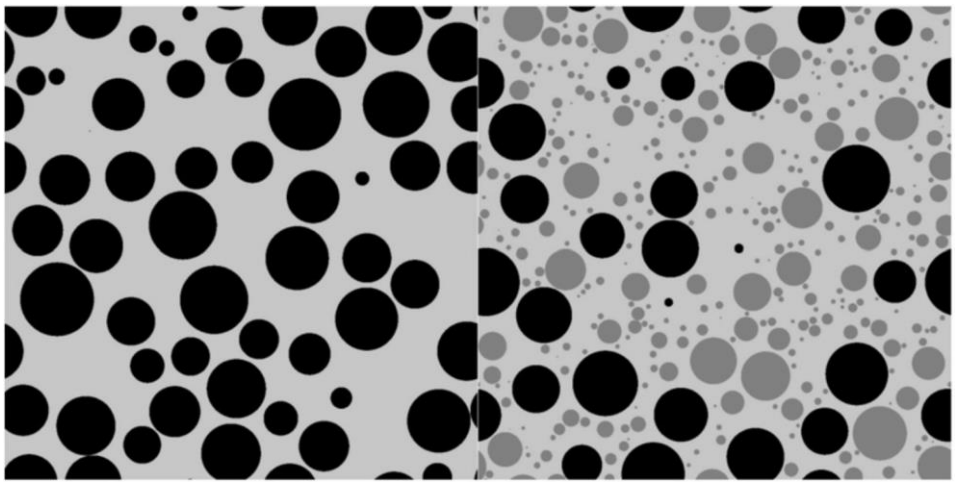

Source: (SCRIVENER et al., 2015).

Limestone is normally used in the industry as a mineral addition in cementitious matrices in order to reduce costs concerning the production of fiber-cement (BENTUR AND MINDESS, 2007). Also, the calcium carbonate mineral addition (limestone) is usually used in research of cement based specimens reinforced with eucalyptus cellulosic pulp subjected to accelerated carbonation curing, in order to apply this technology for the production of fiber-cement at industry (ALMEIDA et al., 2013; SANTOS et al., 2015; PIZZOL et al., 2014). But the mineral addition, even if it consists of inert materials blended with cement, may have a significant effect on the hydration of the clinker phases (GUTTERIDGE et al., 1990).

Various studies showed that the presence of limestone leads to the formation of monocarbonate due to the reaction between the limestone carbonates and existing aluminates (FELDMAN et al., 1965; BENSTED, 1980). The presence of calcite is a few mmol/l and lower compared to

the other main hydration products like portlandite, ettringite and ill crystallized C–S–H (LOTHENBACH et al., 2008). In uncarbonated fiber-cement specimens, the thermogravimetry analysis (TGA) showed decomposition ranged between 650 and 850 °C that is related to the carbon content in as-received cement and calcium carbonate mineral addition (limestone) (ALMEIDA et al., 2013; SANTOS et al., 2015; PIZZOL et al., 2014). Four phases of crystal forms calcium carbonate occur with increasing stability, amorphous calcium carbonate, vaterite, aragonite, and calcite (HOUST et al., 1996).

The extra addition of calcium carbonate at the equilibrium reaction of $CaCO_3$ could impede the formation of calcium carbonate by the chemical equilibrium established in the system, according to the equation:

$$Ca(OH)_{2(s)} + CO_{2(g)} \leftrightarrow CaCO_{3(s)} + H_2O \quad \text{(Eq. 3)}$$

This study examined the implications of calcium carbonate formed during the hydration process in cementitious composites subjected to accelerated carbonation curing process. In this context the use of limestone as mineral addition could make that measurement challenging. In literature, it has been found that inert mineral additions could populate the cementitious matrices without interfering with the calcium carbonate formation, such as ground crystalline silica.

As a strategy to mitigate long term degradation issues, part of the fibre–cement industry worldwide produces fibre–cement composed of Portland cement, finely ground crystalline silica, and cellulose fibre which are autoclaved to confirm appropriate strength, durability and dimensional stability of the composites (COUTTS et al., 1995; COOKE et al., 2000). Crystalline silica is soluble in water at high temperatures and pressures (NEWTON et al., 2009). Quartz has been the most significant crystalline form of SiO_2. The quartz used as mineral addition does not react significantly and is nominally an inert material, offering more space for hydration products of the PC so as to prolong the acceleration period (LOPEZ, 2009; THOMAS et al., 2011).

3. MATERIALS AND METHODS

3.1. Stage 2: Definition of optional parameters for supercritical carbonation process of vegetable Fiber-cement composites at a very early age

The aim of the stage 2 is to study the influence of the bleaching of eucalyptus cellulose pulp, the initial curing duration, the CO_2 exposure time and accelerated aging cycles, on vegetal fiber-cement composites subjected to supercritical carbonation at early age. For this study, samples were made by the slurry-dewatering and pressing technique, the bulk matrix was reinforced with two kinds of pulp: unbleached and bleached. The unbleached eucalyptus pulp reinforced composites were submitted to three different sets of curing conditions, which allowed for a comparison between composite samples with no carbonation and samples carbonated with varying thermal curing durations (24 h v. 48 h). Similarly, the bleached eucalyptus pulp samples were submitted to five different sets of curing conditions, thus allowing a comparison between samples with no carbonation and samples carbonated with varying supercritical carbonation curing durations (1 h v. 2 h) and accelerated ageing cycles (200 soak and dry cycles). A variety of analytical test methods were used to assess the hydration kinetics, the mechanical and the physical properties, and chemical implications in the composites; between them: X-ray diffraction (XRD), thermogravimetric analysis (TG and DTG) and scanning electron microscopy (SEM). The initial period of thermal curing (varying from 24 h to 48 h) and exposure time to carbonation (from 1 h to 2 h) did not affect with statistical significance the mechanical performance of the composites.

3.1.1. Materials and mix design of stage 2

3.1.1.1. Vegetable fiber

For the reinforcement, two kinds of eucalyptus pulp were used: unbleached hardwood kraft pulp of eucalyptus (UB) and commercial bleached hardwood kraft pulp of eucalyptus (Eucalyptus grandis and Eucalyptus urophylla) (B). The unbleached and bleached eucalyptus cellulosic pulp were provided by Suzano Pulp and Paper company and was taken at the beginning of the bleaching process and disintegrated, the moisture content was 65 and 45%, respectively (MEJIA et al., 2015).

3.1.1.2. Chemical analyse of Portland cement

The cement used in this study was the Brazilian brand ordinary Portland cement type CP V-ARI (high initial strength), corresponding ASTM-C150, Type I. This type of cement according

to Santos et al. 2015 is selected for the fibre-cement industry, due to the finer particle size and higher reactivity in comparison to other blended cements available on the Brazilian market. The PC was analyzed through LA-950 Laser Diffraction Particle Size Distribution Analyzer and the result showed that 50% of the particles are finer than 11.88 µm. The use of this cement in this experiment favored the control of the mineral addition to the cement.

3.1.1.3. Chemical analyse of limestone

The mineral addition used in this study was the Brazilian Itaú brand ground limestone. This mineral addition was chosen because it is commonly used in the industry for partial substitution of Portland cement in order to reduce OPC consumption and increase stability (reducing shrinkage) (BENTUR AND MINDESS, 2007). The ground limestone was analyzed through LA-950 Laser Diffraction Particle Size Distribution Analyzer, the result show that 50% of the particles are finer than 12.38 µm.

3.1.1.4. Fibre cement composite mix design

The dry mixture (by mass percent) is composed of 77.2% ordinary Portland cement type OCP V-ARI, 12.8 % calcium carbonate filler (limestone), and 10.0% eucalyptus pulp; is the same formulation as that used by (ALMEIDA et al., 2013), allowing for a comparison between results using a climatic or supercritical chamber for carbonation. Also, this range of fiber contents is compatible to the production method used (a crude reproduction of the Hatschek industrial method), which allows the inclusion of a significant amount of fiber in the inorganic matrix (CORREIA et al., 2014).

The fibre reinforced cement specimens were cast with the dimensions of 200 mm x 200 mm x 5 mm and mean water/binder ratio of 0.40. The specimens were made using a slurry-dewatering process followed by a pressing technique, as simplified reproduction of the Hatschek process used in the industrial production of fiber cement (SAVASTANO et al., 2000). For supercritical carbonation, the samples were cut using a diamond bladed water cooled saw into samples with dimensions (160 mm x 25 mm x 5 mm). These dimensions were necessary for the samples to fit into the carbonation crucible available in the experimental study in laboratory scale.

Table 2 - Dry mixture (in mass percent) proportions of the composite with unbleached pulp of eucalyptus (UB).

Raw material	Mass (%)
ordinary Portland cement (OCP V-ARI)	77.2
Limestone	12.8
Unbleached pulp of eucalyptus [a]	10.00
Total	**100.00**

a. Suzano Pulp and Paper

Source: authorships.

Table 3 - Dry mixture (in mass percent) proportions of the composite with Bleached pulp of eucalyptus (B).

Raw material	Mass (%)
ordinary Portland cement (OCP V-ARI)	77.2
Limestone	12.8
Bleached pulp of eucalyptus [a]	10.00
Total	**100.00**

a. Suzano Pulp and Paper

Source: authorships.

3.1.1.5. Supercritical CO_2 extraction apparatus

The samples were subjected to supercritical carbonation (SC) in a SULAB brand supercritical fluid extractor machine (Figure 9). The machine utilizes a series of pressure valves and a pump to inject CO_2 into a steel crucible. Approximate 99.5% concentration pure carbon dioxide is injected into a crucible capable of holding six samples at once (Figure 10 a-c). The CO_2 employed in the experiments was supplied by the White Martins Gas Industrials Company (Brazil). For the entirety of the carbonation, the steel crucible was immersed in a thermal bath at 45°C (Figure 10 d). The pressure within the crucible can be regulated using the system of seals and gaskets. For this study, a pressure of 20 MPa within the chamber was used, tried to ensuring a nearly complete carbonation of samples (for a duration of 2 h within the chamber) (Figure 10 e). Of course, the change in pressure is not instantaneous, therefore the first hour of carbonation corresponds to a “build-up” period for the pressure to reach 20 MPa, at which point samples remain in the chamber for a second hour in order to complete the carbonation cycle. (SANTOS et al., 2015).

Figure 9 – Supercritical CO_2 extraction apparatus.

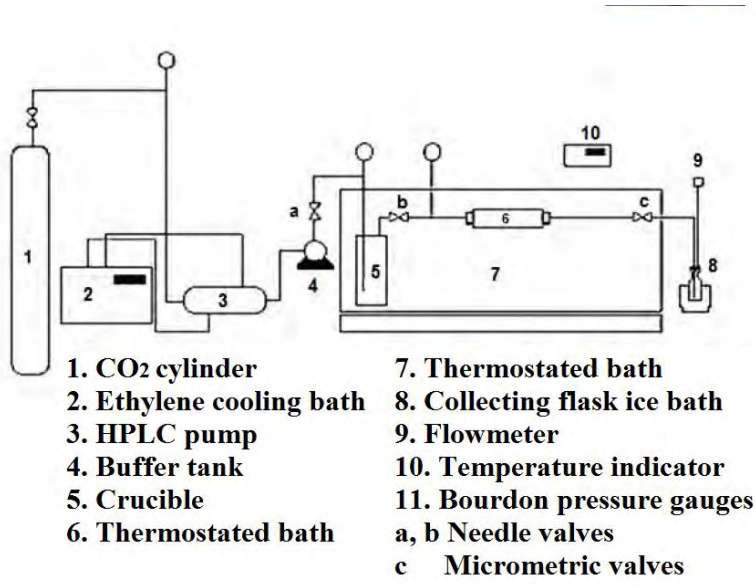

Source: (MARTINEZ et al., 2011).

Figure 10 – Schematic experiment at the chamber: a) Carbonation crucible being loaded with cement samples. b) Samples average size was 25 mm. c) Carbonation crucible loaded with cement samples were connect to extractor. d) Submerged crucible in thermal bath (45° C). e) Pressure gauge of 20 MPa.

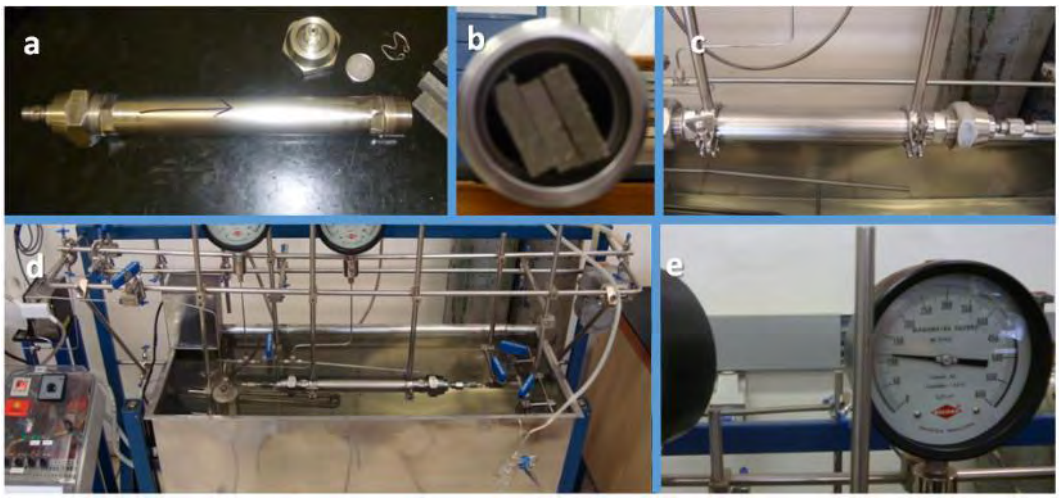

Source: authorships.

3.1.2. Curing and conditioning regimes stage 2

The different sets of curing conditions use the following nomenclature: the first one or two letters indicate what type of pulp was used for that batch of samples (B for bleached, UB for unbleached) which are summarized in Table 4. Close examination of the processes described

in Table 4, reveals that it is possible to isolate the effect of the initial thermal hydration duration (24 h and 48 h); carbonation exposure (0 h, 1 h or 2 h of curing in an environment with close 100% CO_2 concentration); and, accelerated ageing cycles (0 cycles or 200 cycles). The eight conditions shown in Table 4 were cast with the same w/c ratio but with two kinds of eucalyptus pulp as reinforcement and treated with different curing regimes.

3.1.2.1. Uncarbonated curing (UC) regime

After the samples were cast, they underwent 48 hours of thermal curing in a chamber at a RH of 90% at 45°C, some of them correspond to unbleached pulp samples (UB) and the other ones bleached pulp samples (B). The specimens were then removed from the chamber, sealed, stored in air curing at temperature of 25°C, RH of 90%, and atmospheric CO_2 concentration (0.035 vol%). Upon completing the curing process of eleven days, characterization tests were performed. These samples belong to the uncarbonated curing (UC) regime.

3.1.2.2. Supercritical carbonation (SC) curing regime

After the samples were cast, the unbleached pulp samples UB-SC-48-2 underwent 48 hours of thermal curing in an environmental chamber at a RH of 90% at 45°C, while the samples UB-SC-24-2 underwent 24 hours with the same environmental chamber conditions. Following thermal curing, both curing regimes were carbonated for 2 h in a Supercritical CO_2 extraction apparatus. The bleached pulp samples were also subjected to 48 hours of thermal curing. After the thermal curing, the sample B-SC-48-2 was carbonated for 2 h while sample B-SC-48-1 was carbonated for 1 h in a Supercritical CO_2 extraction apparatus (SANTOS et al., 2015). The specimens were then removed from the apparatus, sealed, stored in air curing at temperature of 25 °C, RH of 90%, and atmospheric CO_2 concentration (0.035 vol%) (SANTOS et al., 2015). Upon completing the curing process of eleven days, characterization tests were performed. These samples bellows to the supercritical curing (SC) regime.

3.1.2.3. Accelerated ageing: soak-dry cycles

The accelerated ageing test was conducted on two sets of samples, one set of specimens that had not undergone the carbonation curing regime, namely, B-AAC, and one set of specimens that had been exposed to the 2 h carbonation curing in a SC, namely, B-SC-48-2-AAC. The specimens were then removed from the apparatus, sealed and stored in air curing at temperature of 25 °C and atmospheric CO_2 concentration (0.035 vol%). Upon completing the curing process

of eleven days, samples were subjected to accelerated ageing cycles. Then, characterization tests were performed on both sets.

The accelerated ageing cycles (AAC) aims to simulate the natural ageing with exposure to soaking and drying cycles as tested in previous works (ALMEIDA et al., 2013; TONOLI et al., 2009). The bleached cellulosic pulp samples were successively immersed into water at 20° ± 5°C for 170 min and, after an interval of 10 min, they were heated to the temperature of 60° ± 5°C for 170 min in a ventilated oven. Another interval of 10 min at room temperature elapses before the subsequent cycle, as recommended by the EN 494 Standard (1994). Each soak and dry set represents one cycle, which was repeated 200 times, i.e., 200 ageing cycles.

Table 4 - Description of curing regimes applied at stage 1.

Curing Regime Identification	Thermal Hydration Duration in with: CO_2 = 0.035% Temp. = 60° C RH= 90 %	Carbonation Duration in Chamber with: CO_2 = 99.5% Temp. = 45° C RH= 90 %	Accelerated Ageing Cycles
UB	48 h	0 h	0 cycles
UB-SC-48-2	48 h	2 h	0 cycles
UB-SC-24-2	24 h	2 h	0 cycles
B	48 h	0 h	0 cycles
B-SC-48-1	48 h	1 h	0 cycles
B-SC-48-2	48 h	2 h	0 cycles
B-AAC	48 h	0 h	200 cycles
B-SC-48-2-AAC	48 h	2 h	200 cycles

Source: authorships.

3.1.3. Test methods of stage 2

3.1.3.1. Physical characterization of the fiber-cement composites

Apparent Void Volume (AVV), bulk density (BD), and water absorption (WA) of the composites were obtained from the average of eight test specimens (160 mm x 25 mm x 5 mm) for each condition, following the procedures specified by ASTM C 948-81 (2009). Physical properties were obtained using Eqs.4–6:

$$AVV\ (\%) = \left(\frac{M_{sat} - M_{dry}}{M_{sat} - M_i}\right) \times 100 \quad \text{(Eq. 4)}$$

$$BD\ (g/cm^{-3}) = \left(\frac{M_{dry}}{M_{sat} - M_i}\right) \times \rho \quad \text{(Eq. 5)}$$

$$WA\ (\%) = \left(\frac{M_{sat} - M_{dry}}{M_{dry}}\right) \times 100 \quad \text{(Eq. 6)}$$

where M_{sat} is the saturated with dry surface specimen's mass, M_{dry} is the dry specimen's mass after 24 h at 105 ºC, M_i is the immerse water specimen's mass and ρ is the water real density (g/cm^3)

3.1.3.2. Mechanical characterization of the fiber-cement composites

Mechanical properties were obtained for uncarbonated curing (UC), Supercritical carbonation curing (SC) and composites upon completing the curing process of fourteen days. Each fiber cement specimen was wet cut into four samples measuring 160 mm by 25 mm for the mechanical test, using a water cooled diamond saw.

Eight specimens were evaluated for each condition; mechanical four-point bending flexural tests were performed in an EMIC DL-30000 testing machine equipped with a 1 kN load cell, a four-point bending configuration, a lower span of 135 mm, an upper span of 45 mm and a deflection rate of 1.5 mm/min. The mechanical properties evaluated were: Modulus of rupture (MOR), Limit of proportionality (LOP), Modulus of elasticity (MOE) and Specific Energy (SE). Mechanical properties were obtained using Eqs. 7 – 10 as described in detail by (ALMEIDA et al., 2013; TONOLI et al., 2009).

$$MOR\ (MPa) = \frac{Pmax \cdot L_v}{b \cdot h^2} \quad \text{(Eq. 7)}$$

$$LOP\ (MPa) = \frac{Plop \cdot L_v}{b \cdot h^2} \quad \text{(Eq. 8)}$$

$$MOE\ (MPa) = \frac{276 \cdot L_v^3}{1296 \cdot b \cdot h^3} . m \quad \text{(Eq. 9)}$$

$$SE\ (kJ/m^2) = \left(\frac{Energy}{b \cdot h}\right) \quad \text{(Eq. 10)}$$

where P_{max} is the maximum load rate, P_{lop} is the load at the upper point of the linear portion of the load–deflection curve, L_v is the major span, width (b) and depth (h) and m is the tangent of the slope angle of the load vs. deflection plotting in the elastic behavior. SE, was defined as the energy absorbed during the flexural test and divided by the specimen cross-sectional area (ALMEIDA et al., 2013; TONOLI et al., 2009).

3.1.3.3. Thermal analysis TG/DTG

Chemical changes such degradation of cellulose, as well as transition temperatures in fiber based composites, are studied through derivative thermogravimetry (DTG) (SATYANARAYANA et al., 2009); the samples were ground using a pestle and mortar, sieved until particles smaller than 75 μm, then analyzed in a Thermogravimetric Analyzer NETZSCH STA 449 F3. The experimental conditions were: rates of 10°C/min for heating and 40 mL/min for nitrogen injection. The sample with range (20 – 900°C) at a constant rate (ROSTAMI et al., 2012; PIZZOL et al., 2014), yielding TGA and DTG curves of the extruded cellulosic fiber–cement submitted to supercritical CO_2 curing (SC) and uncarbonated (UC) treatments. The amount of calcium hydroxide, $Ca(OH)_2$, and calcium carbonate, $CaCO_3$, was estimated from the weight loss measured in the TGA curve between the initial and final temperature of the corresponding DTG peak.

Thermogravimetry analysis (TGA) and derivative thermogravimetry (DTG) were used to inspect the nature of hydration products formed in the cement-based systems. The different DTG peaks measured when hydrated cement is heated in a thermobalance correspond to: at 100 °C - weight loss due to the dehydration of water pores, between 100 °C to 300 °C - different stages of dehydration of C–S–H, at 500 °C - dehydroxylation of $Ca(OH)_2$, and at 700 °C - decarbonation of $CaCO_3$ (ROSTAMI et al., 2012).

3.1.3.4. Phases analysis X-Ray diffraction (XRD)

This x-Ray diffraction technique consists in identify crystalline phases presents in samples, characterize for be a qualitative analyze. The diffractometer produces waves at a known frequency, which is determined by their source. This technique was applied in order to identify the main crystalline phases and compere between the specimens for the principal found components in Portland cement hydrated. The single crystal diffraction and the angle between the beam axis and the ring is called the scattering angle and in X-ray crystallography always denoted as 2θ (in scattering of visible light the convention is usually to call it θ). The identification of the phases were made throught the data base “International Centre for Diffraction Data” (ICDD).

The X-Ray Diffraction (XRD) technique, allows the identification of crystalline phases in materials, (CHANG et al., 2006). The analyses were performed using a Rigaku MiniFlex 600, with range 10-60° (2θ) and rate of 15°/min.

3.1.3.5. Microstructural analysis by Scanning Electron Microscopy - (SEM)

Scanning electron microscopy (SEM) was used with a back-scatter electron (BSE) image detector, operated at 15 kV accelerating voltage, for visualization of the microstructure on the surface of the composites. The images were captured by a Hitachi Tabletop Microscope TM3000.

The preparation of specimens for BSE was accomplished with impregnation using epoxy resin. BSE samples were manually polished in a Struers TegraPol-11 machine using silicon carbide abrasive paper with sequential grit sizes 320, 600, 1000 for 6 min, using isopropyl alcohol as lubricant. A final polishing was carried out using in turn 6, 3, l µm diamond polishing compound for 6 min with each size.

Approximately six SEM micrographs were obtained for each composite treatment, with typical images of the observed microstructure being used in this manuscript.

3.2. Stage 3: Comparative study between two kinds of mineral addition in cellulose pulp fiber-cement composites subjected to accelerated carbonation at very early age.

The aim of this stage 3 is to compare two kinds of mineral addition on vegetal fiber-cement composites subjected to accelerated carbonation at a very early age. For this study, samples were produced by the slurry-dewatering and pressing technique. The samples were submitted to carbonation process, with varying the mineral addition (limestone v. ground silica) and the initial curing durations (10 h v. 24 h). A variety of analytical test methods were used to assess the hydration kinetics, the mechanical and the physical properties, and chemical implications in the composites; between them: X-ray diffraction (XRD) and scanning electron microscopy (SEM).

3.2.1. Materials and mix design stage 3

3.2.1.1.Vegetable fibre

Unrefined pine unbleached cellulosic pulp (P) was used in this study. The fiber is produced by the OJSC Solombala Pulp and Paper Mill - brand located in the industrial zone of the city of Arkhangelsk, in North-West Russia. This is a type of fibre Pine Spruce, processed as unbleached northern softwood kraft. Morton et al. (2010) physically describe the Solombala pinus fibre with an average length of 2.7 mm, coarseness of 15.55 mg/100 m, wall thickness of 7.9 µm, and a fibre width of 30.7 µm.

3.2.1.2.Chemical analyse of Portland cement

The cement used in this study was the Brazilian Cauê brand ordinary Portland cement type PC V-ARI (high initial strength), corresponding ASTM-C150, Type I, this type of cement according to Santos et al. 2015 is selected for fibre reinforced cementitious composites, due the finer particle size and higher reactivity in comparison to other blended cements available in the Brazilian market. The PC V-ARI was analyzed through LA-950 Laser Diffraction Particle Size Distribution Analyzer, the result show that 50% of the particles are finer than 8.67 μm.

3.2.1.3. Chemical analyse of Limestone

The mineral addition used in this study was the Brazilian Itaú brand ground limestone (L). This mineral addition was chosen because it is commonly used in the industry for partial substitution of Portland cement in order to reduce OPC consumption and increase stability (reducing shrinkage) (BENTUR AND MINDESS, 2007). The ground limestone was analyzed through LA-950 Laser Diffraction Particle Size Distribution Analyzer, the result show that 50% of the particles are finer than 12.38 μm. Figure 11 shows the XRD, the analysis was made by a Rigaku MiniFlex 600 with range 10-60° (2θ) and rate of 15°/min.

Figure 12 shows the XRD patterns of quantification of the phases for limestone. The chemical compositions of the limestone are calcite with 68.4%, dolomite 29% and quartz 2.6%, determined through the software PANalytical HighScore Plus, using Rietveld method. Various research shows that the reaction occurs on a definite boundary between the lime and carbonate phases (HILLS, 1968).

The presence of dolomite [$CaMg(CO_3)_2$] in this cementitious composite can be explained as it is one of the forms limestone and has a similar crystal structure to that of calcite, having a face-centred rhombohedral cell (MCINTOSH et al., 1990).

Dolomite reaction involves the direct formation of calcium carbonate via Magnesian calcite with a gradual release of Mg^{2+} ions to form calcite. It is proposed that the progression of carbon dioxide from surface defects initiates decomposition, dissociation into the two carbonates as described in eq. (11) (HASHIMOTO et al., 1976; MCINTOSH et al., 1990).

$$CaMg(CO_3)_2 \rightarrow CaCO_3 + MgCO_3 \qquad \text{(Eq. 11).}$$

Figure 11 - XRD patterns of the limestone.

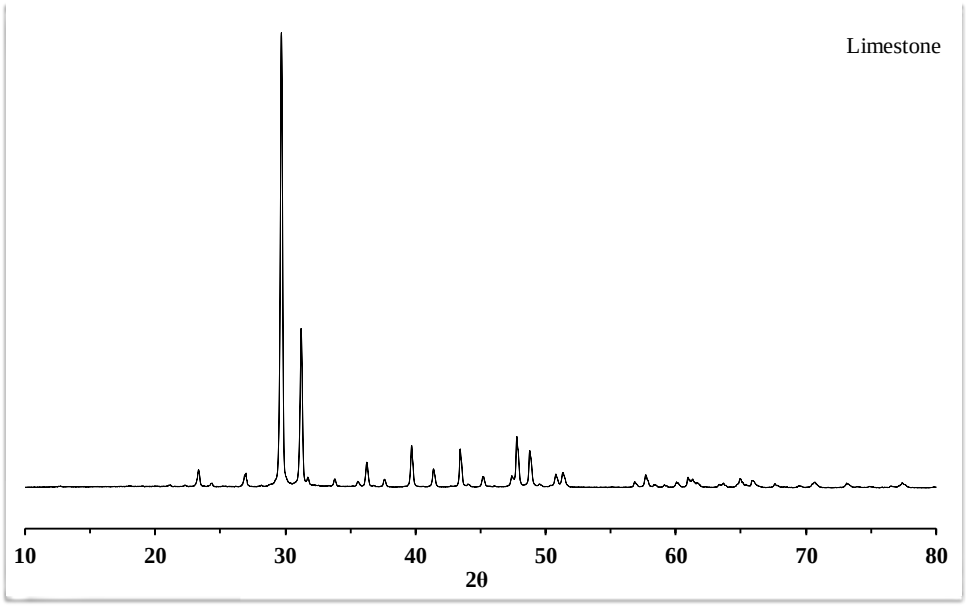

Source: authorships.

Figure 12 - XRD crystalline phases analysis of the limestone.

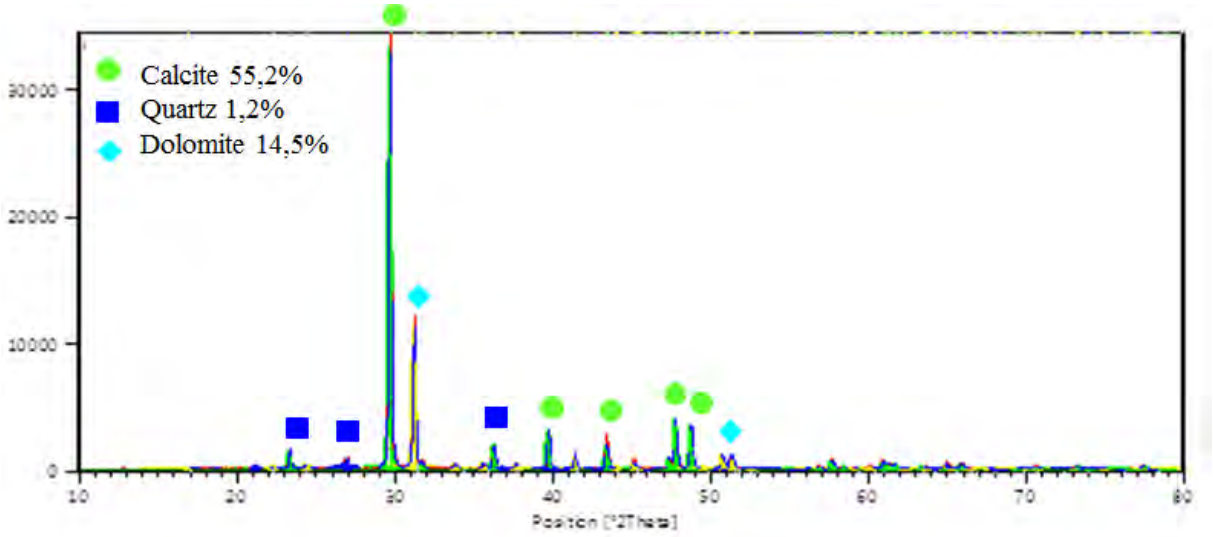

Source: authorships.

3.2.1.4. Chemical analyse of Ground Silica

The silicate used in this work was the Brazilian Mineração Jundu brand crystalline grounded silicate with a real bulk density of 2.65 (g/cm^3). The ground silica was analyzed through LA-950 Laser Diffraction Particle Size Distribution Analyzer, the result shows that 50% of the particles are finer than 17.6 µm. The Figure 13 shows the XRD test results, the analysis was made by a Rigaku MiniFlex 600 with range 10-60° (2θ) and rate of 15°/min.

Figure 13 - XRD patterns of the silica crystalline.

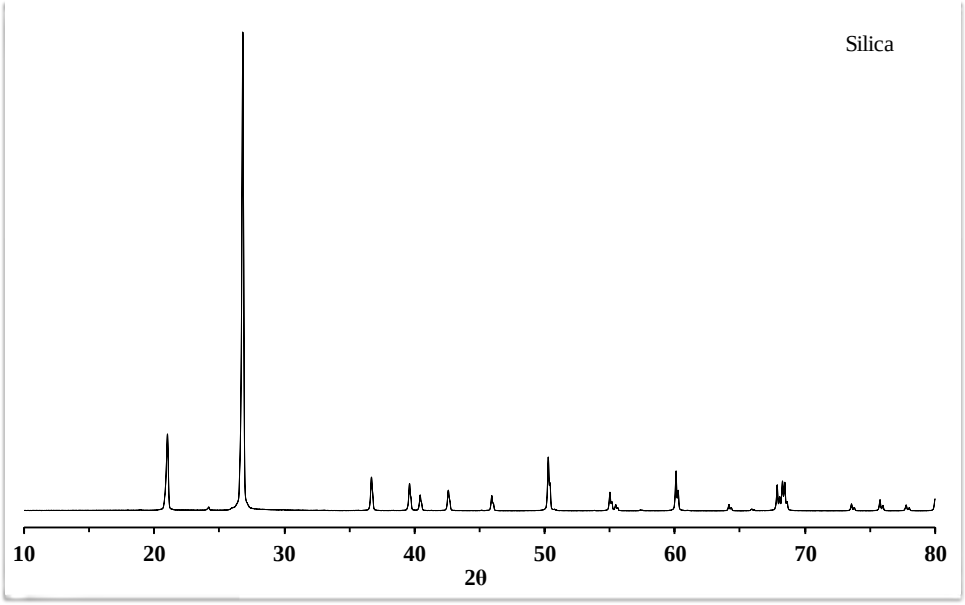

Source: authorships.

Crystalline Silica it is chemically and thermodynamically stable at low temperatures and atmospheric pressure (SINGH et al., 2013). Figure 14 shows that the silica used have a crystal estructure of quartz, determined through the software PANalytical HighScore Plus and Rietveld method. The use of silica as mineral addition with this level of crystallinity in cementitious matrices does not interfere with the formation of cement hydration phases but gives relatively more space for the hydrates of the clinker phases (SINGH et al., 2013; SCRIVENER et al., 2015).

Figure 14 - XRD patterns of quantification of the phases for silica

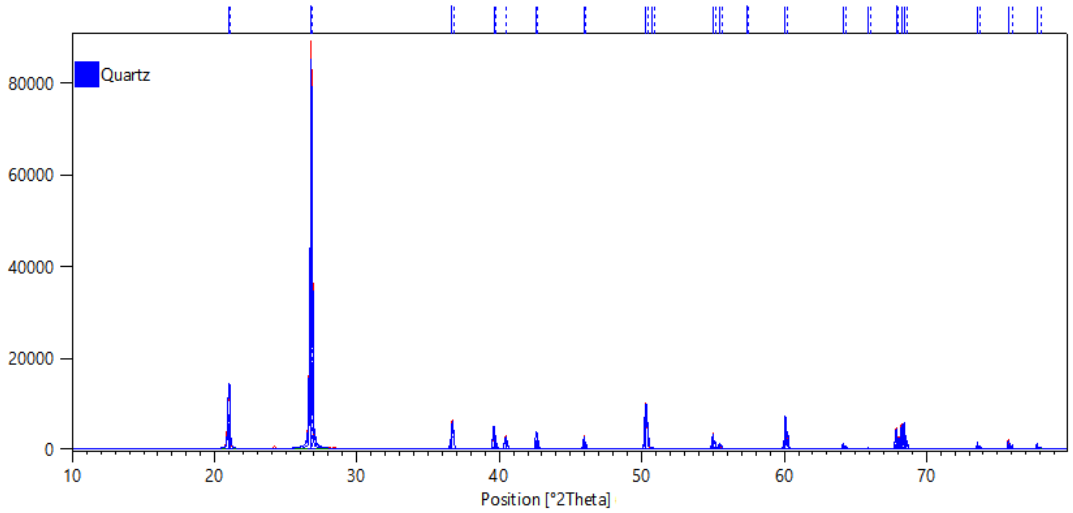

Source: authorships.

3.2.1.5. Analyses of particle size distribution between limestone and silica

The OPC V-ARI, the limestone and the silica was analyzed by the means LA-950 Laser Diffraction Particle Size Distribution Analyzer. The Figure 15 shows the particle size distribution using the ordinary Portland cement type OCP V-ARI (high initial strength) and considering the mix design of dry mass 70% of cement and 30% of mineral addition (ground silica or limestone), the model used was Fuller and Thomson proposed the gradation curves for maximum density, which is well known as Fuller's "ideal" curve. Both formulations had a bimodal profile, almost the same points, there are few differences between the formulations until 10 µm. Comparing the two formulations, this analyses indicates that the ground silica could be used as mineral addition instead the limestone as it was used on the stage two of this thesis.

$$CPFT = \left(\frac{d}{D}\right)^{n} \cdot 100 \qquad \text{(Eq. 12)}$$

Where, CPFT = cumulative (volume) percent finer than, n = 0.5; the value of n was later revised to 0.45; these curves find application in highway pavement mixture design.

Figure 15 – Particle size distribution analyses between limestone and silica

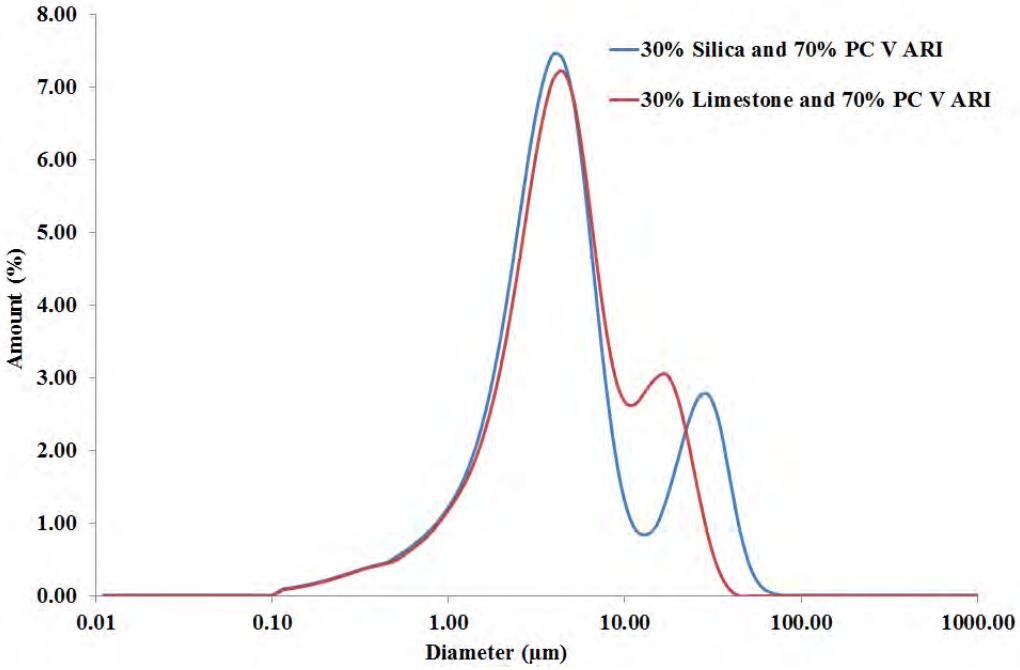

Source: authorships.

3.2.1.6. Fibre cement composite mix design

The materials with respectively amount, used on the composite specimens are shown in Table 5. The formulation is based on previous work carried out by Almeida et al. (2010). The dry mixture (by mass percent) is composed of 64% Brazilian Cauê brand ordinary Portland cement type OPC V-ARI (high initial strength), corresponding to ASTM-C150, Type I, 28% Brazilian brand limestone mineral addition, and 8.0% unrefined pine unbleached cellulosic pulp.

Table 6 shows the second formulation, the dry mixture (by mass percent) is composed of 64% Brazilian Cauê brand ordinary Portland cement type OPC V-ARI (high initial strength), corresponding to ASTM-C150, Type I, 28% silica quartz type mineral addition, and 8.0% unrefined pine unbleached cellulosic pulp.

The fibre reinforced cement specimens were cast with the dimensions of 200 mm x 200 mm x 5 mm and average water/binder ratio of 0.40. The specimens were made using a slurry-dewatering process followed by a pressing technique, as an approximate reproduction of the Hatschek process used in the industrial production of fibre cement (SAVASTANO et al., 2000).

Table 5 - Dry mixture (by mass percent) proportions of the composite with Limestone

Raw material	Mass (%)
ordinary Portland cement (OCP V-ARI)	64.0
Limestone	28.0
unbleached pine cellulosic pulp[a]	8.0
Total	**100.0**

a. Sol. Pulp/Paper Mill

Source: authorships.

Table 6 - Dry mixture (by mass percent) proportions of the composite with Silica

Raw material	Mass (%)
ordinary Portland cement (OCP V-ARI)	64.0
Silica	28.0
unbleached pine cellulosic pulp[a]	8.0
Total	**100.0**

a. Sol. Pulp/Paper Mill

Source: authorships.

3.2.2. Curing and conditioning regimes of stage 3

This experiment exposes the composite specimens to four different curing conditions on fibre-cement composite properties which are summarized in Table 7. The processes described in Table 7, reveals that it is possible to isolate the effect of hydration duration (10 h and 24 h); and the effect of the mineral addition (limestone vs ground silica). Short form 'curing regime identification' names that are shown in the first column of the Table 7, will be used from here onwards in the results, discussion and labels in figures.

Table 7 - Description of curing regimes applied

Mineral addition	Curing Regime Identification	Hydration Duration in Chamber with: CO_2 = 0.035% Temp. = 25°C RH = 90%	Carbonation Duration in Chamber with: CO_2 = 20% Temp. = 45°C RH = 90%	Hydration Duration with: CO_2 = 0.035% Temp. = 45°C RH = 90%
Limestone	P-LAC-10	10 h	10 h	6 days
Limestone	P-LAC-24	24 h	10 h	6 days
Silica	P-AC-10	10 h	10 h	6 days
Silica	P-AC-24	24 h	10 h	6 days

Source: authorships.

3.2.3. Test methods of stage 3

3.2.3.1. Physical characterization of the fiber-cement composites

Apparent Void Volume (AVV), bulk density (BD), and water absorption (WA) of the composites were obtained from the average of eight test specimens (160 mm x 25 mm x 5 mm) for each condition, following the procedures specified by ASTM C 948-81 (2009). Physical properties were obtained using Eqs.4–6:

$$AVV\ (\%) = \left(\frac{M_{sat} - M_{dry}}{M_{sat} - M_i}\right) \times 100 \quad \text{(Eq. 4)}$$

$$BD\ (g/cm^{-3}) = \left(\frac{M_{dry}}{M_{sat} - M_i}\right) \times \rho \quad \text{(Eq. 5)}$$

$$WA\ (\%) = \left(\frac{M_{sat} - M_{dry}}{M_{dry}}\right) \times 100 \quad \text{(Eq. 6)}$$

where M_{sat} is the saturated with dry surface specimen's mass, M_{dry} is the dry specimen's mass after 24 h at 105 ºC, M_i is the immerse water specimen's mass and ρ is the water bulk density (g/cm^3)

3.2.3.2. Mechanical characterization of the fiber-cement composites

Mechanical properties were obtained for carbonated curing (AC), and composites upon completing the curing process of seven days. Each fiber cement specimen was wet cut into four samples measuring 160 mm by 25 mm for the mechanical test, using a water cooled diamond saw.

Eight specimens were evaluated for each condition. Mechanical four-point bending flexural tests were performed in an EMIC DL-30000 universal testing machine with a 1 kN load cell, a four-point bending configuration, a lower span of 135 mm, an upper span of 45 mm and a deflection rate of 1.5 mm/min. The mechanical properties evaluated were: Modulus of rupture (MOR), Limit of proportionality (LOP), Modulus of elasticity (MOE) and Specific Energy (SE). Mechanical properties were obtained using Eqs. 7 – 10 as described in detail by (ALMEIDA et al., 2013; TONOLI et al., 2009).

$$MOR\ (MPa) = \frac{Pmax \cdot L_v}{b \cdot h^2} \quad \text{(Eq. 7)}$$

$$LOP(MPa) = \frac{Plop \cdot L_v}{b \cdot h^2} \quad \text{(Eq. 8)}$$

$$MOE\ (MPa) = \frac{276 \cdot L_v^3}{1296 \cdot b \cdot h^3} . m \quad \text{(Eq. 9)}$$

$$SE\ (kJ/m^2) = \left(\frac{Energy}{b \cdot h}\right) \quad \text{(Eq. 10)}$$

where P_{max} is the maximum load rate, P_{lop} is the load at the upper point of the linear portion of the load–deflection curve, L_v is the major span, width (b) and depth (h) and m is the tangent of the slope angle of the load vs. deflection plotting in the elastic behavior. SE, was defined as the energy absorbed during the flexural test and divided by the specimen cross-sectional area (ALMEIDA et al., 2013; TONOLI et al., 2009).

3.2.3.3. X-Ray diffraction (XRD) analysis

This XRD technique consists in identifying crystalline phases present in samples, as a qualitative analysis. The diffractometer produces waves at a known frequency, which is determined by their source. This technique was applied in order to identify the main crystalline phases and compare between the specimens for the main components in Portland cement hydrated. The single crystal diffraction and the angle between the beam axis and the ring is called the scattering angle and in X-ray crystallography always denoted as 2θ (in scattering of the convention is usually to call it θ). The identification of the phases was made throughout the data base "*International Centre for Diffraction Data*" (ICDD).

The X-Ray Diffraction (XRD) technique, allows the identification of crystalline phases in materials, (CHANG et al., 2006). The analyses were performed using a Rigaku MiniFlex 600, with range 10-60° (2θ) and rate of 15°/min.

International Centre Diffraction Data (2003) and PANalytical HighScore Plus Inorganic Crystal Structure Database (2007) were applied to identify crystalline phases. The PANalytical HighScore Plus was used too for made a quantification estimative of the clinker phases, considering only the crystalline part of the material and excluding the amorphous part.

3.2.3.4. Microstructural analysis by Scanning Electron Microscopy - (SEM/EDS)

Scanning electron microscopy (SEM) was used with a back-scattered electron image (BSEI) detector and was carried out the Energy-dispersive X-ray spectroscopy analysis (EDS), operated at 15 kV accelerating voltage, for visualization of the microstructure on the surface of the composites. The images were captured by a Hitachi Tabletop Microscope TM3000.

The preparation of specimens for BSE was accomplished with impregnation using epoxy resin. BSE samples were manually polished in a Struers TegraPol-11 machine using silicon carbide

abrasive paper with sequential grit sizes 320, 600, 1000 for 6 min, using isopropyl alcohol as lubricant. A final polishing was carried out using in turn 6, 3, l μm diamond polishing compound for 6 min with each size.

Approximately SEM micrographs were obtained for each composite treatment, with typical images of the observed microstructure being used in this manuscript.

3.3. Stage 4: Durability and hydration kinetics study in carbonated fiber-cement composites using silica as a mineral addition.

The aim of this stage 4 is to study the durability and hydration kinetics in carbonated composites reinforced with unbleached pines cellulose pulp fiber and used silica as a mineral addition. Samples were prepared by the slurry-dewatering and pressing technique. The samples were submitted to two different sets of curing conditions, which allowed for a comparison between uncarbonated samples and samples carbonated with varying initial curing durations (10 h v. 24 h) and then subjected to 200 accelerated ageing cycles. A variety of analytical test methods were used to assess the hydration kinetics, the mechanical and the physical properties, and chemical implications in the composites: X-ray diffraction (XRD), thermogravimetric analysis (TG), Infrared spectrometer (FTIR), scanning electron microscopy (SEM) and B.E.T. surface area analyzer.

3.3.1. Materials and mix design of stage 4

3.3.1.1. Vegetable fibre

Unrefined pine unbleached cellulosic pulp was used in this study. The fiber is produced by the OJSC Solombala Pulp and Paper Mill, from Arkhangelsk, in North-West Russia. This is a type of fibre Pinus Spruce, processed as unbleached northern softwood kraft. Morton et al. (2010) physically describe the solombala pinus fibre with an average length of 2.7 mm, coarseness of 15.55 mg/100 m, wall thickness of 7.9 μm, and a fibre width of 30.7 μm.

3.3.1.2. Chemical analyse of Portland cement

The cement used in this study was the Brazilian Cauê brand ordinary Portland cement type OCP V-ARI (high initial strength), corresponding ASTM-C150, Type I, this kind of cement according to Santos et al. (2015) is selected for fibre reinforced cementitious composites, due the finer particle size and higher reactivity in comparison to other blended cements available in the Brazilian market. The OPC V-ARI was analyzed through LA-950 Laser Diffraction Particle

Size Distribution Analyzer, the result showed that 50% of the particles are finer than 8.67 μm. Oxide composition of the OPC V material was accomplished by X-ray fluorescence spectrometry. Table 8 shows these compositions. The oxide composition was investigated by a Philips PW 1410 type wavelength-dispersive X-ray fluorescence spectrometer controlled by Philips X31 version 2.13 software. X-rays are generated at 50 mA and 50 kV by X-ray tube with chromium anode.

3.3.1.3. Chemical analyse of Ground silica

The silica used in this work was crystalline ground silica with a real bulk density of 2.65 (g/cm^3) furnished by the Brazilian Mineração Jundu Ltda. The particle size distribution of the silica mineral addition showed that 50% of the particles are finer than 17.59 μm. Oxide composition of the silica material was accomplished by X-ray fluorescence spectrometry, as shown in Table 8. The Diffraction Particle Size Distribution Analyzer and X-ray fluorescence spectrometry were in the same equipment mentioned at 3.3.1.2.

Table 8 - Oxide compositions of the OPC and ground silica.

	CaO	MgO	SiO_2	Al_2O_3	Fe_2O_3	Na_2O	K_2O	SO_3	MnO	P_2O_5	TiO_2
*OPC V-ARI (% by mass)	63.433	2.715	16.823	3.421	2.468	0.442	1.189	6.032	0.065	0.144	0.64
**Silica (% by mass)	0.02	-	99.56	-	0.047	-	-	-	0.006	0.005	0.015

*Brazilian Cauê brand Portland Cement OPC-ARI (high initial strength), corresponding to ASTM-C150, Type I
**Brazilian Mineração Jundu brand silica quartz type

Source: authorships.

3.3.1.4. Fibre cement composite mix design

The materials used on the composite preparation with their respectively amounts, are shown in Table 9. The formulation is based on previous work carried out by Almeida et al. (2010). The dry mixture (by mass percent) is composed of 64% Brazilian Cauê brand ordinary Portland cement type PC V-ARI (high initial strength), corresponding to ASTM-C150, Type I, 28% Brazilian Mineração Jundu brand silica quartz type mineral addition, and 8.0% unrefined pine unbleached cellulosic pulp.

The fibre reinforced cement specimens were cast with the dimensions of 200 mm x 200 mm x 5 mm and approximate water/binder factor of 0.4. The specimens were produced using a slurry-dewatering process followed by a pressing technique, as simplified reproduction of the Hatschek process usually applied in the industrial production of commercial fibre cement (SAVASTANO et al., 2000).

Table 9 - Dry mixture (by mass percent) proportions of the composite

Raw material	Content (%)
Ordinary Portland cement (CP V-ARI)	64.0
Ground silica	28.0
Unbleached pine cellulosic pulp[a]	8.0
Total	**100.0**

a. Solombala Pulp/Paper Mill

Source: authorships.

3.3.2. Curing and conditioning regimes of stage 4

This experiment exposes the composite specimens to eight different curing and ageing conditions, which are summarized in Table 10. Close examination of the processes described in Table 10, reveals that it is possible to isolate the effect of hydration duration (10 h and 24 h); carbonation exposure (0 h or 10 h of curing in an environment with 20% CO_2 concentration); and, accelerated ageing cycles (0 cycles or 200 cycles).

3.3.2.1. Uncarbonated curing (UC) regime

After the samples were casted, some of them were stored in favorable conditions for hydration during 10 h (P-UC-10), and the others were stored in the favorable hydration conditions for 24 h (P-UC-24) in the Thermotron climate chamber, at temperature of 25°C and relative humidity (RH) of 90%. After that initial curing conditions, for both hydration durations, the settings of the Thermotron ESPEC environmental test chamber were 45°C temperature, 90% relative humidity (RH) and atmospheric CO_2 concentration (0.035 vol%) for 10 h. The specimens were then removed from the chamber and stored in thermal curing at temperature of 60°C and 90% relative humidity (RH), composites upon completing the thermal curing process of six days were subjected to the characterization tests (ROJAS et al., 2002).

3.3.2.2. Accelerated carbonation (AC) curing regime

After the samples were casted, some specimens were stored in the favorable hydration conditions for 10 h (P-AC-10) and the other group was stored in the hydration condition for 24 h (P-AC-24) in the Thermotron environmental test chamber, at temperature of 25°C relative humidity (RH) of 90%. Both sets of samples were then subjected to 10 h of accelerated carbonation in the ESPEC brand environmental test chamber at temperature of 45°C and relative humidity (RH) of 90%. The CO_2 content in the climate chamber was monitored to 20 vol%. The specimens were then removed from the chamber and stored in thermal curing at

temperature of 60°C and 90% relative humidity (RH), composites upon completing the thermal curing process of six days were subjected to the characterization tests (ROJAS et al., 2002).

3.3.2.3. Accelerated ageing: soak-dry cycles

The accelerated ageing test was conducted on four sets of samples which are two sets of specimens that had not undergone the carbonation curing regime, namely, P-UC-10-ACC and P-UC-24-AAC, and two sets of specimens that had been exposed to the 10 h carbonation curing, namely, P-AC-10-ACC and P-AC-24-AAC. The specimens were successively immersed into water at 20 ± 5°C for 170 min and, after 10 min, they were heated to the temperature of 60 ± 5°C for 170 min in a ventilated oven. Another interval of 10 min at room temperature elapses before the subsequent cycle, as recommended by the EN 494 Standards 1994. Each soak-dry set represents one cycle, which was repeated 200 times, or in other words, 200 ageing cycles (TONOLI et al., 2009; ALMEIDA et al., 2013).

Table 10 - Description of curing regimes

Curing Regime Identification	Hydration Duration in Chamber with: CO_2 = 0.035% Temp. = 25°C RH = 90%	Carbonation/Hydration Chamber with: Duration = 10 h Temp. = 45°C RH = 90%	Accelerated Soak & Dry Ageing Cycles
P-UC-10	10 h	CO_2 = 0.035%	0 cycles
P-UC-24	24 h	CO_2 = 0.035%	0 cycles
P-AC-10	10 h	CO_2 = 20%	0 cycles
P-AC-24	24 h	CO_2 = 20%	0 cycles
P-UC-10 - AAC	10 h	CO_2 = 0.035%	200 cycles
P-UC-24 - AAC	24 h	CO_2 = 0.035%	200 cycles
P-AC-10 - AAC	10 h	CO_2 = 20%	200 cycles
P-AC-24 - AAC	24 h	CO2 = 20%	200 cycles

Source: authorships.

Figure 14 – Carbonation and Hydration curing processes. a) Samples stored in climate chamber for initial hydration at 25ºC, 90% RH and atmospheric CO_2 concentration; b.) Samples stored in climatic test chamber at 45ºC, 90% RH for carbonation (with CO_2 20%) or hydration (atmospheric CO_2); c.) Before exposure to thermal curing,

water was sprayed for further hydration of the samples.

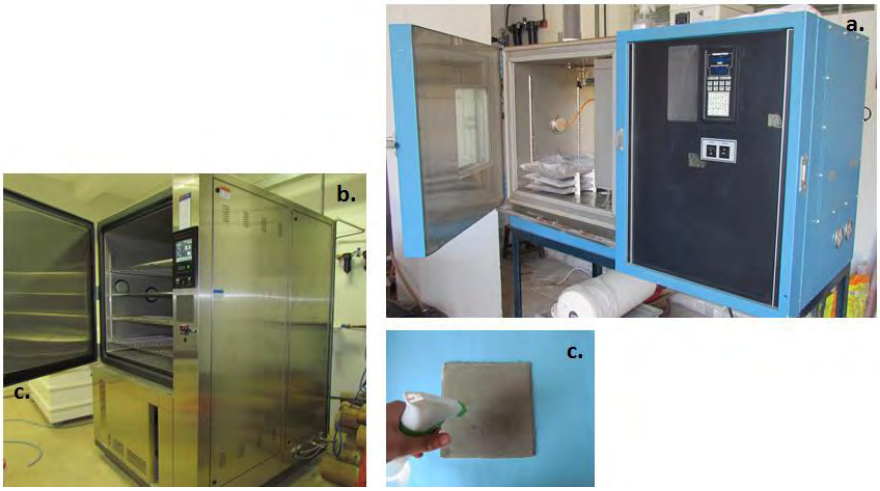

Source: authorships.

3.3.3. Test methods stage 4

3.3.3.1. Physical characterization of the fiber-cement composites

Apparent Void Volume (AVV), Bulk Density (BD), and Water Absorption (WA) of the composites were obtained from the average of eight test specimens (160 mm x 25 mm x 5 mm) for each condition, following the procedures specified by ASTM C 948-81 (2009). Physical properties were calculated by Eqs.4 to 6:

$$AVV\ (\%) = \left(\frac{M_{sat} - M_{dry}}{M_{sat} - M_i}\right) \times 100 \quad \text{(Eq. 4)}$$

$$BD\ (g/cm^{-3}) = \left(\frac{M_{dry}}{M_{sat} - M_i}\right) \times \rho \quad \text{(Eq. 5)}$$

$$WA\ (\%) = \left(\frac{M_{sat} - M_{dry}}{M_{dry}}\right) \times 100 \quad \text{(Eq. 6)}$$

where M_{sat} is the saturated with dry surface specimen's mass, M_{dry} is the dry specimen's mass after 24 h at 105ºC, M_i is the immersed in water specimen's mass and ρ is the water bulk density (g/cm^3)

3.3.3.2. Mechanical characterization of the fiber-cement composites

Mechanical properties were obtained for uncarbonated curing (UC), accelerated carbonated curing (AC) and composites upon completing the curing process of seven days. Each fiber cement specimen was wet cut into four samples measuring 160 mm x 25 mm for the mechanical test, using a water cooled diamond saw.

Eight specimens were evaluated for each condition; mechanical flexural tests were performed in an EMIC DL-30000 universal testing machine equipped with a 1 kN load cell, a four-point bending configuration, a lower span of 135 mm, an upper span of 45 mm and a deflection rate of 1.5 mm/min. The mechanical properties evaluated were: modulus of rupture (MOR), limit of proportionality (LOP), modulus of elasticity (MOE) and specific energy (SE). Mechanical properties were determined by Eqs. 7 to 10 as described in detail by (ALMEIDA et al., 2013; TONOLI et al., 2009).

$$MOR\ (MPa) = \frac{Pmax \cdot L_v}{b \cdot h^2} \quad \text{(Eq. 7)}$$

$$LOP\ (MPa) = \frac{Plop \cdot L_v}{b \cdot h^2} \quad \text{(Eq. 8)}$$

$$MOE\ (MPa) = \frac{276 \cdot L_v^3}{1296 \cdot b \cdot h^3} . m \quad \text{(Eq. 9)}$$

$$SE\ (kJ\ \cdot m^{-2}) = \left(\frac{Energy}{b \times h}\right) \quad \text{(Eq. 10)}$$

where P_{max} is the maximum load rate, P_{lop} is the load at the upper point of the linear portion of the load–deflection curve, L_v is the major span, width (b) and depth (h) and m is the tangent of the slope angle of the load vs. deflection plotting in the elastic behavior. SE was defined as the energy absorbed during the flexural test and divided by the specimen cross-sectional area (ALMEIDA et al., 2013; TONOLI et al., 2009).

3.3.3.3. Thermal analysis TG/DTG

The efficiency of the carbonation process for the eight sets of curing regimes, was studied through thermogravimetry analysis (TGA) and differential thermogravimetry analysis (DTG) (SATYANARAYANA, et al., 2009). The samples were ground using a pestle and mortar, sieved until particles smaller than 75 μm, then analyzed in a Thermogravimetric Analyzer with NETZSCH TASC 414/3 T6. Experimental test was performed in the temperature range of 20 to 900°C and rates of 10°C/min for heating and 40 mL/min of nitrogen injection (PIZZOL et al., 2014; ROSTAMI et al., 2012). Thermogravimetry analysis (TGA) and differential thermogravimetry (DTG) were used to inspect the nature of hydration and carbonate products formed in the cement-based systems. The different DTG peaks measured when hydrated cement was heated in the thermobalance correspond to:

- 100°C - weight loss due to the dehydration of water pores;
- 100 to 300°C - different stages of dehydration of C–S–H;

- 500°C - dehydroxylation of $Ca(OH)_2$;
- 700°C - decarbonation of $CaCO_3$.

The accelerated carbonation increased the mass loss at the range between 650 and 750°C related to decomposition of the poorly crystallized $CaCO_3$ and at the range between 750 and 850°C related to decomposition of the well-crystallized $CaCO_3$, as also reported elsewhere (ROSTAMI et al., 2012; PIZZOL et al., 2014).

3.3.3.4. FTIR Spectrometer analysis

The molecular identification of the composite of the eight sets of curing regimes, were studied through the diffuse reflection Fourier transform infrared spectroscopy. The vibrations of molecules were measured with a TENSOR 27 FTIR with an insert cell for diffuse reflection spectroscopy. The measurement range lies between 400 and 4,000 cm^{-1} with a nominal resolution of 2 cm^{-1}.

The DR-FTIR spectroscopy technique relies on the vibration modes of characteristic groups in a compound, i.e. not on the crystallinity of the sample. FTIR spectra of the uncarbonated and carbonated samples also confirm CO_3^2 from calcium carbonate polymorphs (between 850–890 cm^{-1} and 1400–1500 cm^{-1}), SO_4^2(between 900–1000 cm^{-1}) and OH- (between 3200–3500 cm^{-1}) groups from ettringite and S-rich phases. Thus DR-FTIR spectroscopy is a very suitable method for monitoring the formation of compounds such as carbonates in cement (YLMÉN et al., 2013).

3.3.3.5. Phases analysis X-Ray diffraction (XRD)

The crystalline phases identification of the composite of the eight sets of curing regimes, were studied through the X-Ray Diffraction (XRD). The phase identification and structural changes of the products was investigated by a Philips PW-1730 X-ray diffractometer (XRD) equipment. Peak position (2θ) with range 10-60°, the full-width at half maximum (FWHM), and area under peak (A) were obtained from the XRD spectra.

International Centre Diffraction Data (2003) and PANalytical HighScore Plus Inorganic Crystal Structure Database (2007) were applied to identify crystalline phases. The PANalytical HighScore Plus was also applied for a quantitative estimative of the clinker phases, considering only the crystalline part of the material and excluding the amorphous part.

3.3.3.6. Microstructural analysis by Scanning Electron Microscopy - (SEM)

Scanning electron microscopy (SEM) was applied with a back-scattered electron (BSE) image detector, operated at 15 kV accelerating voltage, for visualization of the microstructure on the surface of the composites. The images were captured by a JEOL machine, model 6610 LV. Magnification ranged from 300 up to 750x.

The preparation of specimens for BSE was accomplished with impregnation using epoxy resin. BSE samples were manually polished in a Struers TegraPol-11 machine using silicon carbide abrasive paper with sequential grit sizes 320, 600, 1000 for 6 min, using alcohol as lubricant. A final polishing was carried out using in turn 6, 3 and l µm diamond polishing compound during 6 min each size.

Around six SEM micrographs were obtained for each composite treatment and just the most relevant images of the microstructure observed were displayed in this manuscript. The energy-dispersive X-ray spectroscopy (EDS) analysis was carried out through Inca software.

3.3.3.7. Dynamic water vapor sorption- BET method

Dynamic vapor sorption (DVS) was also used to investigate the mesopore structure of the eight curing regimes composites. The dynamic vapor adsorption method is performed using a facility provided by Surface Measurement System Ltd. London, UK. Approximately 0.1 g of dry sample in small pieces was placed on a dish in the chamber in which the RH could be precisely and automatically controlled by mixing a proportional amount of nitrogen gas and moisture. The RH was then changed by step each time until the mass change was lower than 0.002% (by mass fraction, the same below) per minute until the target RH of 30% (LIWU AND PANESAR, 2014).

The Brunauer Emmett Teller BET method deduces the adsorption branch of an isotherm to provide an amount of the specific surface area of the inner pore area, an indication of overall porosity (International Union of Pure and Applied Chemistry, 1985). This measure, referred to as the BET specific surface area, is derived from the humidity content of the sample when a complete sorptive monolayer has formed. It is assumed that a complete monolayer is formed on all available inner surfaces prior to any multilayer condensation due to the difference between heats of adsorption and liquefaction of the adsorbent (BRUNAUER et al., 1938). The

BET specific surface area, ABET, is calculated as (COLLETT et al., 2008; PANESAR et al., 2014):

$$A_{BET} = \sigma_m N \frac{w_m}{M_m} \quad \text{(Eq. 13)}$$

where σ_m is the surface area of an adsorbed molecule of water (10 Å$_2$), N is Avogadro's number (6.023×10^{23}), w_m is the moisture content at monolayer saturation (kg/kg), and M_m is the molar mass of water (18.07 g/mol) (BRUNAUER et al., 1938).

3.4. Stage 5: Evolution of the hydration kinetics on unbleached cellulose pulp fiber-cement composites subjected to accelerated carbonation at very early age

The aim of stage 5 is to study the carbonation kinetic hydration at very early age on unbleached pines cellulose pulp fiber-cement composites using silica as a mineral addition. For this study, samples were prepared by the slurry-dewatering and pressing technique. The carbonation process was monitored along 10 h, each hour corresponds to a condition. A variety of analytical test methods was used to assess the hydration kinetics, the chemical implications in the composites; between them: X-ray diffraction (XRD), thermogravimetric analysis (TG and DTG), Infrared spectrometer (FTIR) and scanning electron microscopy (SEM).

3.4.1. Materials and mix design stage 5

3.4.1.1. Vegetable fibre

Unrefined pine unbleached cellulosic pulp was used in this study. The fiber is produced by the OJSC Solombala Pulp and Paper Mill - brand located in the industrial zone of the city of Arkhangelsk, in North-West Russia. This is a type of fibre Pine Spruce, processed as unbleached northern softwood kraft. Morton et al. (2010) physically describe the Solombala pinus fibre with an average length of 2.7 mm, coarseness of 15.55 mg/100 m, wall thickness of 7.9 μm, and a fibre width of 30.7 μm.

3.4.1.2. Chemical analyse of Portland Cement

The cement used in this study was the Brazilian Cauê brand ordinary Portland cement type OCP V-ARI (high initial strength), corresponding to the ASTM-C150, Type I. According to Santos et al. (2015), this type of cement is selected for fibre reinforced cementitious composites, due to the finer particle size and higher reactivity in comparison to other blended cements available in the Brazilian market. The OPC type V-ARI is well known to be high sulfate resistant, as the chemical reaction between cement compounds and sulfates causes undesirable expansion of the

mixture. The OPC was characterized through LA-950 Laser Diffraction Particle Size Distribution Analyzer, and the results show that 50% of the particles are finer than 8.67 μm.

3.4.1.3. Chemical analyse of Ground silica

Silica quartz type is a neutral material, chemically and thermodynamically very stable at low temperatures (e.g. 45°C) and atmospheric pressure. This material could be used as mineral addition in carbonated cementitious composites for avoiding interference with the main crystalline phases formed along the accelerated carbonation process (FOURNIER AND ROWE, 1977; SINGH et al. 2013).

The crystalline silica used in this work was supported by Brazilian Mineração Jundu with a real density of 2.65 (g/cm^3). The particle size distribution of the silica mineral addition shows that 50% of the particles are finer than 17.6 μm.

3.4.1.4. Fibre cement composite mix design

The raw materials with their respective amount, used on the fiber-cement composites are shown in Table 11. The formulation is based on previous work carried out by Almeida et al. (2010). The dry mixture (by mass percent) is composed of 64% Brazilian Cauê brand ordinary Portland cement type OPC V-ARI (high initial strength), corresponding to ASTM-C150, Type I (PICANÇO et al., 2008), 28% Brazilian Mineração Jundu brand silica quartz type mineral addition, and 8% unrefined pine unbleached cellulosic pulp.

The fibre reinforced cement specimens were cast with the dimensions of 200 mm x 200 mm x 5 mm and mean water/binder factor of 0.40. The specimens were elaborated using a slurry-dewatering process followed by a pressing technique, as a simplified reproduction of the Hatschek process used in the industrial production of fibre cement (SAVASTANO et al., 2000).

Table 11 - Dry mixture proportions (% by mass) of the composite

Raw material	Mass (%)
Ordinary Portland cement (CP V-ARI)	64.0
Silica	28.0
Unbleached pine cellulosic pulp[a]	8.0
Total	**100.0**

a. Solombala Pulp/Paper Mill

Source: authorships.

3.4.2. Curing and conditioning regimes of stage 5

This experiment exposes the composite specimens to eleven different curing conditions, which are summarized in Table 12 and the curing process shows at Figure 15. Close examination of the processes described in Table 12 reveals that it is possible to isolate the effect of hydration duration (10 h and 24 h) and carbonation exposure (from 0 h up to 10 h of curing in an environment with 20% CO_2 concentration).

3.4.2.1. Accelerated carbonation (AC) curing regime

After preparation, the samples were stored in the chamber for initial hydration condition for 24h at climatic test chamber at 25°C and relative humidity (RH) of 90% (Figure 15 - a.). Then they were removed from the chamber and each fibre-cement specimen was cut into four samples measuring 100 mm by 50 mm (Figure 15 - c.). All samples were introduced at the same time in the climate chamber for the accelerated carbonation at 45°C and relative humidity (RH) of 90%. The CO_2 content in the climate chamber was monitored to be 20 vol%. One hour after the initiation of the carbonation process, two cut samples were removed from the chamber, then immersed in acetone, in order to stop the hydration; this process was repeated until the completion of the 10 conditions corresponding to each hour of carbonation process along 10 h. The samples were monitored during carbonation process using phenolphthalein indicator. For each hour of carbonation, small pieces of the specimens were removed for checking the status of the internal region of the cross section, according to the intensity of the color displayed by the indicator (Figure 15 - d.). Table 12 shows the description of curing regimes applied.

Figure 15 - Study of the hydration kinetic of accelerated carbonation along 10 h. a.) Specimens at climatic test chamber; b.) Cut of the samples; and c.) Monitoring with phenolphthalein indicator during carbonation process along 10 h.

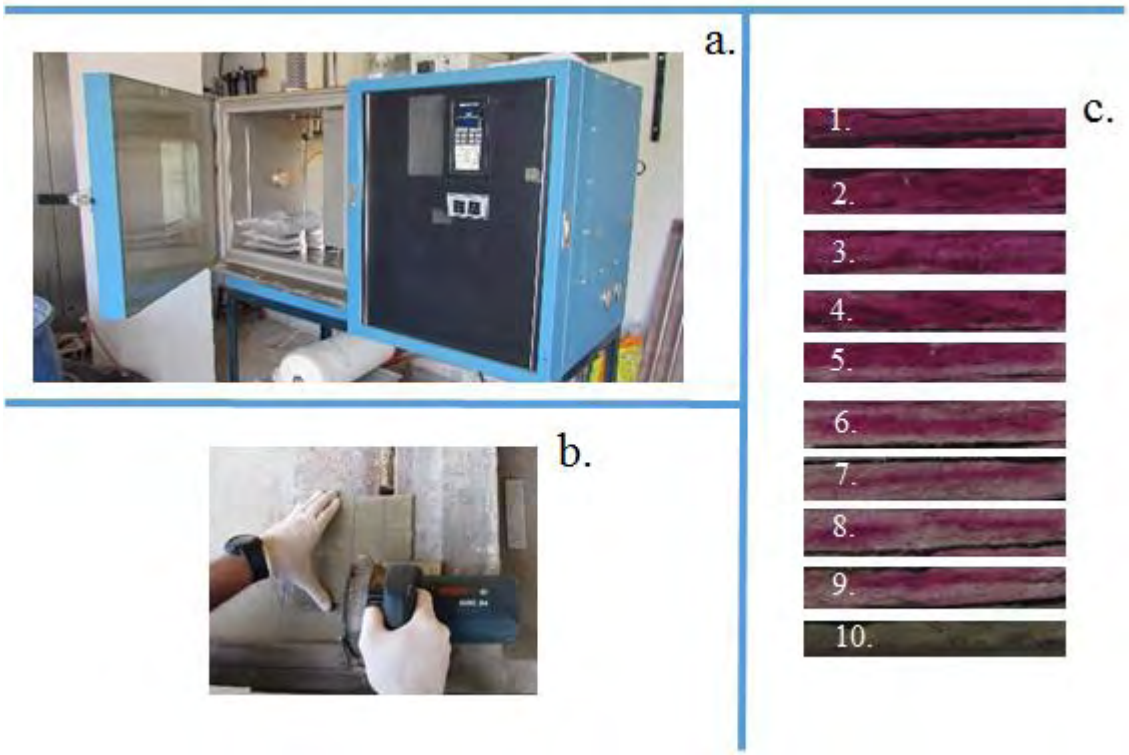

Source: authorships.

Table 12 - Description of the curing regimes.

Curing Regime Identification	Hydration Duration in Chamber with: CO_2 = 0.035% Temp. = 25°C RH = 90%	Carbonation Duration in Chamber with: CO_2 = 20% Temp. = 45°C RH = 90%
P-AC-24 - 0 h	24 h	0 h
P-AC-24 - 1 h	24 h	1 h
P-AC-24 - 2 h	24 h	2 h
P-AC-24 - 3 h	24 h	3 h
P-AC-24 - 4 h	24 h	4 h
P-AC-24 - 5 h	24 h	5 h
P-AC-24 - 6 h	24 h	6 h
P-AC-24 - 7 h	24 h	7 h
P-AC-24 - 8 h	24 h	8 h
P-AC-24 - 9 h	24 h	9 h
P-AC-24 - 10 h	24 h	10 h

Source: authorships.

3.4.3. Test methods of stage 5

3.4.3.1. Thermal analysis DTA/TGA

The efficiency of carbonation process for the eleven sets of curing regimes, was studied through the differential thermal analysis (DTA) and thermogravimetry analysis (TG) (SATYANARAYANA, et al., 2009). The samples were ground using a pestle and mortar, sieved until particles smaller than 75 μm, then analyzed in a Thermogravimetric Analyzer with NETZSCH TASC 414/3 T6. Equipment was used in a temperature range of 20 to 900°C and rates of 10°C/min for heating and 40 mL/min for nitrogen injection (PIZZOL et al., 2014; ROSTAMI et al., 2012).

For the uncarbonated samples there is one clear endothermic peak at 460°C which matches with $Ca(OH)_2$. For the carbonated samples, there is also a clear endothermic peak at 800°C corresponding to $CaCO_3$ (SKOOG et al., 1994; LIWU et al., 2012). Therefore, the accelerated carbonation increased the mass loss at the range between 650 and 750°C related to decomposition of the poorly crystallized $CaCO_3$ and at the range between 750 and 850°C related to decomposition of the well-crystallized $CaCO_3$, as also reported by (ROSTAMI et al., 2012; PIZZOL et al., 2014).

3.4.3.2. Phases analysis X-Ray diffraction (XRD)

The crystalline phases identification of the composite of the eleven sets of curing regimes, were studied through the X-Ray Diffraction (XRD). The phase identification and structural changes of the products were investigated by a Philips PW-1730 X-ray diffractometer (XRD). Peak position (2θ) with range 10-60°, the full-width at half maximum (FWHM), and the area under peak (A) were obtained from the XRD spectra.

International Centre Diffraction Data (2003) and PANalytical HighScore Plus Inorganic Crystal Structure Database (2007) were applied to identify crystalline phases.

3.4.3.3. Chemical analysis FTIR spectrometer

The molecular identification of the composite of the eleven sets of curing regimes, were studied through the diffuse reflection Fourier transform infrared spectroscopy (DR-FTIR) with a TENSOR 27 FTIR with an insert cell for diffuse reflection spectroscopy. The measurement range lies between 400 and 4,000 cm^{-1} with a nominal resolution of 2 cm^{-1}.

The DR-FTIR spectroscopy technique relies on the vibration modes of characteristic groups in a compound, i.e. not on the crystallinity of the sample. FTIR spectra of the uncarbonated and

carbonated samples also confirm CO_3^2 from calcium carbonate polymorphs (between 850–890 cm^{-1} and 1400–1500 cm^{-1}), SO_4^2(between 900–1000 cm^{-1}) and OH- (between 3200–3500 cm^{-1}) groups from ettringite and S-rich phases. Thus DR-FTIR spectroscopy is a very suitable method for monitoring the formation of compounds such as carbonates in cement (YLMÉN et al.,2013).

3.4.3.4. Microstructural analysis by Scanning Electron Microscopy - (SEM)

Scanning electron microscopy (SEM) was used with a back-scattered electron image (BSEI) detector, operated at 15 kV accelerating voltage, for visualization of the microstructure on the polished surface of the composites. The images were captured by a JEOL machine, model 6610 LV. Magnification ranged 300 times.

The preparation of specimens for BSEI SEM was accomplished with impregnation using epoxy resin. BSEI samples were manually polished in a Struers TegraPol-11 machine using silicon carbide abrasive paper with sequential grit sizes 320, 600, 1000 for 6 min, using alcohol as lubricant. A final polishing was carried out using in turn 6, 3, l µm diamond polishing compound during 6 min each size.

Around six SEM micrographs were obtained for each composite treatment and just the most relevant images of the microstructure observed were used in this manuscript.

4. RESULTS AND DISCUSSIONS

4.1. Stage 2: Definition of optional parameters for supercritical carbonation process of vegetable Fiber-cement composites at a very early age

4.1.1. Mechanical and physical characteristics of stage 2

Table 13 presents a summary of the average values and corresponding standard deviation of the physical properties (AVV, BD and WA) and mechanical properties (MOR, LOP, MOE and SE), under flexural loading respectively for all curing scenarios.

The curing conditions were conducted on eight sets of samples which were three sets reinforced with unbleached eucalyptus pulp and five sets reinforced with bleached eucalyptus pulp. For both types of reinforcing pulp, the effect of supercritical carbonation exposure was studied (0 h, 1 h or 2 h of curing in an environment with close 100% CO_2 concentration); for the set of unbleached pulp the effect of thermal hydration duration was studied (24 h and 48 h); and for bleached pulp samples the effect of accelerated ageing cycles was studied (0 and 200 soak and dry cycles). A summary of the statistical significance testing is presented in Table 14 for the physical and mechanical properties. A '0' in the table averages that there is no statistically significant difference between the averages, '+' indicates that there is a statistically significant difference between the means with the first listed condition having higher averages than the second, and '-' indicates the first listed condition had a lower mean than the second. E.g. for the AVV column of UB vs. UB-SC-48-2, the '+' indicates that the averages AVV of UB was greater than that of UB-SC-48-2, whereas the '-' in the BD column indicates the UB samples had a lower average BD than the UB-SC-48-2 samples.

Table 13 - Physical and mechanical properties of specimens exposed to various curing regimes (average ± standard of deviation).

Curing Regime Identification	**AVV (%)**	**BD (g/cm^3)**	**WA (%)**	**MOR (MPa)**	**LOP (MPa)**	**MOE (GPa)**	**SE (J/m2)**
UB	34.36 (1.4)	1.41 (0.03)	24.48 (1.6)	7.49 (1.4)	3.15 (0.8)	7.718 (0.8)	3.22 (1.5)
UB-SC-48-2	30.80 (0.5)	1.61 (0.03)	19.10 (0.4)	12.83 (2.8)	6.59 (0.7)	10.676 (1.7)	2.57 (0.7)
UB-SC-24-2	33.10 (0.3)	1.61 (0.02)	20.57 (0.4)	11.27 (2.2)	5.85 (1.1)	10.446 (1.4)	2.54 (0.8)
B	34.79 (0.6)	1.49 (0.02)	23.35 (0.7)	8.97 (0.6)	4.23 (2.1)	8.559 (0.9)	2.30 (1.1)
B-SC-48-1	31.50 (0.4)	1.68 (0.02)	18.78 (0.4)	15.79 (2.4)	7.91 (1.1)	13.711 (1.13)	3.28 (1.1)
B-SC-48-2	30.20 (0.6)	1.69 (0.02)	17.92 (0.03)	16.94 (2.0)	8.73 (0.7)	14.758 (1.2)	3.42 (0.9)
B-AAC	30.28 (2.8)	1.52 (0.04)	19.94 (5.8)	7.20 (2.5)	6.03 (1.7)	11102.67 (1.5)	0.34 (0.2)
B-SC-48-2-AAC	28.78 (1.3)	1.76 (0.03)	16.40 (4.6)	12.09 (2.5)	7.52 (1.6)	17269.83 (1.5)	1.27 (0.7)

Source: authorships.

Table 14 - Statistically Significance of the Difference between the average of stage one (at 95% confidence level)

Experimental Variable	Comparison of average between Curing Regimes:	AVV (%)	BD (g/cm^3)	WA (%)	MOR (MPa)	LOP (MPa)	MOE (MPa)	SE (J/m^2)
Carbonation	UB vs. UB-SC-48-2	+	-	+	-	-	-	0
Carbonation	UB vs. UB-SC-24-2	0	-	+	-	-	-	0
Carbonation	B vs. B-SC-48-1	+	-	+	-	-	-	-
Carbonation	B vs. B-SC-48-2	+	-	+	-	-	-	-
Carbonation	B-AAC vs. B-SC-48-2-AAC	0	-	+	-	0	-	-
Hydration time	UB-SC-48-2 vs. UB-SC-24-2	-	0	0	0	0	0	0
Carbonation time	B-SC-48-1 vs. B-SC-48-2	+	0	+	0	0	0	0
Cellulosic Pulp	UB vs. B	0	-	0	-	-	0	0
Cellulosic Pulp	UB-SC-48-2 vs. B-SC-48-2	0	+	0	-	-	-	-
Ageing cycles	B vs. B-AAC	+	0	+	+	0	-	+
Ageing cycles	B-SC-48-2 vs. B-SC-48-2-AAC	+	-	+	+		-	+

* 0 no statistically significant difference between the average

** + statistically significant difference with a higher average for the first listed regime

*** - statistically significant difference with a lower average for the first listed regime

Source: authorships.

The effect of Exposure to Carbonation Curing: The supercritical carbonation at early stages in the curing process resulted in many improvements to the mechanical properties of cement composites, reinforced with both bleached and unbleached eucalyptus pulp. Between samples UB vs. UB-SC-48-2, UB vs. UB-SC-24-2, B vs. B-SC-48-1, B vs. B-SC-48-2, and B-AAC vs B-SC-48-2-AAC, the statistically significant difference shows that carbonation had an effect on specimen's bulk density, water absorption, and modulus of elasticity.

Almeida et al. (2013) studied cement based specimens reinforced with eucalyptus cellulosic pulp subjected to accelerated carbonation curing (AC) with similar mechanical behavior. There is also a noticeable improvement to the flexural toughness of sisal and eucalyptus cellulosic pulp fiber-reinforced cement composites as a result of the supercritical carbonation curing (SANTOS et al., 2015). In these previous studies, the mechanical improvement was attributed to the elimination of calcium hydroxide due to the carbonation treatment (PIZZOL et al., 2014).

The production of calcium carbonate during carbonation results in a better connected cement fiber matrix with fewer voids, responsible for the added strength and stiffness of the material. Observations showed that the major product formed for supercritically carbonated samples was calcium carbonate (Calcite). This product fills the voids in the cement matrix increasing bulk density, stiffness and strength, while decreasing the apparent void volume (AVV); these effects are a result of calcium carbonate's higher density than calcium hydroxide.

The effect of Hydration time: Samples UB-SC-48-2 vs. UB-SC-24-2 compared the effect of increasing the thermal hydration time from 24 h to 48 h, the statistically significant difference shows that the change had no effect on specimen's bulk density, water adsorption, modulus of rupture, modulus of elasticity or specific energy. So, it would seem the initial 24 h of thermal curing yields a substantial amount of hydration products, enough so as to not limit the carbonation process, because once carbon dioxide dissolves and reacts with hydration products (CH and C–S–H) or with anhydrous phases (C_3S and C_2S), it forms $CaCO_3$ by the combination of moist CO_2 with Ca^{2+} (FERNANADEZ-BERTOS et al., 2004; ROSTAMI et al., 2012; ALMEIDA et al., 2013).

However, the AVV was affected, a short thermal hydration time (24 h) resulted in a higher AVV for UB-SC-24-2. The difference of AVV is due to the progression of the hydration process (TONOLI et al., 2009). There are many aspects that can influence the reaction kinetics and the amounts of the hydrated phases produced (MURAT, 1983; TAHA et al., 1985; SILVA et al.,

1990). The most important one is the curing temperature, because it influences the stability and the transformation of the hydrates (ROJAS et al., 2002). The AVV values decreased with longer durations of thermal curing (between UB-SC-48-2 and UB-SC-24-2).

The effect of Carbonation time: Samples B-SC-48-1 vs. B-SC-48-2, compared the effect of decreasing the carbonation time from 2 h to 1 h, the statistically significant difference shows that the variation had no effect on specimen's bulk density, modulus of rupture, modulus of elasticity and specific energy. Santos et al. (2015) proposed 2 h for the whole accelerated supercritical carbonation process, the first hour to reach the equilibrium treatment and the second hour to extend the treatment after achieving the equilibrium treatment conditions. Due to the negligible difference between 1 h and 2 h (Table 14), it would appear that for guaranteed improvement to the mechanical properties of the composites, the accelerated supercritical carbonation process can be 1 h of treatment, the first hour when equilibrium conditions are reached.

The effect of cellulosic Pulp: Samples created with the unbleached pulp had lower average values of mechanical properties than their bleached pulp counterparts having undergone the same curing process, as shown in Figure 16 which describes the typical stress x strain curves of the two kinds of composites. The comparison between carbonated samples UB-SC-48-2 vs. B-SC-48-2 resulted in average values of MOR, LOP, MOE, and SE that were 24%, 24%, 27% and 25% higher for the bleached pulp samples. This is due in part to the lignin content difference between the types of fibers. The bleached cellulose fiber used in this study was subjected to an oxygen delignification process (MANOIR et al., 1993), which is a removal of: 92-95% of lignin from wood, the residual lignin (hexenuronic acid groups and extractives), and a destruction of chromophores (SJÖSTRÖM, 1993; DENCE AND REEVE, 1996), which are the amorphous components of the fiber (DENCE AND REEVE, 1996; CORREIA et al., 2016). The bleached fibers with higher crystallinity and lower amounts of phenolic polymer, resulted in an increased stiffness and embrittlement of the fiber (WEI AND MEYER, 2015). This argument is reiterated by numerous authors with similar results, that the degree of crystallinity influences the physical and mechanical properties of the fibers (STURCOVA et al, 2005), particularly the elastic modulus (CHEN et al., 2012). Also, inside microfibrils of the pulp the cellulose networks could have an organized structure and increased crystallinity (CORREIA et al., 2014). The degree of crystallinity and the organized structure could be influence the effect of carbonation process in bleached pulp fiber-cement composite with higher tensile strength, void content and interfacial adhesion of the composite.

The amorphous regions in cellulose are weaker due to hydrophobic properties, reagent attacks and the enzymes, this requires investigations on the use of amorphous samples, understanding the thermal, chemical and mechanical behavior in crystal regions (LENGOWSKI et al., 2013). When vegetal fibers are exposed to chemical treatments that result in significant hydrolysis, oxidation, dehydration reactions, etc. (SAHA et al., 2012; PITARELO, 2013) or mechanical treatments, the crystallinity of cellulose could be altered (MEJIA et al., 2015). In alkaline cementitious matrices, the amorphous regions protect the fiber from the attack, but when the pH of the composite is reduced, the amorphous areas do not work as well as those of a fiber that has a higher crystallinity. Which average the degree of crystallinity of the natural fiber influences the improvement of the mechanical behavior of a cementitious composite subjected to carbonation.

The comparison between uncarbonated samples UB vs. B indicated the toughness and Bulk Density of B was statistically higher than that of UB. The B samples tended to have higher bulk density, but lower AVV and WA than the UB samples. Alkaline attacks occur in both types of samples, resulting in mineralization that is caused by diffusion and precipitation of minerals rich in Ca. The literature indicates that the lignin, hemicelluloses, and pectin act as chemical and physical walls to the penetration of Ca^{2+} ions into the fibers (TONOLI et al., 2010). The bleached pulp has higher crystallinity and fewer amorphous components, which resulted on a stronger fiber-cement interface and a fewer barriers to the precipitation of Ca^{2+} ions, it other words the mineralization process.

Effect of Accelerating Ageing Cycles: The superior performance of carbonated samples persisted after 200 cycles of accelerated aging, with MOE of B-SC-48-2-AAC and B-AAC samples presenting 17% to 30% higher average values than aged B-SC-48-2 and B samples. Additionally, after accelerated aging, the average values of specific energy for the carbonated and uncarbonated composites decreased approximately 62% and 87%, respectively. Figure 17 shows typical stress x strain curves during flexural tests of the composites reinforced with bleached pulp before and after accelerated ageing cycles.

The physical properties of accelerated aging cycles were similar to those of the carbonation process, but with milder changes in bulk density which only increased by 5% after aging. This is a result of the aging process, during which CO_2 causes the precipitation of calcium carbonate, but also because of the greater duration over which hydration can occur and produce hydration products that fill the cement-fiber matrix.

The supercritical carbonation treatment helped diminish the annihilation of macromolecular chains during the partial alkaline hydrolysis of the cellulose, which causes their rupture and the consequent reduction to the degree of polymerization. During soak and dry cycles, the fibers' natural degradation occurs as the movement of the pore water towards the surface of the fibers is facilitated (SANTOS et al., 2015).

Figure 16 - Typical stress x strain curves during flexure tests of the composites reinforced with unbleached and bleached pulp.

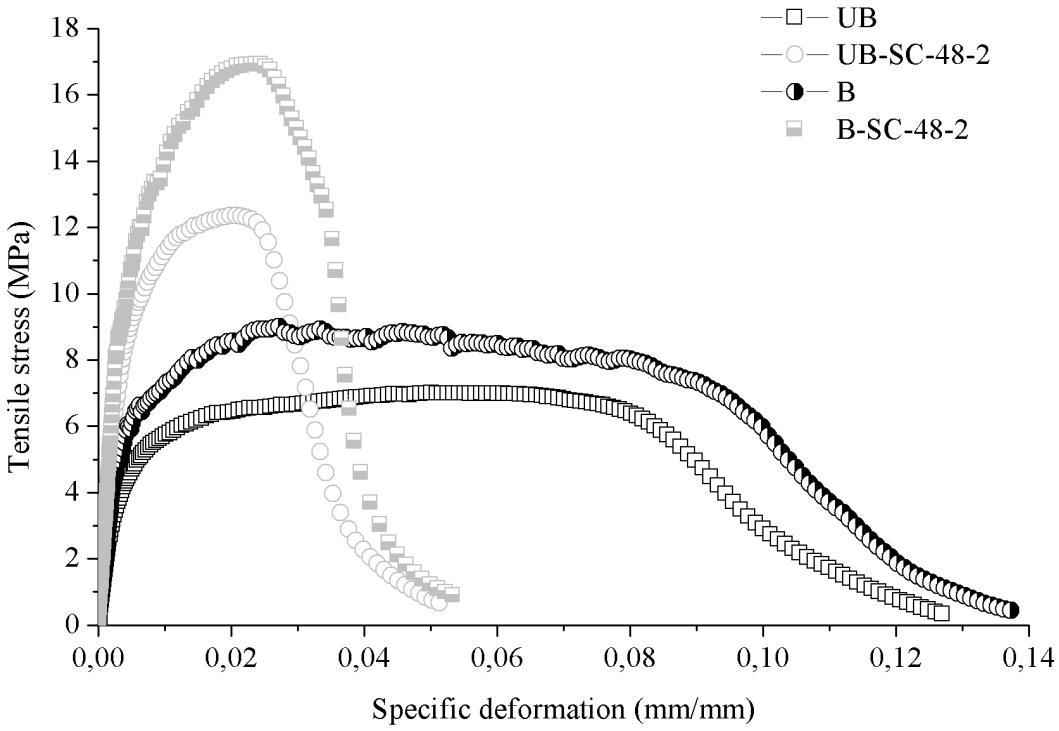

Source: authorships.

Figure 17 - Typical stress x strain curves during flexure tests of the composites reinforced with bleached pulp before and after accelerated ageing cycles.

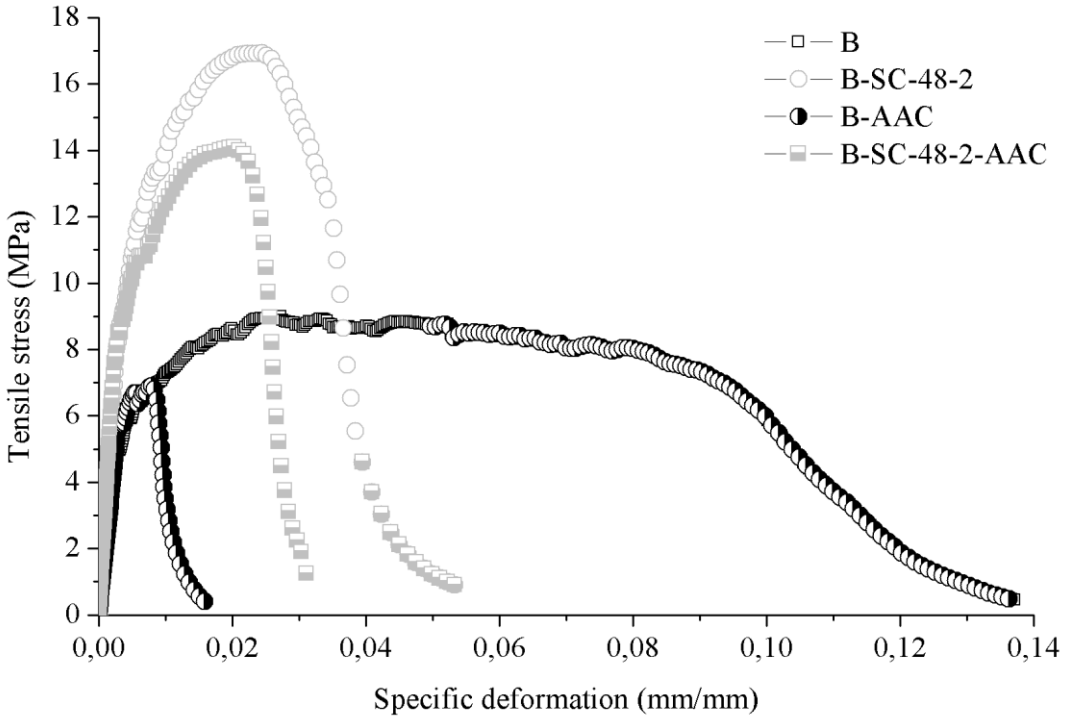

Source: authorships.

4.1.2. Thermogravimetric analysis

Figure 18 depicts the mass loss (TG) and differential mass loss (DTG) of the different curing processes. The changes in the mass loss between 90 and 200°C corresponds to the C–S–H, ettringite (Aft), monosulfoaluminate (AFm) and monocarboaluminate (Mc). The mass loss in the range of 200 to 420°C corresponds to C_3A and C_4AF hydration products (RAMACHANDRAN et al., 2001; SHA et al., 1999). Moreover, if water is more determinedly bonded in the C–S–H, it is even likely that some C–S–H dehydration will occur up to 300°C (RAMACHANDRAN et al., 1971). The most important hydration product of cement based materials is calcium silicate hydrate (C–S–H) gel (SANTOS et al., 2015; JENNINGS et al., 2008; CHEN et al.,2004). The solid phase containing Ca^{2+} also contributes to calcite formation (GARCIA-GONZALEZ et al., 2008), promoted by the accelerated carbonation through the adsorption of the CO_2 by the cementitious matrix, as was also observed by Pizzol et al. (2014) and Almeida et al. (2013) under different curing conditions.

The researchers Bentur and Mindess (2007) noted that the cellulose phase in fiber-cement composites can be detected in the temperature interval between 295 and 370°C, corresponding to the degradation of the cellulose fibers. Figure 18 shows peaks at 340°C for UB and B samples, and at 350°C for UB-SC-48-2 and B-SC-48-2. For AAC samples it is possible to see an increase to mass loss at 360°C for B-AAC and B-SC-48-2-AAC conditions when compared to unaged samples, indicating the degradation of the cellulose fibers due to exposure to aged cycles.

Figure 18 – DTG results of the fiber-cement composites with different curing conditions of (a) unbleached samples and (b) bleached samples.

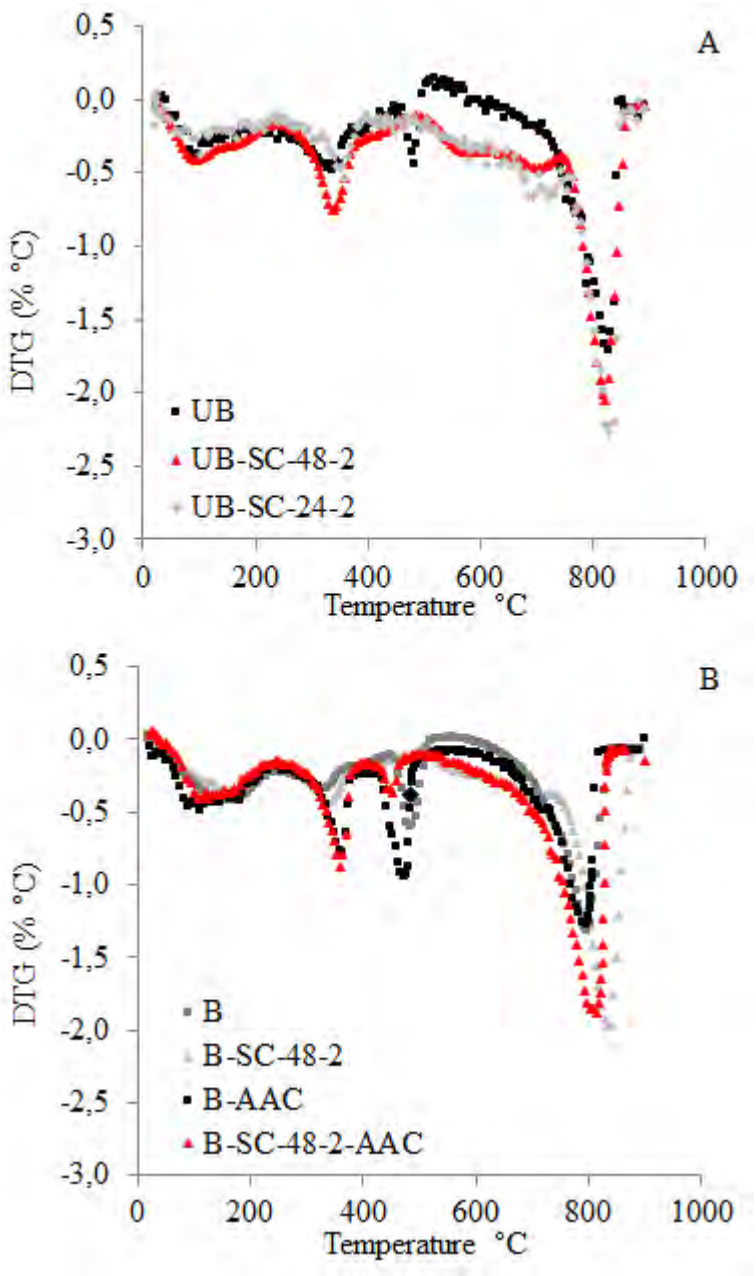

Source: authorships.

According to Shaaban (1991), approximately 30% of $Ca(OH)_2$ has potential to be carbonated during CO_2 exposure in controlled environmental chambers. The estimated amount of mass loss of calcium hydroxide $Ca(OH)_2$ (CH) and calcium carbonate $CaCO_3$ (CC) is calculated following the procedure proposed by Borges et al. (2010) using the equations (14) and (15), which, considering increased molecular mass resulting from the carbonation process, as shown

in Table 15, would suggest an increase to the percentage of mass lost, confirmed in the thermogravimetric data (DTG) presented in Figure 18. Dehydroxylation, L1, occurs between 450 and 500°C, the mass loss in this range decreases as the carbonation exposure time increases, and decarbonation losses, L2, occurs between 600–750°C. The initial amount of $Ca(OH)_2$ may be directly calculated from Eq. (16). The corresponding amount of $CaCO_3$ resulting from the total $Ca(OH)_2$ that carbonated was estimated using Eq. (17).

$$\%CH = L1 \cdot \frac{74}{18} = 4.11 \cdot L1 \quad \text{(Eq. 14)}$$

$$\%CC = L2 \cdot \frac{100}{44} = 2.27 \cdot L2 \quad \text{(Eq. 15)}$$

$$\%CH_{\,\text{Initial}} = \%CH + (0.74 \cdot \%CC) \quad \text{(Eq. 16)}$$

$$\%CC = 1.35 \cdot \%CH \quad \text{(Eq. 17)}$$

Table 15 - Molecular Mass weight reagents

Reagent	**Molecular Mass (g/mol)**
$Ca(OH)_{2(solid)}$	74.09
$CaCO_{3(solid)}$	100.08
$CaO_{(solid)}$	56.07
H_2O	18.00

Source: (BORGES et al., 2010)

Table 16 - The estimation of the extent of carbonation of C‑S‑H from TGA data, before and after supercritical carbonation treatment, non-aged and aged.

Curing Regimes	**Uncarbonated composite**			**Curing Regimes**	**Carbonated composite**				
	CH from TGA (%)	CC from TGA (%)	Calculation of initial CH (%)		CH from TGA (%)	CC from TGA (%)	Amount carbonated of CH (%)	Expected CC from carbonating CH (%)	Carbonates formed by C–S–H (%)
UB	5.6	28.01	26.40	UB-SC-48-2	1.5	38.1	24.9	33.6	4.4
				UB-SC-24-2	1.6	43.7	24.7	33.4	10.3
B	12.6	27.7	23.6	B-SC-48-1	2.05	42.2	21.5	29.1	13.11
				B-SC-48-2	0.57	41.6	23.0	31.1	10.5
B-AAC	15.7	23.85	21.47	B-SC-48-2-AAC	4.5	36.2	16.9	22.8	13.3

Source: authorships.

Table 16 presents the estimated % $Ca(OH)_2$ and % $CaCO_3$ between the uncarbonated and carbonated conditions with different parameters. It is apparent that the effect of hydration time, the effect of carbonation exposure, and the effect of the cellulose pulp, did not influence the $Ca(OH)_2$ and $CaCO_3$ formation.

For the specimen submitted to 200 accelerated soak and dry aging cycles and carbonation (B-SC-48-2-AAC), the results suggest an increase of calcium hydroxide and reduction of calcium carbonate compared with non-aged and carbonated samples (B-SC-48-2), for example at 476°C (Figure 18b) it is possible to estimate the amounts of $Ca(OH)_2$ to be 4.5% and 0.57%, respectively. On the other hand, at 830°C estimated amounts of $CaCO_3$ for the same conditions were 36,11% and 41,58%. This could be attributed to progress of hydration process of the cement.

Hence, the supercritical accelerated carbonation increased the mass loss between 650 and 750°C related to the decomposition of poorly crystalized $CaCO_3$, as well as between 750 and 850°C related to the decomposition of well-crystalized $CaCO_3$, as reported by Rostami et al. (2012) and Pizzol et al. (2014). In all samples subjected to the carbonation regime, weight loss was observed at approx. 800°C which represents well-crystallized $CaCO_3$.

According to Alvarez and Abanades (2005), the carbonation process of calcium hydroxide can generate carbonate polymorphs to be oxidized in the same temperature range, which explains the presence of a large peak around 830°C.

4.1.3. X-ray diffraction analysis

The XRD results shown in Figure 19 present the patterns for the eight sets of curing regimes. Calcium carbonate ($CaCO_3$) is the main mineralogical phase observed and the second phase is calcium hydroxide ($Ca(OH)_2$).

Four phases of calcium carbonate occur with increasing stability, amorphous calcium carbonate, vaterite, aragonite, and calcite (BLACK et al., 2007). In Figure 19, it is possible to observe the increase of the peak at $2\theta = 29.5°$ in supercritically carbonated samples (UB-SC-48-2, UB-SC-24-2, B-SC-48-1, B-SC-48-2 and B-SC-48-2-AAC). This corresponds to $CaCO_3$ in the form of calcite (HUNNICUT, 2013), this increase is due to the primary reaction process of CO_2 that dissolves into the matrix and reacts with hydration products, such as calcium hydroxide (CH) and calcium silicate hydrate (C–S–H), and also reacts with polymerized silica gel leading to secondary carbonation.

Figure 19 compares the uncarbonated samples (UB, B and B-AAC) vs supercritical carbonated samples (UB-SC-48-2, UB-SC-24-2, B-SC-48-1, B-SC-48-2 and B-SC-48-2-AAC), there is a noticeable reduction of portlandite (around $2\theta = 18°$ or 35°) according to Pizzol et al. (2014)

and Santos et al. (2015). The carbonation reactions and effects are the same as those described in the previous section for bleached and unbleached pulp samples.

International Centre Diffraction Data (2003) and PANalytical HighScore Plus Inorganic Crystal Structure Database (2007) were applied to identify crystalline phases. The PANalytical HighScore Plus was used too for made a quantification estimative of the clinker phases, considering only the crystalline part of the material and excluding the amorphous part.

Figure 19 – XRD patterns for UB, UB-SC-48-2, UB-SC-24-2, B, B-SC-48-1, B-SC-48-2, B-AAC and B-SC-48-2-AAC. Their respective peaks associated with CH disappeared after supercritical carbonation treatment. Cu Kα radiation was used.

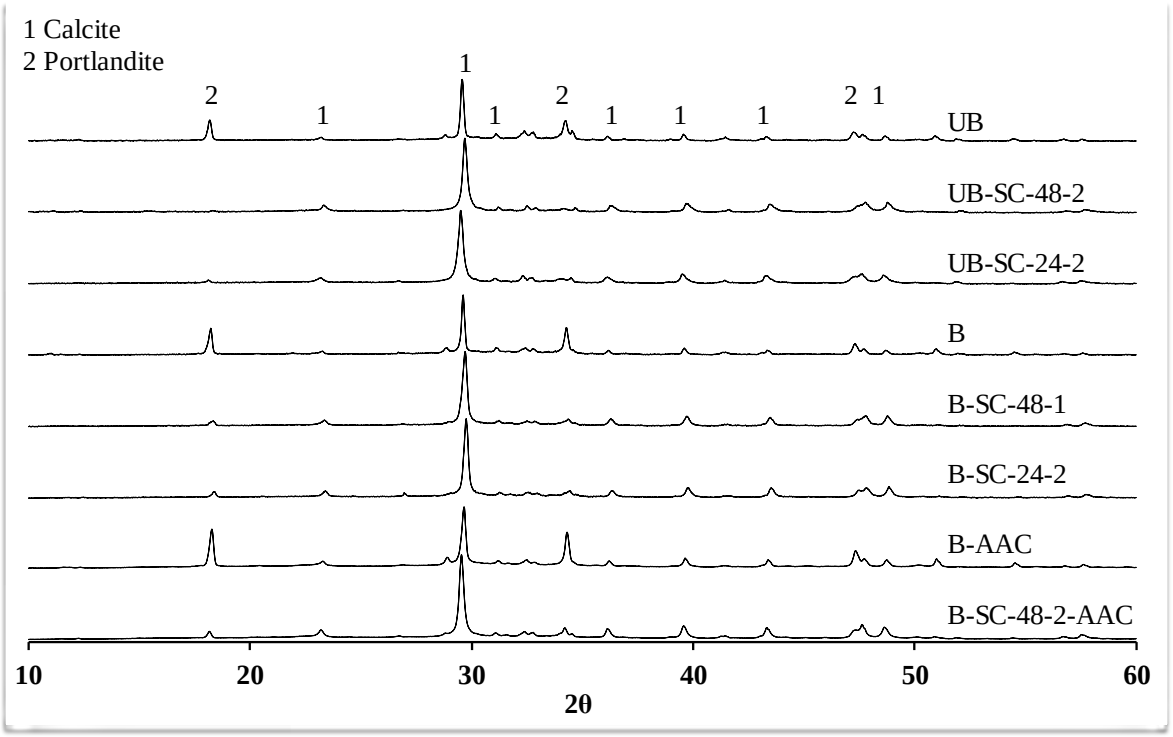

Source: authorships.

4.1.4. Evaluation of the changes in the microstructure

Figures 20 and 21 present micrographs that were obtained by a SEM in Back-Scatter Electron mode (BSE) image detector operating at approximately 15.0 kV. The electron scattering is related to the atomic number.

Previous studies have shown that accelerated carbonation enhanced the interface between cellulose and the cementitious matrix (PIZZOL et al., 2014; ALMEIDA et al., 2013), which develops good mechanical anchorage and interlocking effects since carbonated composites are

denser and more compact, due to calcite filling the pores of the system (PIZZOL et al., 2014). Carbonated composites micrographs emphasize the difference between cellulose pulp at the adhesion fibers-matrix. Arrow 1 in Figure 20 shows the cracks and pores observed in the cement matrix surrounding the unbleached cellulose fibers; as a result, during mechanical testing, the deficient fiber-matrix interface is linked to weaker mechanical properties (SAVASTANO et al., 2003; SAVASTANO et al., 2005). The carbonation process is accompanied with a reduction to the pH of the matrix, although the accelerated carbonation did not avoid the mineralization process inside the cellulose fibers, as shown by arrow 2 in Figure 20.

The carbonated composite shows unbleached cellulose fiber agglomeration (arrow 3 in Figure 20). On the other hand, the bleached fibers in the carbonated composites had improved fiber–matrix interfaces with the cellulose when compared to the unbleached fibers (Arrow 4 in Figure 21 compared to arrow 1 in Figure 20). Nevertheless, bleached fiber presents the mineralization process inside the cellulose fibers, as shown by arrow 5 in Figure 21. Homogeneous distribution of the of eucalyptus fibers over the matrix is noted by arrow 6 on Figure 21. In summary, the carbonated bleached fiber-reinforced composites presented better fiber distribution, improved fiber-matrix adhesion and mechanical behavior, than carbonated unbleached fiber-reinforced composites.

Figure 20 - SEM/BSE micrographs of the cut and polished surface of carbonated unbleached natural fiber-cement composite. Arrow 1: cracks and pores around the fibers; Arrow 2: mineralized cellulose fiber; Arrow 3: agglomeration of fibers.

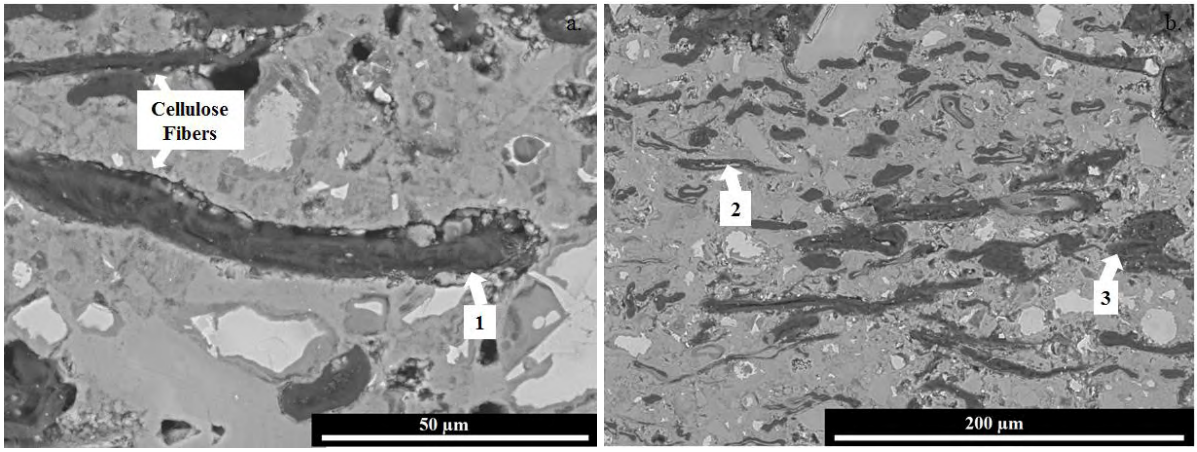

Source: authorships.

Figure 21 - SEM/BSE micrographs of the cut and polished surface of carbonated bleached natural fiber-cement composite. Arrow 4: improved interface between fibers and matrix; Arrow 5: mineralization process inside the cellulose fibers. Arrow 6: homogeneous distribution.

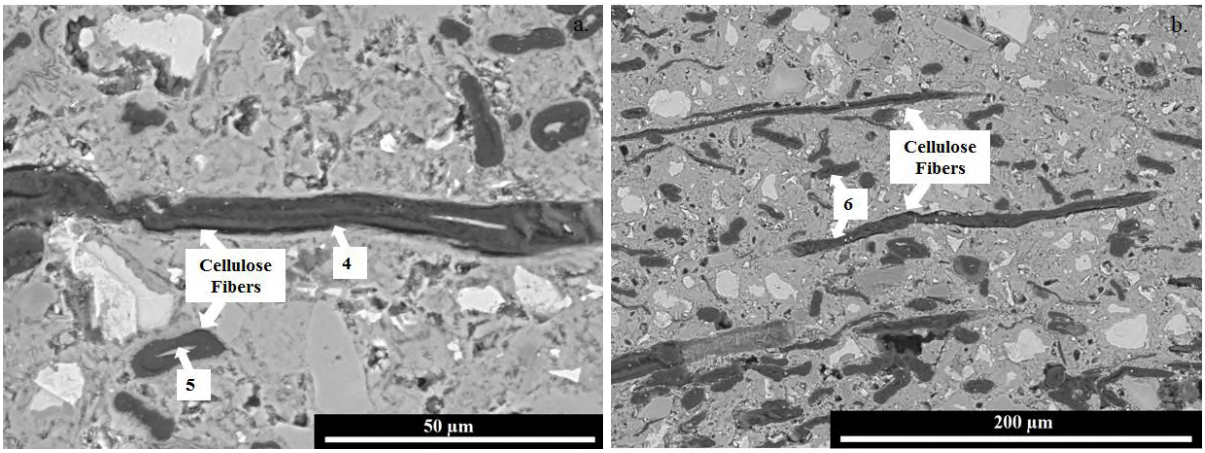

Source: authorships.

4.2. Stage 3: Comparative study between two kinds of mineral addition in cellulose pulp fiber-cement composites subjected to accelerated carbonation at very early age.

4.2.1. Mechanical and physical characteristics of stage 3

Table 17 presents a summary of the average values and corresponding standard deviation of the physical results (AVV, BD and WA) and the mechanical results (MOR, LOP, MOE and SE), respectively for all curing scenarios of the stage 3.

The student's t-test was conducted to a confidence level of 95%. By analyzing the physical and mechanical property results for the four curing regimes we can isolate the influence of hydration time (10 h vs. 24 h); the mineral addition effect (Limestone vs. Silica) and the four conditions in carbonation processes (20% CO_2). For example, to evaluate the effect of the mineral addition on the properties of the matrix, specimen's properties were compared between curing regimes: P-LAC-10 vs. P-AC-10 and P-LAC-24 vs. P-AC-24. The average values represent an average of all measurements and exclude the outliers (spurious) values. A '0' in Table 18 averages that there is no statistically significant difference between the averages, '+' indicates that there is a statistically significant difference between the average with the first listed condition having a higher average than the second, and '-' indicates the first listed condition had a lower average than the second.

Table 17 - Mechanical properties specimens exposed to various curing regimes. (average ± standard of deviation).

Curing Regime Identification	AVV (%)	BD (g/cm^3)	WA (%)	MOR (MPa)	LOP (MPa)	MOE (GPa)	SE (J/m^2)
P-LAC-10	31.47 (1.4)	1.48 (0.02)	21.19 (1.2)	9.17 (1.01)	3.59 (0.4)	8.748 (1.1)	3.01 (1.1)
P-LAC-24	32.41 (1.6)	1.51 (0.03)	21.51 (1.2)	8.80 (0.8)	3.55 (1.7)	8.232 (1.4)	2.00 (0.6)
P-AC-10	33.74 (0.9)	1.51 (0.05)	22.32 (1.3)	9.74 (1.3)	4.99 (0.9)	8.847 (0.8)	3.09 (1.2)
P-AC-24	32.95 (0.9)	1.51 (0.04)	21.79 (1.2)	10.90 (1.9)	5.19 (1.3)	10.324 (2.1)	2.65 (0.9)

Source: authorships.

Table 18 - Statistically Significance Difference between the average (at 95% confidence level)

Experimental Variable	Comparison of average between Curing Regimes:	AVV (%)	BD (g/cm^3)	WA (%)	MOR (MPa)	LOP (MPa)	MOE (MPa)	SE (J/m^2)
The effect of the mineral addition	P-AC-10 vs P-LAC-10	0	0	+	0	+	0	0
	P-AC-24 vs P-LAC-24	+	0	0	+	+	+	0
The effect of the hydration time	P-LAC-10 vs P-LAC-24	0	0	0	0	0	0	+
	P-AC-10 vs P-AC-24	0	0	0	0	0	0	0

Source: authorships.

The effect of the Mineral addition: To compare the effect of the carbonation curing phase on the specimens, a comparison of the properties of the following curing regimes was examined: P-LAC-10 vs. P-AC-10 and P-LAC-24 vs. P-AC-24 (Figure 22). Comparing the four curing regimes, as shown in Table 18, the effect of the mineral addition on the samples P-LAC-24 vs. P-AC-24 had an effect on the specimen's, resulted in average values of MOR, LOP, MOE, and SE of the composition of the silica were 24%, 46%, 25% and 32%. This could be attributed to the difference in enhancing the hydration of the clinker as a result of the mineral addition effect; the fine particle size distribution of the limestone, influence on the chemistry or the packing (HAWKINS et al., 2003), as well to be high affinity between calcium aluminate and carbonate phases to form monocarbonate (FELDMAN et al. 1965; BENSTED, 1980). The performance of limestone-cementitious materials is impacted by all main aggressive species (sulfates, chlorides, carbonation) and main pathologies (freezing-thawing, ASR, corrosion). On the other hand, the use of silica particles to substitute clinker particles, led to more available space for the hydrates of the clinker phases to form, and it is considering for the heterogeneous precipitation and growth of hydrates (SCRIVENER et al., 2015) and as an inner mineral addition it seems that there is almost no influence on the heat evolution curve during the acceleration period (LOTHENBACH et al., 2011). In both cementitious matrices, the presence of CO_2 during the curing period (early carbonation) led to disappearing of calcium hydroxide (portlandite—P). The CH and C–S–H become carbonated simultaneously. The initial rate of carbonation is quite similar, but while C–S–H is still carbonating, CH carbonation slows down and stops. This is due to the fact that CH becomes less and more accessible for carbonation front (MORANDEAU et al., 2014; TONOLI et al., 2016).

Effect of Hydration Time: To compare the effect of the carbonation curing phase on the specimens, a comparison of the properties of the following curing regimes was examined: P-LAC-10 vs. P-LAC-24 and P-AC-10 vs. P-AC-24. Comparing the four curing regimes, as shown in Table 18, increasing the hydration time from 10 h to 24 h had no effect on the specimen's bulk density, modulus of rupture and modulus of elasticity.

Figure 22 - Typical stress x strain curves during flexural tests of the composites using Limestone and Silica as mineral addition.

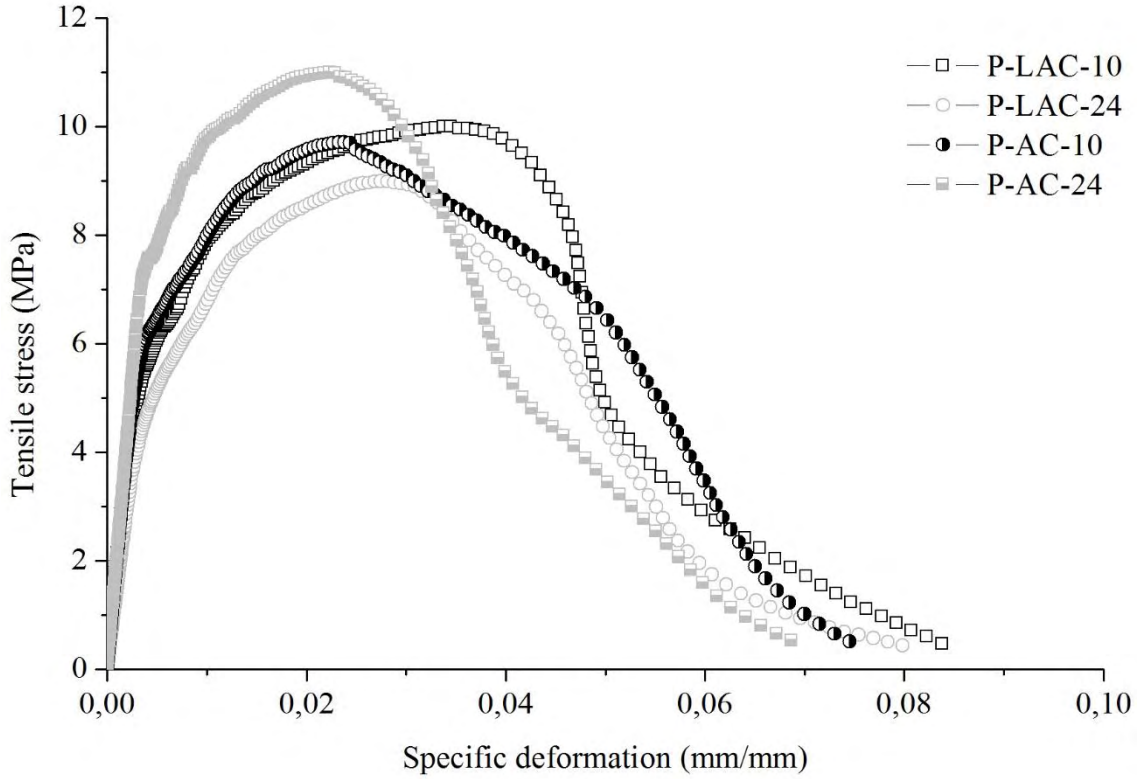

Source: authorships.

4.2.2. X-ray diffraction analysis

Figure 23 presents the XRD patterns for the four different sets of curing and formulations conditions. Calcium carbonate (calcite) is the main mineralogical phase observed in the carbonated samples due to the presence of the calcium carbonate, the second phase is calcium hydroxide (Portlandite) observed at a much lower rate. Figure 23 compares the carbonated samples using different mineral additions, Limestone (P-LAC-10 and P-LAC-24) vs Silica (P-AC-10 and P-AC-24). There is a noticeable absence of portlandite (around $2\theta = 18°$ or 36°) and

the notorious peak around 2θ = 26.6°, correspond to the silica type quartz, in the samples with silica mineral addition.

In Figure 23, it is possible to observe the increase of the peak at 2θ = 29.5° in all carbonated samples. This corresponds to $CaCO_3$ in the form of calcite (TONOLI et al., 2016), this increase is due to the primary reaction process of CO_2 that dissolves into the matrix and reacts with hydration products, such as calcium hydroxide (CH) and calcium silicate hydrate (C–S–H), and also reacts with polymerized silica gel leading to secondary carbonation.

Figure 23 - XRD patterns of the sets of curing regimes. Limestone vs Silica.

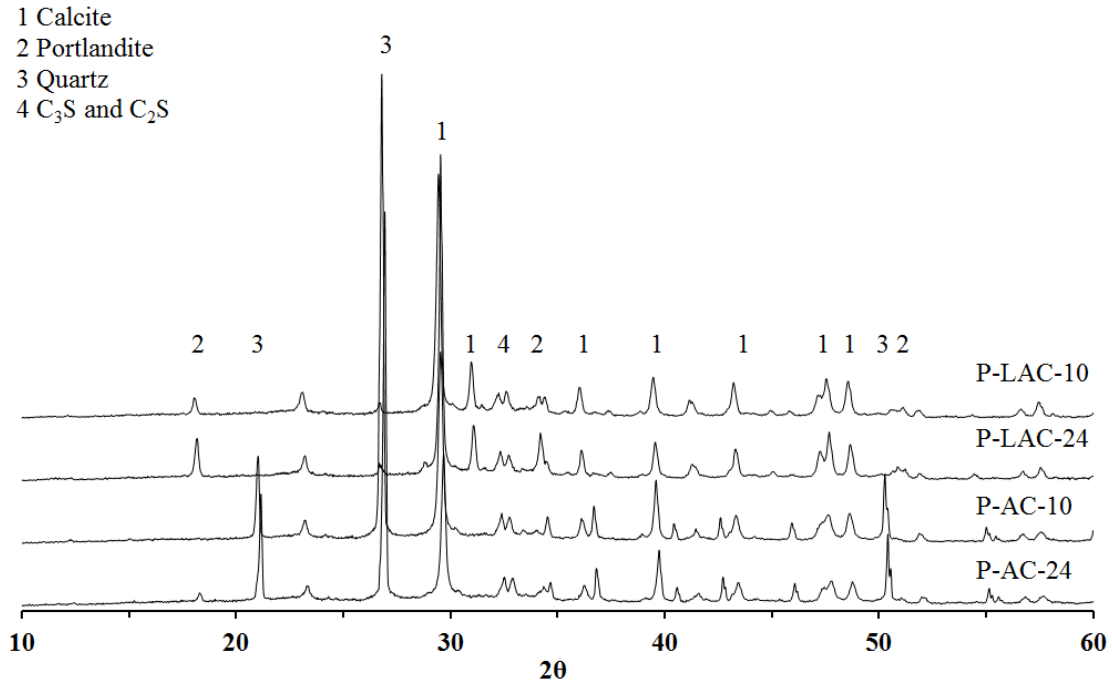

Source: authorships.

Figure 24 shows estimated percentages of calcium hydroxide (Portlandite), calcium carbonate (Calcite), tricalcium silicate (alite), dicalcium silicate (belita), quartz, and calcium carbonate and magnesium (dolomite), these were determined using the software PANalytical HighScore Plus. The estimated percentages correspond to the crystalline percent of the material and did not take into account the amorphous percent of the material.

The percent quantification and formation of each one those phases on limestone composites subjected to carbonation curing depends mostly on two main chemical processes: primarily the dissolution of $Ca(OH)_2$, which releases Ca^{2+} and OH^- ions, and precipitates forming calcium carbonate ($CaCO_3$). Even though the carbonation process reduces the amount of portlandite, this phase was not completely consumed in the limestone composite, as shown in Figure 24, nevertheless the principal component, with significantly greater quantities, is calcium carbonate. Secondly, the calcium carbonate formation is attributed to the reduction of Ca/Si in calcium silicate hydrate gel, as well from other solid phases containing Ca^{2+}. The progressive decalcification ultimately leads to S–H and $CaCO_3$. This reaction process between CO_2 and the C–S–H produces $CaCO_3$ and a polymerised silica gel (SANTOS et al., 2015; FERNANDEZ-BERTOS et al., 2004).

Figure 24 - XRD patterns of quantification of the phases for Limestone Composite P-LAC-24.

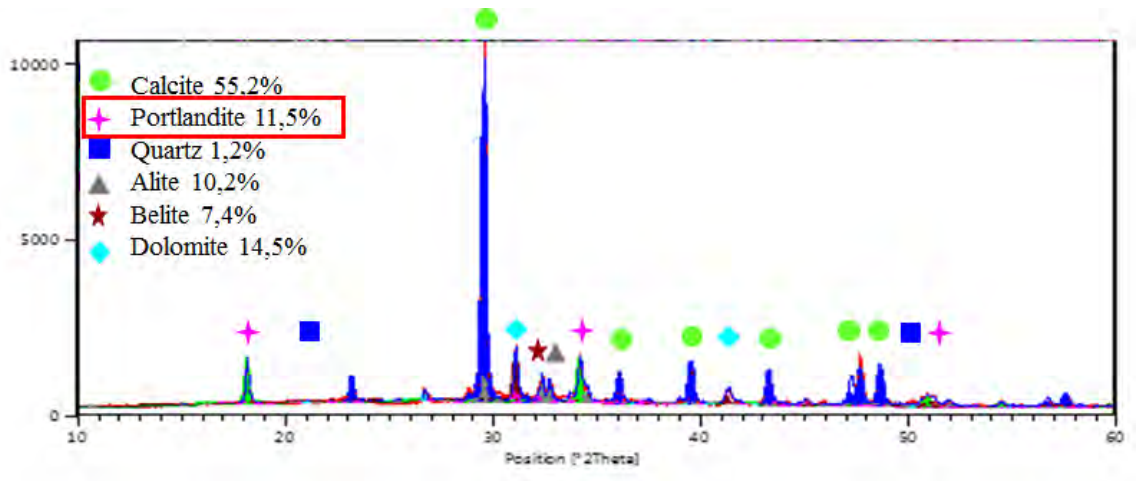

Source: authorships.

Figure 25 shows estimated percentages of calcium hydroxide (Portlandite), calcium carbonate (Calcite), tricalcium silicate (alite), dicalcium silicate (belita) and quartz, also determined using the software PANalytical HighScore Plus. As was previously mentioned, these estimated percentages correspond to the phases of crystalline amount of the material and did not take into account the amorphous amount of the material.

In this case, the principal component of the matrix is the quartz, instead of $CaCO_3$. The presence of quartz (SiO_2) is due to the inert mineral addition used, silica. In this composite, it is considered the total reduction of portlandite, because it is around 3%, clarify that is the percent correspond to the quantification of the crystalline part of the composite. In other words, with

the use of silica as mineral addition can conduct to a better reduction of the alkalinity than using limestone.

Figure 25 - XRD patterns of quantification of the phases for Silica Composite P-AC-24.

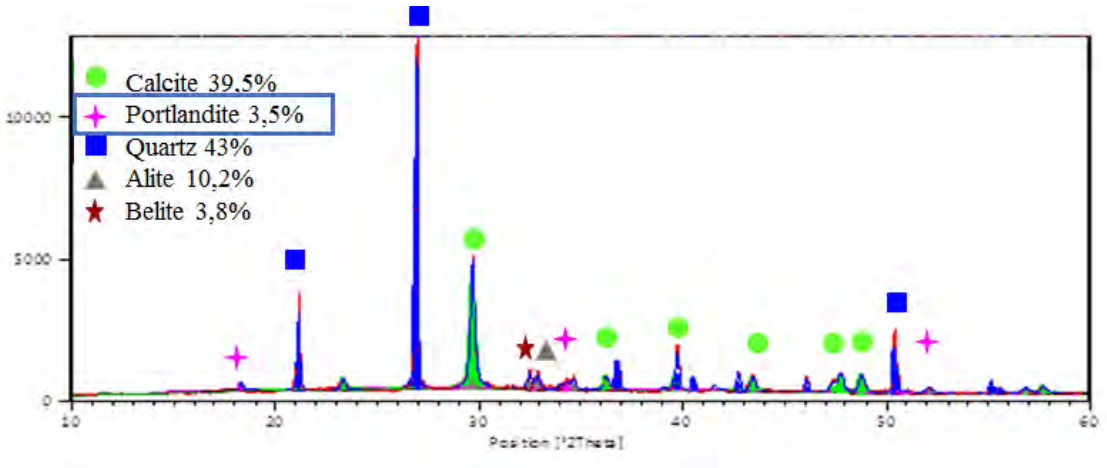

Source: authorships.

A few global crystallographic parameters of each phase are: calcite ($CaCO_3$), with reference code 969009669, it has a hexagonal crystallographic structure and the space group number of cataloguing data R -3c (167) (SITEPU et al., 2005); the portlandite $Ca(OH)_2$, with a reference code 969000114, corresponds to hexagonal crystallographic structure and the space group number of cataloguing data P-3 m 1 (164) (HERNDERSON et al., 1962); the alite, with a reference code 990010019, compound name 1540705, corresponds to monoclinic crystallographic system and bellows to a space group number of cataloguing data C 1 m 1 (8) (DE LA TORRE et al., 2002); the belite, with a reference code 969012790, corresponds to monoclinic crystallographic system and the space group number of cataloguing data P 1 21/c 1 (14) (TSURUMI et al., 1994); the quartz, with a reference code 962100189, corresponds to hexagonal crystallographic structure and the space group number of cataloguing data P 31 2 1 (152) (CASPI et al., 2005).

4.2.3. Evaluation of the changes in the microstructure

Figure 26 and Figure 27 presents micrographs that were obtained using a SEM in Back-Scatter Electron mode (BSE) image detector operating at approximately 15.0 kV. Both images correspond to carbonated cementitious matrices, which average they are denser and more

compact, and have improved contact between cellulosic fibers and the cement matrix, when compared to uncarbonated cementitious matrices (SAVASTANO AND AGOPYAN, 1999). The EDS analysis allows to see the differences between these composites, which are the chemical components; on limestone composites, it is well known and previously discussed that the porosity is sufficiently high to permit constant CO_2 diffusion, therefore the CH is further reduced and the interlayer calcium from C–S–H also reacts with carbon dioxide, as a result the main composite is $CaCO_3$ and secondary composite is silicate gel (FERNÁNDEZ-BERTOS et al., 2004). (Fig. 26 and Fig. 27) In both cases the microstructure is compact and formed by layered structures, (cross1 in Fig. 26 and Fig. 27) likely related to the C–S–H phases. These results corroborate with the higher content of $CaCO_3$ (cross 2 in Fig. 26), observed in the XRD quantification of the crystalline part of the limestone material. Across 3, Fig. 27 presents the main component of this composite that is the quartz.

Figure 26 - a) SEM image. b) EDS analysis of limestone composite. Arrow 1: Alite (C_3S); Arrow 2: Calcium carbonate ($CaCO_3$).

a.

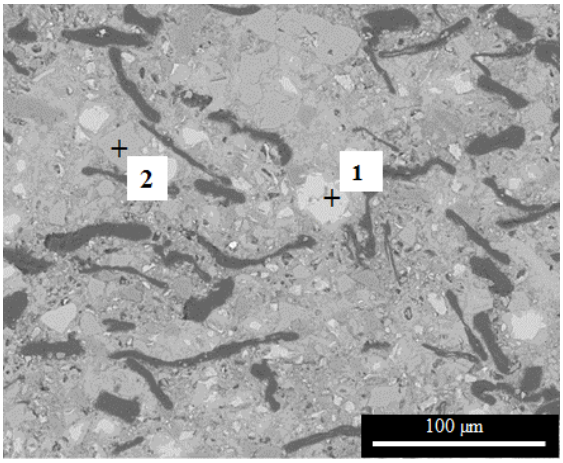

b.

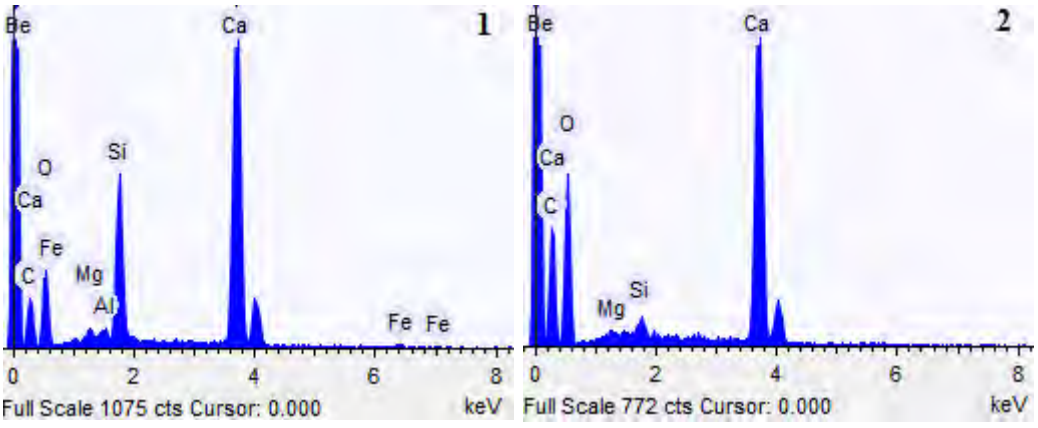

Source: authorships.

Figure 27 - a) SEM image. b) EDS analysis of Silica composite. Arrow 1: Alite (C_3S); Arrow 3: Quartz (SiO_2).

a.

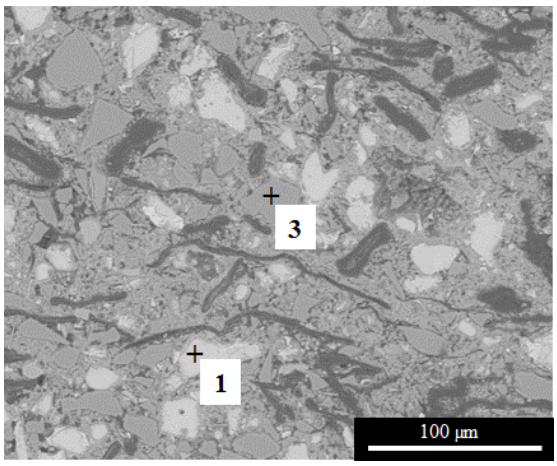

b.

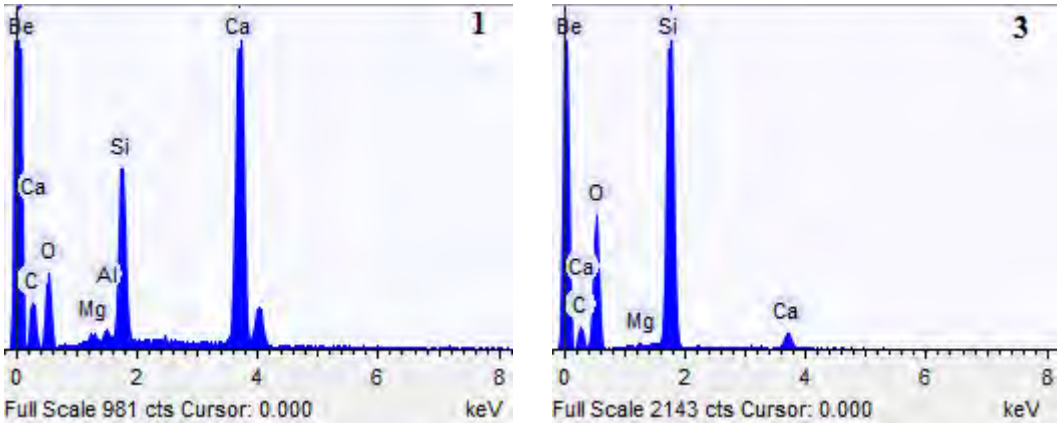

Source: authorships.

4.3. Stage 4: Durability and hydration kinetics study in carbonated fiber-cement composites using silica as a mineral addition.

4.3.1. Mechanical and Physical Properties of stage 4

Table 19 presents a summary of the average values and corresponding coefficient of variation (COV) of the physical properties (AVV, BD and WA) and the mechanical properties (MOR, LOP, MOE and SE), respectively for all curing scenarios.

The student's t-test was conducted to a confidence level of 95%. By analyzing the physical and mechanical property results for the eight curing regimes we can isolate the influence of hydration time (10 h vs. 24 h); carbonation processes (atmospheric CO_2 level (0.035%) vs. 20% CO_2); and also the degradation performance by way of exposure to accelerated ageing (soak-dry) cycles (no cycles vs. 200 cycles). To evaluate the effect of the hydration time duration on the properties of the matrix, the following comparisons are assessed: P-UC-10 vs. P-UC-24; P-AC-10 vs P-AC-24; P-UC-10-AAC vs. P-UC-24-AAC; and P-AC-10-AAC vs. P-AC-24-AAC. A summary of the statistical significance testing is reported in Table 20 for the physical and mechanical properties. The average values represent an average of all measurements and exclude the outliers (spurious) values. A '0' in the table averages that there is no statistically significant difference between the averages, '+' indicates that there is a statistically significant difference between the means with the first listed condition having a higher average than the second, and '-' indicates the first listed condition had a lower average than the second.

Table 19 - Physical and mechanical properties of specimens exposed to various curing regimes (average ± standard of deviation).

Curing Regime Identification	**AVV (%)**	**BD (g/cm^3)**	**WA (%)**	**MOR (MPa)**	**LOP (MPa)**	**MOE (GPa)**	**SE (kJ/m^2)**
P-UC-10	34.45 (0.8)	1.43 (0.03)	24.18 (0.6)	6.51 (0.41)	2.84 (0.8)	7.021 (0.7)	4.47 (1.3)
P-UC-24	33.38 (0.41)	1.43 (0.03)	23.30 (0.4)	6.49 (0.8)	2.93 (0.7)	7.111 (0.9)	3.78 (1.5)
P-AC-10	33.74 (0.6)	1.51 (0.03)	22.32 (0.74)	9.74 (1.34)	4.99 (0.9)	8.847 (0.8)	3.09 (1.2)
P-AC-24	32.95 (1.5)	1.51 (0.03)	21.79 (1.14)	10.90 (1.9)	5.19 (1.3)	10.324 (2.1)	2.65 (0.9)
P-UC-10 – AAC	30.85 (2.01)	1.41 (0.05)	22.10 (2.1)	6.17 (1.2)	3.76 (0.9)	8.765 (1.8)	0.93 (0.7)
P-UC-24 – AAC	30.82 (0.9)	1.42 (0.03)	21.67 (0.8)	7.40 (1.3)	5.03 (0.7)	8.704 (0.8)	0.77 (0.6)
P-AC-10 – AAC	29.88 (1.9)	1.57 (0.02)	19.03 (1.5)	9.39 (2.0)	4.35 (1.5)	11.936 (1.2)	2.64 (1.1)
P-AC-24 – AAC	28.17 (0.7)	1.54 (0.04)	18.33 (0.8)	8.21 (1.6)	6.51 (1.3)	11.138 (1.9)	1.35 (0.3)

Table 20 - Statistically Significance of the difference between the average (at 95% confidence level)

Experimental Variable	Comparison of Means between Curing Regimes:	AVV (%)	BD (g/cm^3)	WA (%)	MOR (MPa)	LOP (MPa)	MOE (MPa)	SE (J/m^2)
Hydration time	P-UC-10 vs. P-UC-24	+	0	+	0	0	0	0
Hydration time	P-AC-10 vs. P-AC-24	0	0	0	0	0	0	0
Hydration time	P-UC-10-AAC vs. P-UC-24-AAC	0	0	0	0	-	0	0
Hydration time	P-AC-10-AAC vs. P-AC-24-AAC	+	0	0	0	-	0	+
Carbonation	P-UC-10 vs. P-AC-10	0	-	+	-	-	-	+
Carbonation	P-UC-24 vs. P-AC-24	0	-	+	-	-	-	0
Carbonation	P-UC-10-AAC vs. P-AC-10-AAC	0	-	+	-	0	-	-
Carbonation	P-UC-24-AAC vs. P-AC-24-AAC	+	-	+	0	-	-	-
Ageing cycles	P-UC-10 vs. P-UC-10-AAC	+	0	+	0	-	-	+
Ageing cycles	P-UC-24 vs. P-UC-24-AAC	+	0	+	0	-	-	+
Ageing cycles	P-AC-10 vs. P-AC-10-AAC	+	-	+	0	0	-	+
Ageing cycles	P-AC-24 vs. P-AC-24- AAC	+	0	+	+	0	0	+

* 0 no statistically significant difference between the average

** + statistically significant difference with a higher average for the first listed regime

*** - statistically significant difference with a lower average for the first listed regime

Effect of Hydration Time: To compare the effect of the carbonation curing phase on the specimens a comparison of the properties of the following curing regimes is examined: P-UC-10 vs. P-UC-24; P-AC-10 vs. P-AC-24; P-UC-10-AAC vs. P-UC-241-AAC; and P-AC-10-AAC vs. P-AC-24-AAC. Considering eight curing regimes as shown in Table 19, the effect of increasing the hydration time from 10 h to 24 h had no effect on the specimen's bulk density, modulus of rupture and modulus of elasticity. However, when comparing specimens subjected to the accelerated ageing cycles, the limit of proportionally was affected, whereby, a longer hydration time (24 h) resulted in a higher LOP for both the uncarbonated (P-UC-10-AAC and P-UC-24-AAC) specimens, as well as the carbonated specimens (P-AC-10-AAC and P-AC-24-AAC). The difference of LOP could be due to the progression of the hydration process (TONOLI et a., 2009). Another factor that could influence the initial hydration duration time was the mineral addition effect, in this case the silica, allows the heterogeneous precipitation and growth of hydrates (SCRIVENER et al., 2015).

Effect of Exposure to Carbonation Curing: To evaluate the effect of the carbonation curing phase on the specimens a comparison of the properties of the following curing regimes is examined: P-UC-10 vs. P-AC-10; P-UC-24 vs. P-AC-24; P-UC-10-AAC vs. P-AC-10-AAC; and P-UC-24-AAC vs. P-AC-24-AAC. Examination of the measurements in Table 19 reveals that for all specimens, exposure to carbonation curing increased the mechanical properties, namely, the modulus of rupture, limit of proportionality and the modulus of elasticity, compared to the specimens that were not subjected to carbonation. For the case of specimens without exposure to the accelerated ageing cycles, the statistical analysis reveals that the high concentration of CO_2 (20%) exposure resulted in a statistically significant difference in all physical and mechanical properties. The average values of LOP and MOE show indirectly that there is an improvement in the fibre-matrix interface caused by carbonation processes in the early stage of curing, and furthermore, after exposure to 200 soak-dry cycles. Almeida et al. (2010) and Pizzol et al. (2014) studied cement based specimens reinforced with eucalyptus cellulosic pulp subjected to accelerated carbonation curing (AC) resulting in an increase of matrix resistance to the crack propagation, if compared to uncarbonated fibre–cement. The mechanical improvement was attributed to the elimination of calcium hydroxide due to the carbonation treatment, that creates a microstructure with more strength-contributing solids than conventional hydration (PIZZOL et al., 2014; ROSTAMI et al., 2012; ALMEIDA et al., 2013).

Specimens of carbonated specimens (AC) were compared to the uncarbonated (UC) specimens after they were exposed to the accelerated ageing cycles. The specimens P-UC-10-AAC and P-UC-24-AAC have greater mean apparent porosity values, and lower mechanical performance compared to P-AC-10-AAC and P-AC-24-AAC respectively. $CaCO_3$ is precipitated in the pore structure of the composite, filling the voids and through blocking the absorption of water due to the decrease of pore size (HYVERT et al., 2010).

According with Santos et al. (2015), the fibre-matrix interactions are dependent on physical and chemical adhesion, shear stress resistance and mechanical anchorage induced by overall complex geometry and orientation effects of the cellulosic fibres. Unbleached pine fibre is low density and hydrophilic. Therefore, the amount of water absorbed by this fibre depends on the void volume and the amount of cellulose material present; both parameters have an effect upon density of the matrix (COUTTS, 1995).

Effect of Accelerating Ageing Cycles: To evaluate the effect of the accelerated ageing soak-dry cycles on the properties of the specimens, the following curing regimes are compared: P-UC-10 vs. P-UC-10-AAC; P-UC-24 vs. P-UC-24-AAC; P-AC-10 vs. P-AC-10-AAC; and P-AC-24 vs. P-AC-24-AAC. No clear trends are apparent when examining the average mechanical properties or physical properties of specimens subjected to 200 soak-dry cycles compared to specimens that were not submitted to the aging cycles. In some cases, the mechanical properties are greater for the specimens subjected to the accelerated ageing cycles, but in other cases they are not. In some cases, the difference of the mean properties between samples exposed and not exposed to 200 soak-dry cycles is statistically significantly different, but in other cases it is not, as shown in Table 20. However, close examination of the data in Table 20, representing the physical and mechanical properties, reveals that the vegetable fibre -cement composite can exhibit good durability properties even after being subjected to 200 soak-dry ageing cycles. For example, the range in modulus of rupture of samples not exposed to any ageing cycles compared to those exposed to 200 ageing cycles is 6.49 to 10.9 MPa, and 6.17 to 9.39 MPa respectively. The range in limit of proportionality of samples not exposed to any ageing cycles compared to those exposed to 200 ageing cycles is 2.84 to 5.19 MPa, and 3.76 to 6.51 MPa respectively. The range in the elastic modulus of samples exposed to no ageing cycles compared to those exposed to 200 ageing cycles is 7022 to 10325 MPa, and 8705 to 11936 MPa respectively. Therefore, it is clear, the range in mechanical properties of specimens exposed to accelerated soak-dry cycles is within a similar range as that of the specimens that have not been subjected to any soak-dry cycles.

The accelerated carbonation treatment interferes with the reduce of the destruction macromolecular chains during the partial alkaline hydrolysis of the cellulose, which causes their rupture and the consequent decrease in the degree of polymerisation. Also, this treatment is a gradual process of filling up the inner cores of the vegetable fibres with the hydration products that leads to the embrittlement of the reinforcement (MELO FILHO et al., 2013). Furthermore, a it was proposed that on carbonated composites the toughening mechanisms were better preserved the fracture process (SANTOS et al., 2015). Nevertheless, judging by the results of both composites, carbonated and uncarbonated, was found that the mechanical properties were maintained and this could be attribute to the use of an inert filler in the cementitious matrix.

The use of an inert mineral addition as ground silica allows to isolate the effect of the accelerated carbonation curing process on cementitious composites, but it also seems to work as appropriate strategy to mitigate degradation of the composite, even for air curing (with no autoclave) condition. In conjunction with the use of unbleached pine fiber, it works for the good interfacial fibre-matrix bonding strength and lower vulnerability of the fiber for degradation in the cement matrix (COOKE, 2000; SANTOS et al., 2015). The typical stress x strain curves of the composites are shown at Figure 28 before and after accelerated ageing cycles for 10 h of initial hydration; and Figure 29 before and after accelerated ageing cycles for 24 h of initial hydration. Comparing specimens subjected to the accelerated ageing cycles, the specific energy affected, whereby, a longer hydration time (24 h) resulted in a higher SE for the carbonated specimens (P-AC-24-AAC); but a short hydration time (10 h) resulted in a higher MOR for the carbonated specimen (P-AC-10-AAC)

Figure 28 - Typical stress x strain curves during flexure tests of the composites reinforced before and after accelerated aging cycles. Initial hydration period of 10 h.

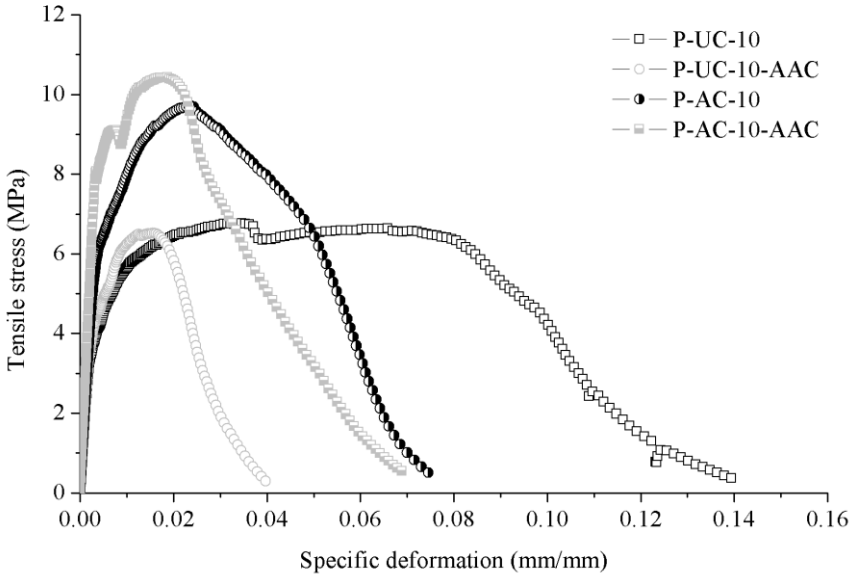

Source: authorships.

Figure 29 - Typical stress x strain curves during flexure tests of the composites reinforced before and after accelerated aging cycles. Initial hydration period of 24 h.

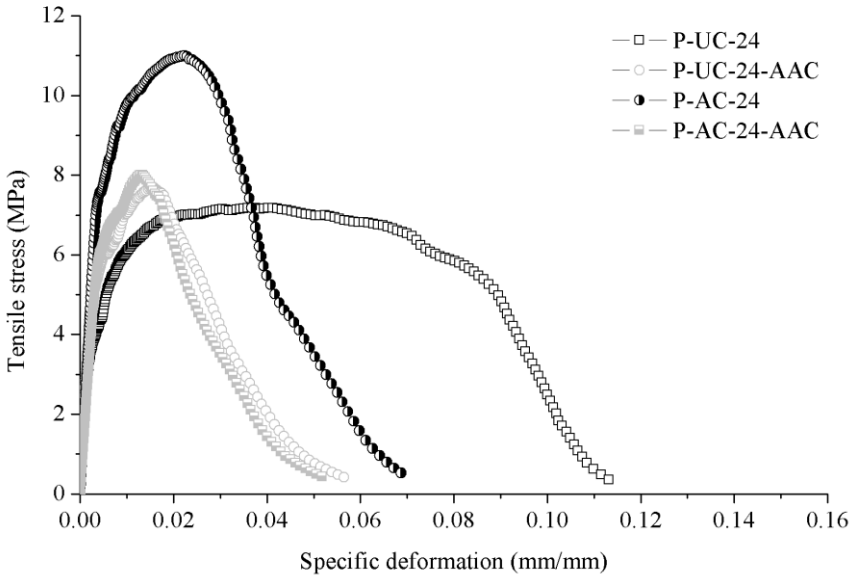

Source: authorships.

4.3.2. Thermogravimetry analysis (TG/DTG)

The comparison of the mechanical properties of the uncarbonated and carbonated samples before and after accelerated aging cycles shows statistically significant improvement of the carbonated samples due to the carbonation reaction. The efficiency of the carbonation reaction was evaluated for the eight sets of curing regimes, through the differential thermogravimetry analysis (DTG).

The most important hydration product of cementitious composites is still calcium silicate hydrate (C–S–H) gel (CHEN et al., 2004; SHI et al., 2009) and it is responsible for most of the properties of cement-based materials (SANTOS et al., 2015). For the carbonation process, the dissolution of $Ca(OH)_2$ generally takes place more readily, while decalcification of C–S–H occurs when $Ca(OH)_2$ is inaccessible or locally reduced (FERNANDEZ-BERTOS et al., 2004), it is known as secondary carbonation process (FERNANDEZ-BERTOS et al., 2004). On DTG Figure 30a and Figure 30b there is a clear difference between uncarbonated (UC) and carbonated (AC) conditions; the AC conditions presents a lower mass loss between 0°C and 240°C compared with the UC conditions, this is attributed to the formation of different phases. The abrupt mass loss between 105 and 150°C is evident in the uncarbonated (UC) samples; the DTG curve indicates C-S-H and ettringite dehydration (RAMACHANDRAN et al., 2001). In addition, in the UC samples, a weight loss at approximately 180°C is observed, indicating the presence of monosulfate (LOTHENBACH et al., 2008). Also, the UC conditions presents a higher mass loss between 105 and 420°C compared with the UC conditions, this range represents the loss of combined water due to dehydration of (C–S–H), aluminate hydrate and ferroaluminate hydrate (RAMACHANDRAN et al., 2001; SHA et al., 1999; SHARMA et al., 1999).

Bentur and Mindess (2007), observed that cellulose phase in fiber-cement composites detected in the temperature interval 295 - 370°C corresponding to the degradation of the cellulose fibers. Exposure of specimens to elevated levels of carbon dioxide is known to be one mechanism to minimize cellulose fibre degradation in the fibre-cement products. The beneficial effects on the mechanical and physical properties were apparently. The mass loss in the range of 295 - 370°C could be related to the degradation of the fibre as a result of the soak-dry cycles, in particular at 340°C for the specimen P-AC-10-AAC (Figure 30a) have a higher peak compare with P-AC-24-AAC (Figure 30b) at 350°C.

One potential mechanism of degradation which has been reported in the literature is the mineralization of the cellulose fibres, which is produced by the free ions from the dissolution of Portland cement phases that penetrate into the fibre cavity (lumen). This is the principal reason for the re-precipitation of calcium hydroxide into the fibre. This re-precipitation of solids into the fibre voids induces the embrittlement of the cellulose fibres (MOHR et al., 2005; MOHR et al., 2006). This influences significant losses in mechanical properties in the long-term and has specifically been observed in vegetable fibre-cement composites after natural or accelerated ageing (e.g. soak/dry cycling), due to the degradation mechanisms of cellulose fibres in the cementitious environment (MOHR et al., 2005; TONOLI et al., 2009).

Table 21 presents the TG results by way of quantifying the mass loss percentage of carbonation precipitate. According with Borges et al. (2010), the increase in molar mass with carbonation process, allows inferring an increase in the percentage of mass lost. The amount of calcium hydroxide (CH) and calcium carbonate (CC) was determined using the molar mass balance, since that 74 g/mol, 44 g/mol, 100 g/mol and 18 g/mol are the molar masses of $Ca(OH)_2$, CO_2, $CaCO_3$ and H_2O respectively. Using the method of Borges et al. (2010), withthe equations (14) and (15). Dehydroxylation, L1, occurs between 450 and 500°C, the mass loss in this range decreases as the carbonation exposure time increases, and decarbonation losses, L2, occurs between 600–750°C. The initial amount of $Ca(OH)_2$ may be directly calculated from Eq. (16). The corresponding amount of $CaCO_3$ resulting from the total $Ca(OH)_2$ that carbonated was estimated using Eq. (17).

$$\%\mathrm{CH} = \mathrm{L1} \cdot \frac{74}{18} = 4.11 \cdot \mathrm{L1} \qquad \text{(Eq. 14)}$$

$$\%\mathrm{CC} = \mathrm{L2} \cdot \frac{100}{44} = 2.27 \cdot \mathrm{L2} \qquad \text{(Eq. 15)}$$

$$\%\mathrm{CH}_{\,\mathrm{Initial}} = \%\mathrm{CH} + (0.74 \cdot \%CC) \qquad \text{(Eq. 16)}$$

$$\%\mathrm{CC} = 1.35 \cdot \%\mathrm{CH} \qquad \text{(Eq. 17)}$$

Figure 30 - DTG curves of the fibre–cement specimens: a.) before and after ageing cycles for 10 h initial hydration, and b.) before and after ageing cycles for 24 h initial hydration

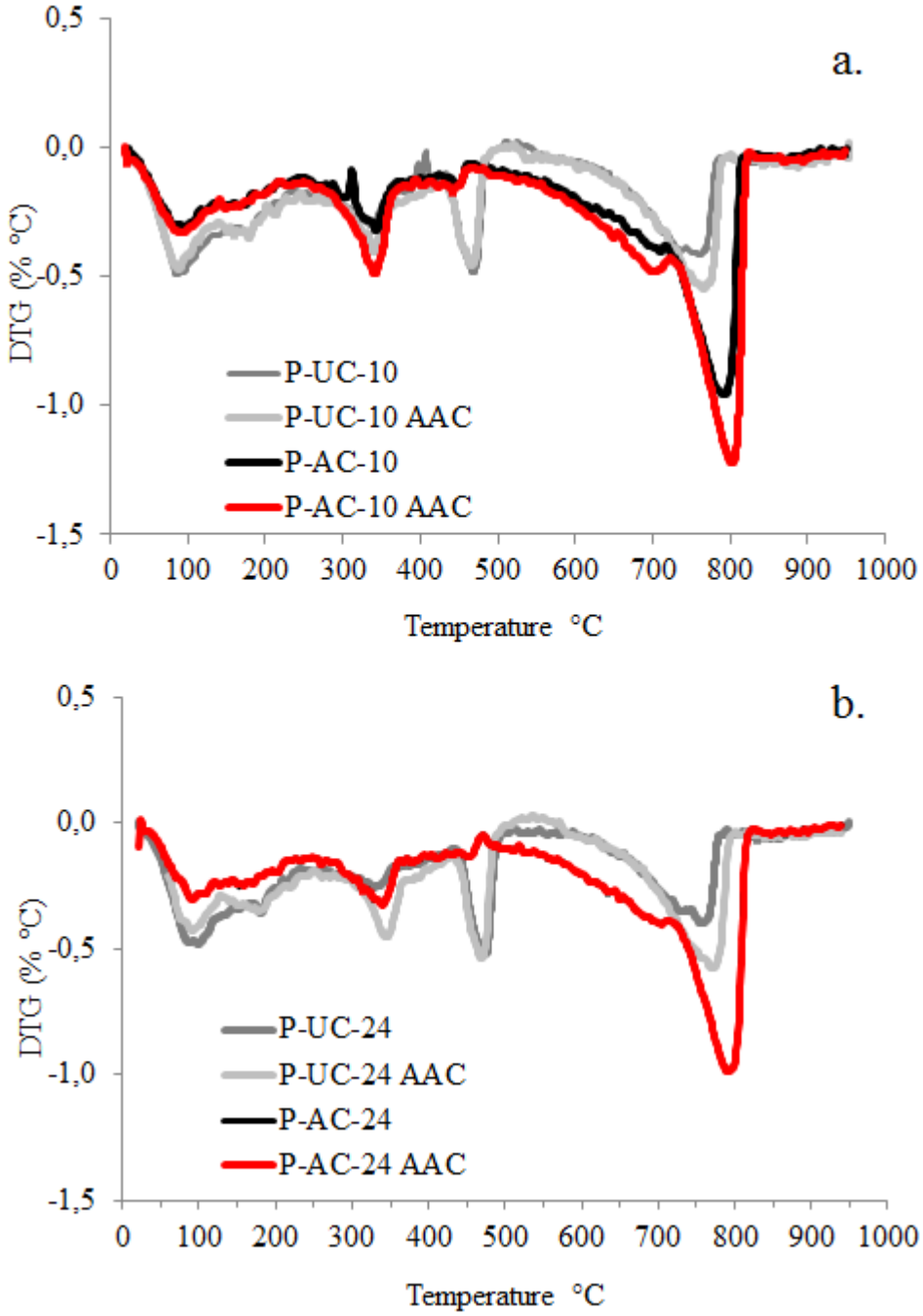

Source: authorships.

From Table 21 comparing the %CH and %CC between the uncarbonated and carbonated samples with different initial hydration durations (10 h v. 24 h), it is apparent that the hydration time did not influence the $Ca(OH)_2$ and $CaCO_3$ formation. In all samples subjected to the carbonation regime, it was observed weight loss at approximately 800°C, which represents well-crystallized $CaCO_3$. According to Alvarez et al. (2005), this indicates that the carbonation

process of calcium hydroxide can generate carbonate polymorphs that may be oxidized in the same region. Considering the relatively weak peak located at 758°C of the uncarbonated samples (P-UC-10 and P-UC-24) in Figure 30a, it suggests only the initial carbon content in as-received cement. This observation is also supported by other researchers such as Rostami et al. (2011).

For the samples under accelerated carbonated conditions, it was observed a considerable decrease in the peak at 470°C indicating the CH consumption due to carbonation, what can surely contribute to the dimensional stabilization of the composite and to the alkalinity reduction of the cement matrix (PIZZOL et al., 2014). Contrarily, the uncarbonated samples show a much greater peak at the same region, which infers a highly alkaline composite. The increase or decrease of these peaks indicate the alkalinity of the matrix, as well as the reaction with phenolphthalein on carbonated composites indicates the composite to be less alkaline. In contrast, the phenolphthalein on the uncarbonated samples is measured to be more alkaline, with a relatively above pH (8.5).

Table 21 - The estimation of the extent of carbonation of C‑S‑H from TGA data, before and after accelerated carbonation treatment, non-aged and aged.

Curing Regimes	**Uncarbonated composite**			**Curing Regimes**	**Carbonated composite**				
	CH from TGA (%)	CC from TGA (%)	Calculation of initial CH (%)		CH from TGA (%)	CC from TGA (%)	Amount of carbonated CH (%)	Expected CC from carbonating CH (%)	Carbonates formed by C–S–H (%)
P-UC-10	6.49	6.44	11.26	P-AC-10	1.35	21.2	9.9	13.37	7.78
P-UC-10-AAC	6.1	5.8	10.38	P-AC-10-AAC	1.93	24.3	8.45	11.41	12.85
P-UC-24	7.35	4.15	10.43	P-AC-24	0.98	23.6	9.44	12.75	10.81
P-UC-24-AAC	5.79	4.74	13.21	P-AC-24-AAC	1.39	24.9	11.81	15.95	9.01

Source: authorships.

4.3.3. FTIR spectrometer analysis

FTIR analysis results are shown in Figure 31 and Figure 32 for specimens with initial hydration of 10 h and initial hydration of 24 h, that were not subjected to ageing cycles and those that were exposed to 200 soak-dry cycles respectively. The results reveal that the calcium carbonate was present in all carbonated samples. In both Figures 31 and 32, a band in the region of 1,300 to 1,700 cm^{-1} is observed, which some researchers have linked to carbonation processes (YLMÉN et al., 2013). For the specimens, P-AC-10 and P-AC-10-AAC, presents peaks at 879, 1085, 1427, 1794 and 2505 cm^{-1} can be observed in all of the spectra and were assigned to

$CaCO_3$. In a CO_2 rich atmosphere there is a noticeable decline in $Ca(OH)_2$, seen as a dip at 3,632 cm-1 in Fig. 31. For the specimen, P-AC-24-AAC (Figure 32), presents peaks at 884, 1089, 1443, 1799 and 2505 cm^{-1} can be observed in all of the spectra and were assigned to $CaCO_3$. There is also a dip at 3,643 cm^{-1} due to a decreased amount of $Ca(OH)_2$ in Fig. 32 the sample P-AC-24. (BJÖRNSTRÖM, 2005; DELGADO et al., 1996; YU et al., 1999). In fibre–cement with a reasonable amount of CH, the principal carbonation product is calcite from higher carbonation rate of CH and C–S–H. (YLMÉN et al., 2013, SANTOS et al., 2015).

There is also a dip at *950–1,100 cm^{-1} corresponding to the peaks for C–S–H in all the samples spectrum in Figure 31 and Figure 32. Some transformations of sulfates appear to occur, emphasized by a shift in absorbance of the S–O stretching between 1,100 and 1,200 cm^{-1}. The spectrum of the product fits well with that of ettringite. In this experiment this was not observed sulfate phases, such as ettringite, this can be concluded because there are no observable signatures of the calcium sulfate species, such as gypsum, formed as a byproduct of the carbonation (GROUNDS et al., 1988; XIANTUO AND RUIZHEN, 1994).

Figure 31 - FTIR patterns of 10 h initial hydration composite before and after accelerated aging curing.

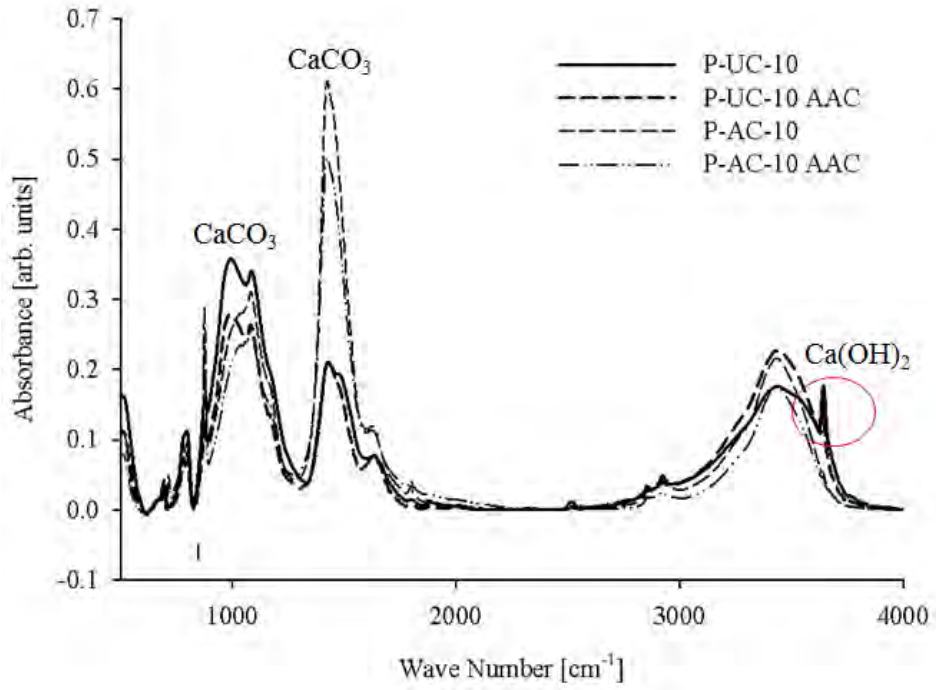

Source: authorships.

Figure 32 - FTIR patterns of 24 h initial hydration composite before and after accelerated aging curing.

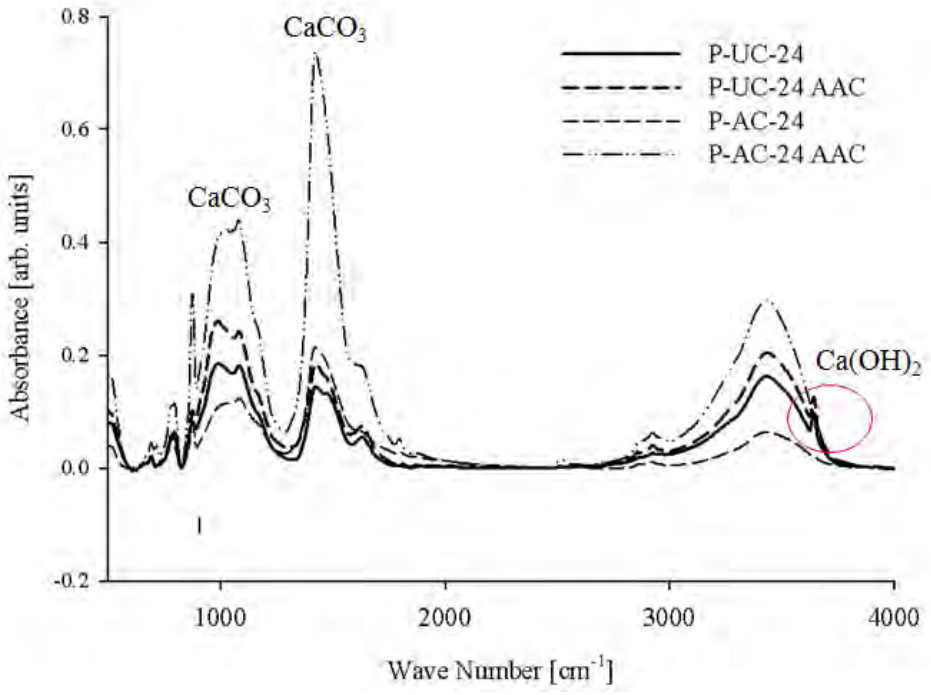

Source: authorships.

4.3.4. X-ray diffraction analysis

The XRD results shown in Figure 33 presents the patterns of the four sets of curing regimes correspond to 24 h of initial hydration. Through the XRD analysis, it was possible to identify the main phases of the composite. Calcium carbonate (calcite) is the main mineralogical phase observed in the uncarbonated samples due to the presence of the calcium carbonate, the second phase is calcium hydroxide (portlandite), third phase is quartz due to the mineral addition in the composition, the fourth is tricalcium silicate (alite) and the last one is dicalcium silicate (belita).

The remaining cement anhydrous phase, such as alite (C_3S) and belite (C_2S) are detected after seven days of thermal curing (Figure 33). Four phases of calcium carbonate can take place with increasing stability, amorphous calcium carbonate, vaterite, aragonite, and calcite (BLACK et al., 2007). It is observed the reduction of the amorphous background (broad band between 2θ = 25–40°C) from the uncarbonated to the carbonated composite, which means an increase of the crystallinity of the phases. In Figure 33, it is possible to observe the increase of the peak 2θ = 29.5° in the conditions P-AC-24 and P-AC-24-AAC this corresponds to calcite, due the primary reaction process of CO_2 that dissolves into the matrix and reacts with hydration products, such as calcium hydroxide (CH) and calcium silicate hydrate (C–S–H), and also reacts

with polymerized silica gel is known as secondary carbonation. Other $CaCO_3$ polymorphs (vaterite—Va and aragonite—Ar) were not detected.

The uncarbonated samples (P-UC-24, and P-UC-24-AAC) presented a higher intensity in the region of 2θ = 18° corresponding to the portlandite (calcium hydroxide) (ALMEIDA et al., 2013). The carbonation process in the early stages of hydration resulted in the decrease of portlandite, as shown by the lower intensity of the characteristic peak of the carbonated samples. Another important peak 2θ = 26.6°, correspond to the silica type quartz.

Figure 33 - XRD patterns of the four sets of curing regimes.

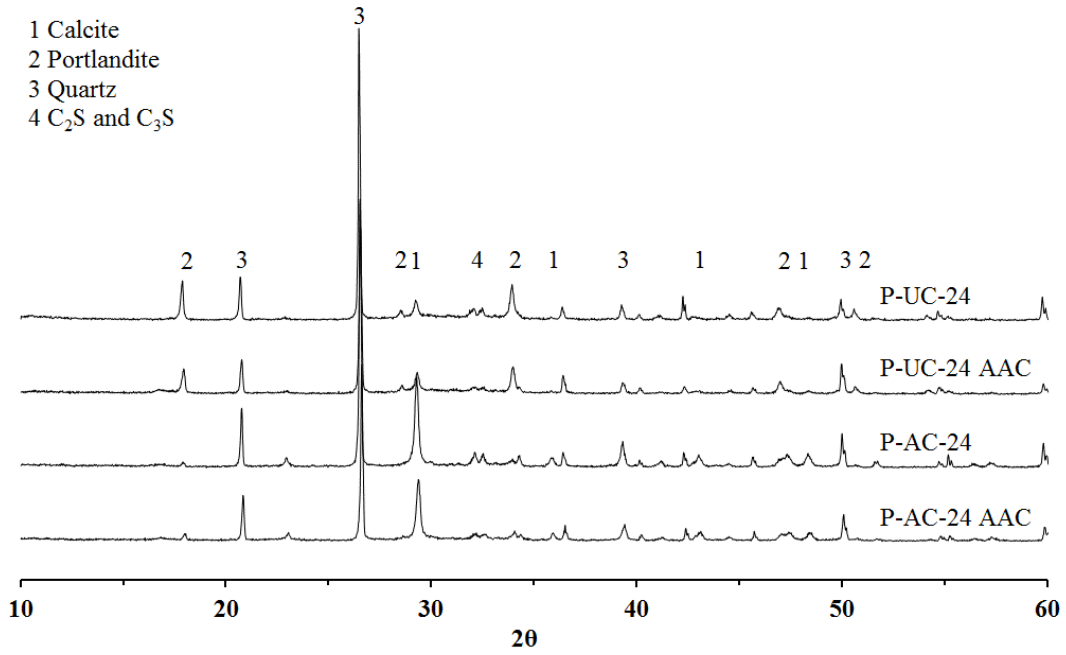

Source: authorships.

The figures 34 and 34 show the estimative amount of the identified phases, following it is mentioned a few global crystallographic parameters of each identified phase are: calcite (CaCO3), with reference cod 969009669, have a hexagonal crystallographic structure and the space group number of R -3c (167) (SITEPU et al., 2005); the portlandita $Ca(OH)_2$, with a reference cod 969000114, corresponds to hexagonal crystallographic structure and the space group number of P-3 m 1 (164) (HERNDERSON et al., 1962); the alite, with a reference cod 990010019, compound name 1540705, correspond to monoclinic crystallographic system and the space group number of C 1 m 1 (8) (DE LA TORRE et al., 2002); the belite, with a reference cod 969012790, correspond to monoclinic crystallographic system and the space group number

of P 1 21/c 1 (14) (TSURUMI et al., 1994); the quarzt, with a reference cod 962100189, corresponds to hexagonal crystallographic structure and the space group number of P 31 2 1 (152) (CASPI et al., 2005).

Figure 34 and Figure 35 shows estimated percentages of calcium hydroxide (Portlandite), calcium carbonate (Calcite), tricalcium silicate (alite), dicalcium silicate (belita) and quartz, were determined using the software PANalytical HighScore Plus for the samples in the initial ages P-UC-24 and P-AC-24, and after ageing P-UC-24-AAC and P-AC-24-AAC.

These estimated percentages correspond to the crystalline content of the material and didn't take into account the amorphous content of the material. The XRD patterns without (Figure 34a) and after (Figure 34b) carbonation indicated at AC condition, the calcium hydroxide (CH) was reduced 17.4% as well the belite was reduced 3.3%, these phases took part on the primary and secondary carbonation process, respectively (SANTOS et al., 2015; FERNANDEZ-BERTOS et al., 2004). A very similar situation was related with the increase of the calcite, corresponding to 23%.

These estimated percentages correspond to the crystalline amount of the material and didn't take into account the amorphous content of the material. The XRD patterns of before (Figure 35a) and after (Figure 35b) carbonation both after accelerated aging cycles indicates at AC condition, the calcium hydroxide (CH) was reduce 18.5% as well the belite 2.5%, this phases made part of the primary and secondary carbonation process, respectively (SANTOS et al., 2015; FERNANDEZ-BERTOS et al., 2004). In this case, the increase of the calcite corresponds to 31.7%.

It is possible to compare the amount of CH of 19.2% (Figure 34a) and 21% (Figure 35a) with 1.8% (Figure 34b) and 2.5% (Figure 35b), which is related to the decrease of alkalinity of the matrix. In the XRD analysis, for a crystallinity quantification, it is considered that below of 3% it is not a significant percentage for an identified phase.

By the other hand, in all the composites the main phase is the quartz and this phase presents a reduction on carbonated composites compared with uncarbonated ones. Also, the calcium carbonate is not the principal phase on the carbonated samples but in the section 3.1, Mechanical and physical properties, the carbonated composites present a statistically significantly better mechanical behavior than the uncarbonated composites. This improvement could be attributed to the reduction of the alkalinity and the amount of calcium carbonate formatted during the accelerated curing process.

Figure 34 - XRD patterns of quantification of the phases for: a) composite P-UC-24 and b) composite P-AC-24

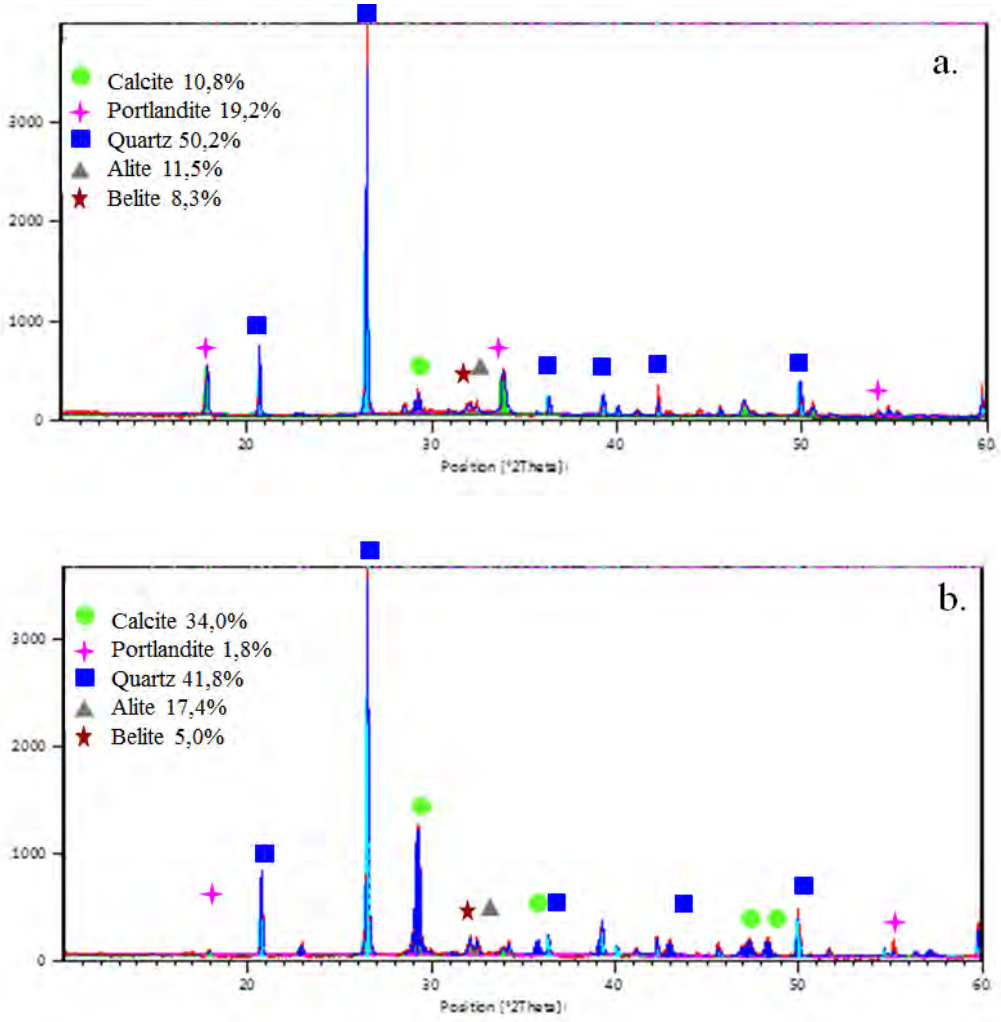

Source: authorships.

Figure 35 - XRD patterns of quantification of the phases for: a) composite P-UC-24-AAC and b) composite P-AC-24-AAC

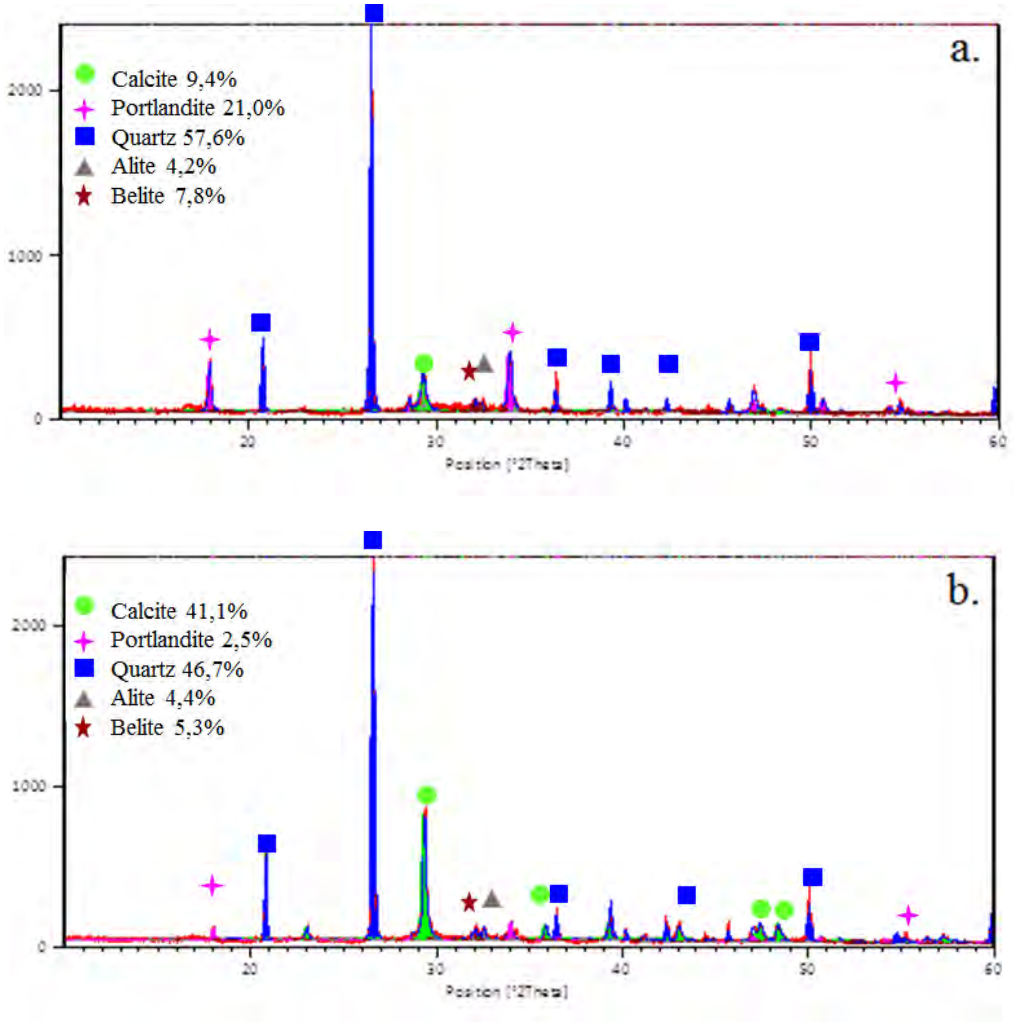

Source: authorships.

4.3.5. Microstructure of the composites by SEM

Micrographs were obtained by a SEM in Back-Scattered Electron Image (BSEI) mode for the observation of the morphological features of cut and polished surfaces of composites subjected to uncarbonated and early age carbonated composites, both after 200 accelerated aging cycles, P-UC-24 and P-AC-24 (Figure 36 a,b), P-UC-24-AAC and P-AC-24-AAC (Figure 37 a,b). All the images have an accelerating voltage of 15 kV. The SEM micrographs shown are typical images of the microstructure chosen from around six representative images for each composite treatment.

Figure 36 depicts cracks (arrow 1) and a more porous matrix is observed in the uncarbonated composite, due the initial porosity of a fiber-cement matrix, especially because of the production by the slurry-dewatering and significant volume of fibers, which eases the

penetration of CO_2 in the composite (TONOLI et al., 2010). The cement matrix of the carbonated composite is denser and compact (Figure 36b).

The uncarbonated composite shows the heterogeneous and distribution of unbleached cellulose fiber (arrow 2 in Figure 36a). Arrow 3 in Figure 36a presents cracks surrounding the cellulose fiber, which are the indicative of a weak contact between cellulose fibers and matrix. The deficient fiber-matrix interface is linked to lower mechanical properties (SAVASTANO et al., 2003; SAVASTANO et al., 2005). However, some fibers in the uncarbonated composites present good contact with the cement matrix (arrow 4 in Figure 36a), this could be attributed to the use of an inert mineral addition, silica, have good packing effect due to the 28% of filler using in the formulation. The accelerated carbonated process is refining the porosity of the cement matrix and improving the contact between cellulosic fibers and the matrix, and possibly favoring the better adhesion between them (arrow 5 in Figure 36b) (PIZZOL et al., 2014). The accelerated carbonation did not avoid some mineralization inside of the cellulose fibers, as shown by arrow 6 in Figure 36b.

Figure 37 shows the uncarbonated and carbonated composite both after accelerated ageing cycles. The water absorption of natural fiber has a direct influence on the reinforcing performance and durability of the fiber in the cement matrix (WEI et al., 2015). At uncarbonated and aged composite, the fibers present creep, due the fibers absorb water, accompanied by volume expansion, from the soak and drying cycles (arrow 7 in Figure 37a). Before and after the aging cycles the uncarbonated composite depicts cracks and a more porous matrix than the carbonated composite (arrow 8 in Figure 37a). At early ages in the carbonated composites it is observed the improved fiber–matrix interface of the cellulose fibers and the diminutive porosity at the interface between aggregate particles and cement matrix. According to Farahi et al. (2013) and Almeida et al. (2013) precipitation of the calcium carbonate during carbonation is formed favorably at the aggregate-matrix interface, since this area is generally the most porous and thus weakest zone in the cement composites. After the aging cycles present some crack propagation in the carbonated composite (arrow 9 Figure 37b). However, most of the fibers do not present rupture (arrow 10 Figure 37b) it means that after the cycles, the energy is still absorbed by the composite due to the frictional slipping process during the pulling-out of fibers giving a good interface with the matrix (FARAHI et al., 2013).

Figure 36 - SEM BSEI of the composites in the early ages. a.) Uncarbonated 50 nm sample P-UC-24. Arrow 1: cracks and pores in the matrix; Arrow 2: distribution of the fiber; Arrow 3: cracks and pores around the fibers; Arrow 4: interface between the fibers. b.) Carbonated sample P-AC-24. Arrow 5: adhesion between fibers; Arrow 6: mineralization of the fiber.

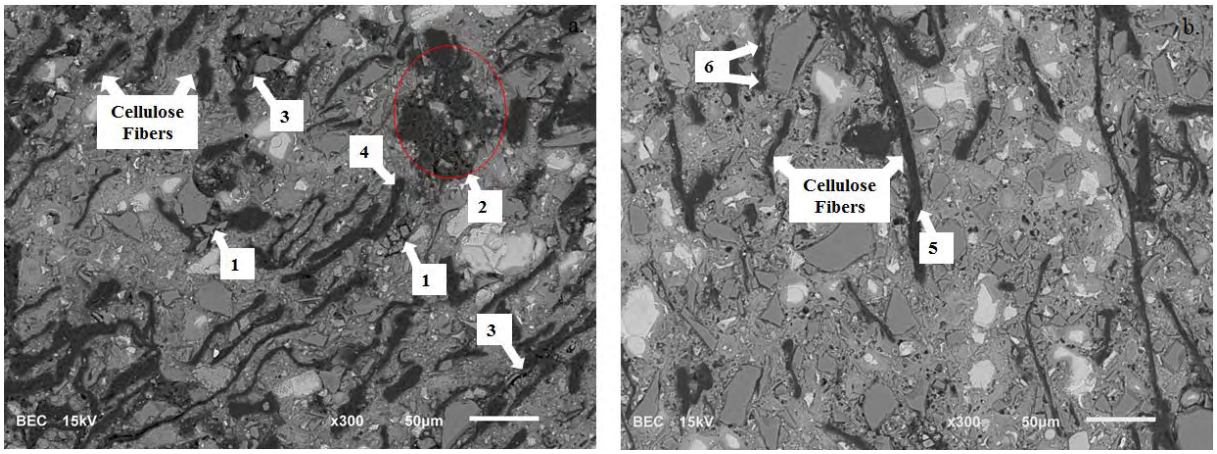

Source: authorships.

Figure 37 - SEM BSEI of the composites after the accelerated aging tests. a.) Uncarbonated sample P-UC-24-AAC. Arrow 7: fibers present creep. Arrow 8: cracks and pores in the matrix b.) Carbonated sample P-AC-24-AAC. Arrow 9: crack propagation. Arrow 10: fibers without rupture.

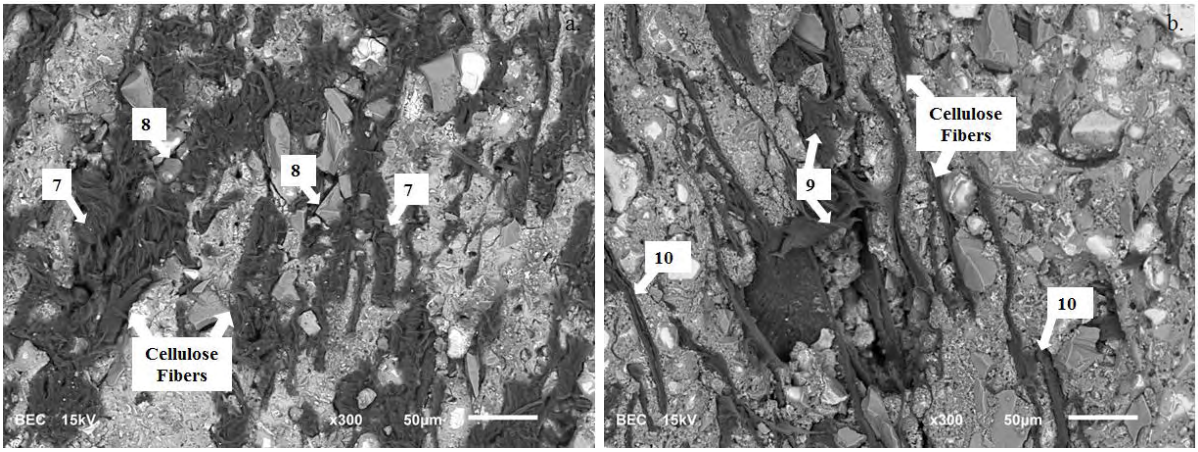

Source: authorships.

Figure 38 and 39 present typical SEM micrographs of uncarbonated and carbonated samples that were obtained by SEM in Back-Scattered Electron Image (BSEI) mode. Figure 38 shows the composite before carbonation (P-UC-24), EDS analyses depict strong peaks of Ca and Si. The high content of the selected elements indicates the presence of quartz (Fig. 38 b-1), typical amorphous C–S–H (Figure 38 b-2), crystalline CH (Fig. 38 b-3) and CH into the fiber cavity (lumen) (Fig. 38 b-4) after complete seven days of thermal hydration process.

Figure 39 shows the composite after carbonation (P-AC-24). Generally, the carbonated composite has finer texture compared to the uncarbonated sample (P-UC-24 in Fig. 38). While the corresponding XRD pattern suggests formation of carbon products, the SEM picture does not provide any evidence of the crystalline form of carbonates. However, it is observed relatively high carbon content can be distinguished into the fiber cavity (lumen) based on the Energy Dispersive Spectroscopy (EDS) spot analysis (Fig. 39 b-4). The biggest amount of carbon in fiber cavity correspond to the main element of the organic constitution of the fiber.

The EDS analysis of the spots shown reveals strong intensities of Ca, Si, O and C (Figure 39 b1-4), suggesting the presence of a hybrid of hydrates and carbonates. Comparison of relative intensities of carbon and oxygen in Fig. 4.12 with those in Fig. 39 suggests that O/C is evidently greater in the P-AC-24 sample. Similar result was found by Rostami et al., (2012).

Figure 39b-2 carbonation of C–S–H, whatever seems to be even more dependent on the permeability of the matrix. Fast decalcification of C–S–H is expected in highly permeable composite, accompanied by carbonation shrinkage, which is accelerated when the $CaO:SiO_2$ molar ratio (C/S) is reduced below 1.2 (CHEN et al., 2006). Also, suggesting carbonation modified C–S–H is Si-rich but its binding capacity by Ca–O structure is maintained (ROSTAMI et al., 2012). Figure 39 b-1 is related to the silica hydrated; the remaining silica gives an absorption profile resembling condensed silica (YLMÉN et al., 2008).

Figure 38 - Uncarbonated sample P-UC-24: a) SEM image. b) EDS analysis

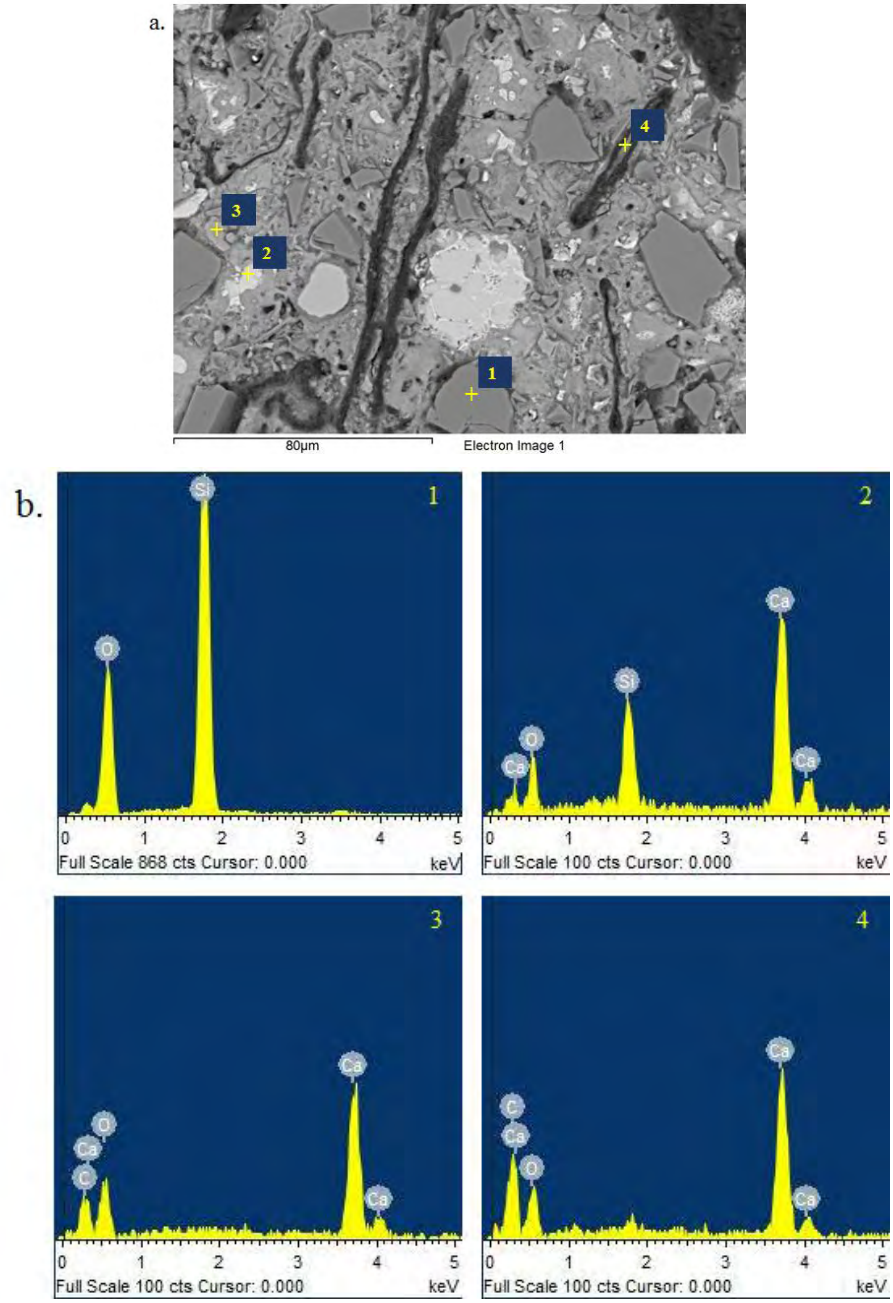

Source: authorships.

Figure 39 - Carbonated sample P-AC-24: a) SEM image. b) EDS analysis

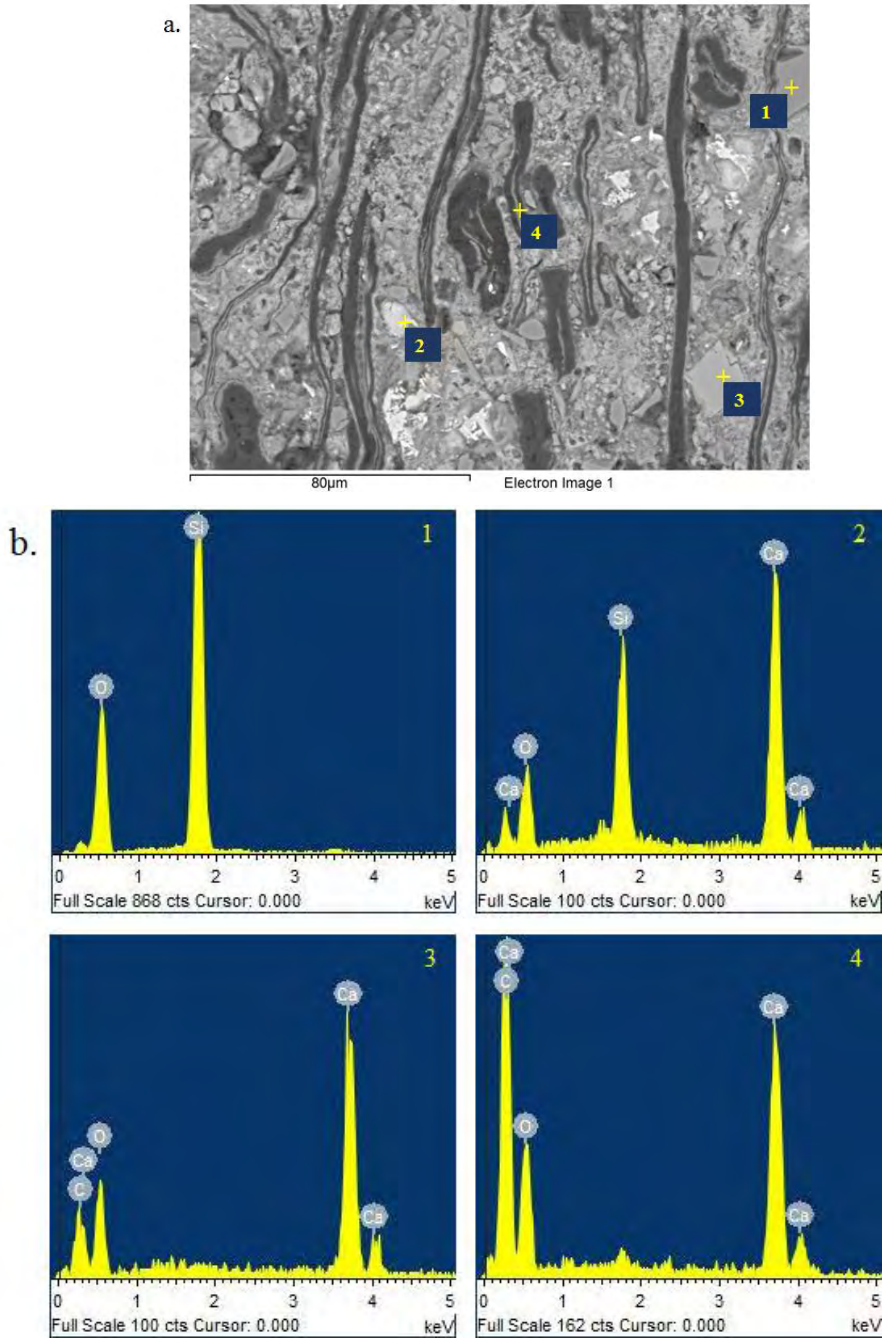

Source: authorships.

4.3.6. Specific surface area

The specific surface area of hardened cementitious composite indicates the amount of accessible fine pores (THOMAS et al., 1999). The surface area of well-hydrated cement composite as measured using water vapor, is remarkably consistent values between 100 and 200 m^2/g of dry cementitious composite (RARICK et al., 1996; THOMAS et al., 1999). BET

method includes internal surfaces present in microcracks or in open pores at only one end (TAYLOR, 1990).

Evaluated according to the BET method detailed in Section 3.3.3.7, experimental specific surface areas for the eight paste mixtures in this study are reported in Table 22. The BET specific surface area values for specimens stored in air curing, range from 39 to 57 m2/g in the initial ages and range from 37 to 50 after aging cycles. Unaged samples present bigger specific surface area than the aged samples. The carbonated samples present bigger specific surface area than the uncarbonated samples, due the carbonation of portlandite is manifested by the crystallisation of numerous calcite crystals on the portlandite platelets (CHRISTOPHE et al., 2006; PHAM AND PRINCE, 2014). The greatest specific surface area was for the condition P-AC-24 follow by the P-AC-10, but these two composites had a pore structure less accessible to water vapor in comparison to the other regimes as it shows at table 19 the physical properties.

Table 22 - Specific surface areas from Dynamic vapor sorption DWVS.

Curing Regime	A_{BET} (m^2/g)
P-UC-10	39.32
P-UC-24	45.98
P-AC-10	54.82
P-AC-24	56.87
P-UC-10 - AAC	37.82
P-UC-24 - AAC	40.78
P-AC-10 - AAC	49.83
P-AC-24 - AAC	42.83

Source: authorships.

4.4. Stage 5: Evolution of the hydration kinetics on unbleached cellulose pulp fiber-cement composites subjected to accelerated carbonation at very early age

4.4.1. Thermogravimetry (TG) analyse and X-ray diffraction analyse

Along 10 h with the eleven sets of samples it is possible to evaluate the kinetics of carbonation through the differential thermogravimentric analysis (DTA) and thermogravimetry analysis (TG), corresponding to Figure 40, 41 and Figure 42. According to the literature, the mass loss at 100°C is associated to the escape of the pore water. The peak temperatures depend on the technique and amount present, and probably on the degree of crystallinity, being typically shifted to 180-190°C for the material present in cement composites. DTA curves have been reported for other AFm phases (TAYLOR, 1990). But the absence of ettringite (AFt) peaks from an XRD pattern at Figure 43, could be a proof that this phase may not be formed in the fiber-cement carbonated composite that use silica as a mineral addition. This could be beneficial considering that ettringite (AFt) formation has been previously suggested as one of the degradation mechanisms of cellulose pulp fiber into cement matrix (MOHR et al., 2005; MOHR et al., 2006). The remaining cement anhydrous phase, such as alite (C_3S), belite (C_2S) and tricalcium aluminate (C_3A) are also detected peaks from an XRD pattern at Figure 43.

DTA curves of C-S-H preparations show endotherms at 100°-200°C and exotherms at 835°-900°C. CH begins to decompose at an easily detectable rate at about 370°C; under typical conditions for TG, decomposition is 98% complete at the end of the step at 580°C (TAYLOR, 1990). Figure 42 shows the TG curve range of CH decomposition, it could be observed the slopes of mass loss in times of 0 h, until 7 h. DTA curves (Figure 40) and TG curves (Figure 41) show what is evidence in the literature, that CO_2 simultaneously reacts with C–S–H and CH and that the decalcification of C–S–H takes place prior to the formation of silica gel, the latter starting at later stages of carbonation (GROVES et al., 1991). Based on the evolution of 10 h carbonation process in a fiber-cement composite that uses silica as a mineral addition, it is possible to split in two groups from P-AC-24-0h to P-AC-24-5h and P-AC-24-6h to P-AC-24-10h. The first group presents the rapid rate of calcium hydroxide carbonation process and the second group shows the slow rate of carbonation process due to the mass of loss percent observed for this phase. CH carbonation may be initially more rapid than that of the C–S–H gel, but this situation soon reverses because of the formation of a layer of $CaCO_3$ micro crystals at the surface of CH (GROVES et al., 1991; THIERY et al, 2007).

On both groups, the rate of calcium carbonate formation is constantly growing. The dissociation

pressure of calcite reaches at 894°C and the decarbonation reaction is highly endothermic. The rate of decarbonation becomes significant at 500-600°C if a sufficiently low partial pressure of CO_2 is maintained or if the calcite is intimately mixed with materials, such as quartz at 560°C (TAYLOR, 1990). The C–S–H is progressively decalcified, being converted to $CaCO_3$ and silicate hydrates. The porosity of fibre–cement composites is typically high enough to permit constant CO_2 diffusion, which results in the $Ca(OH)_2$ to be further reduced and the calcium ions released from C–S–H react with carbon dioxide (FERNANDEZ-BERTOS et al., 2004).

Figure 40 – DTA curves of Carbonated Curing process along 10 h in fiber–cement specimens

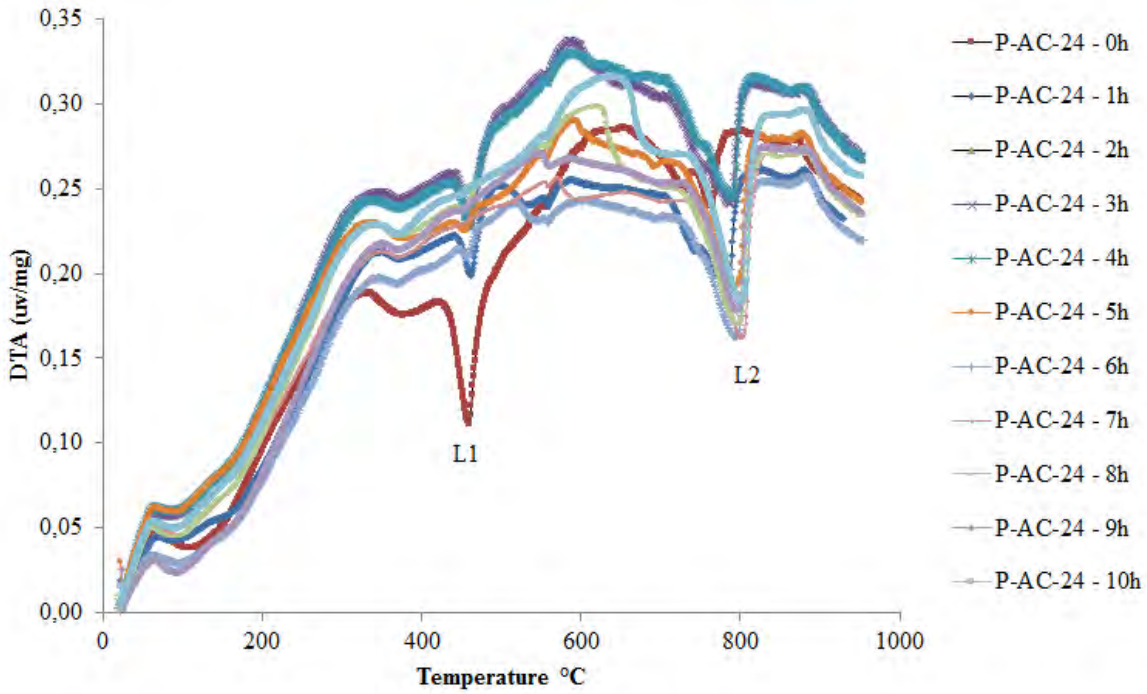

Source: authorships.

Figure 41 – TG curves of Carbonated Curing process along 10 h in fiber–cement curing regimes

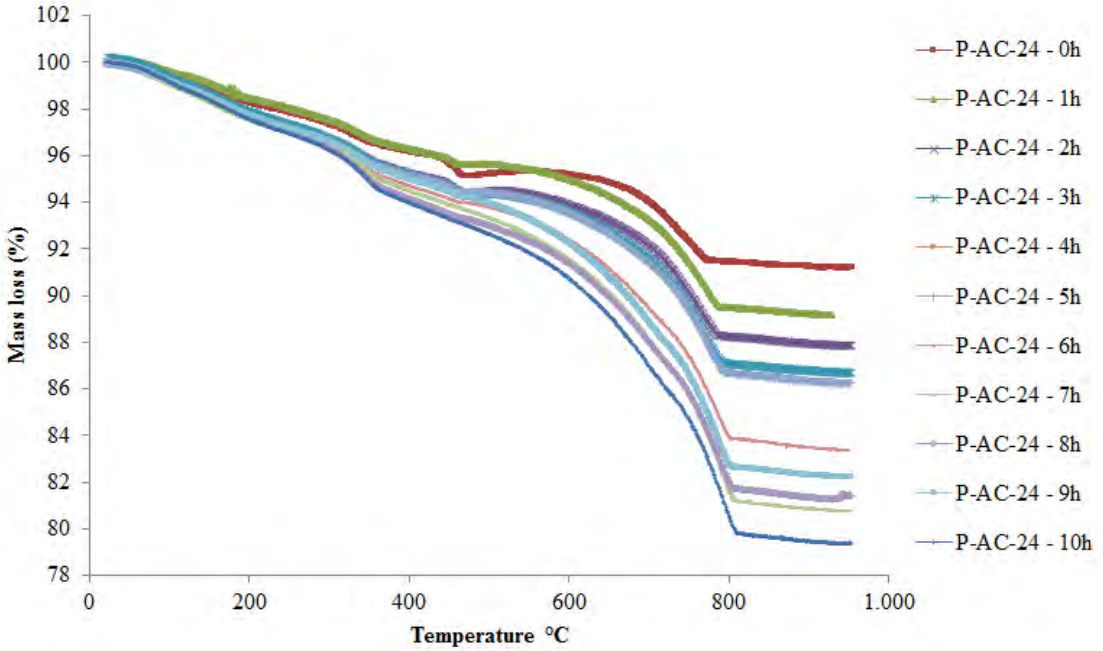

Source: authorships.

Figure 41 – TG curves of Carbonated Curing process along 10 h in fiber–cement specimens, range of CH decompose.

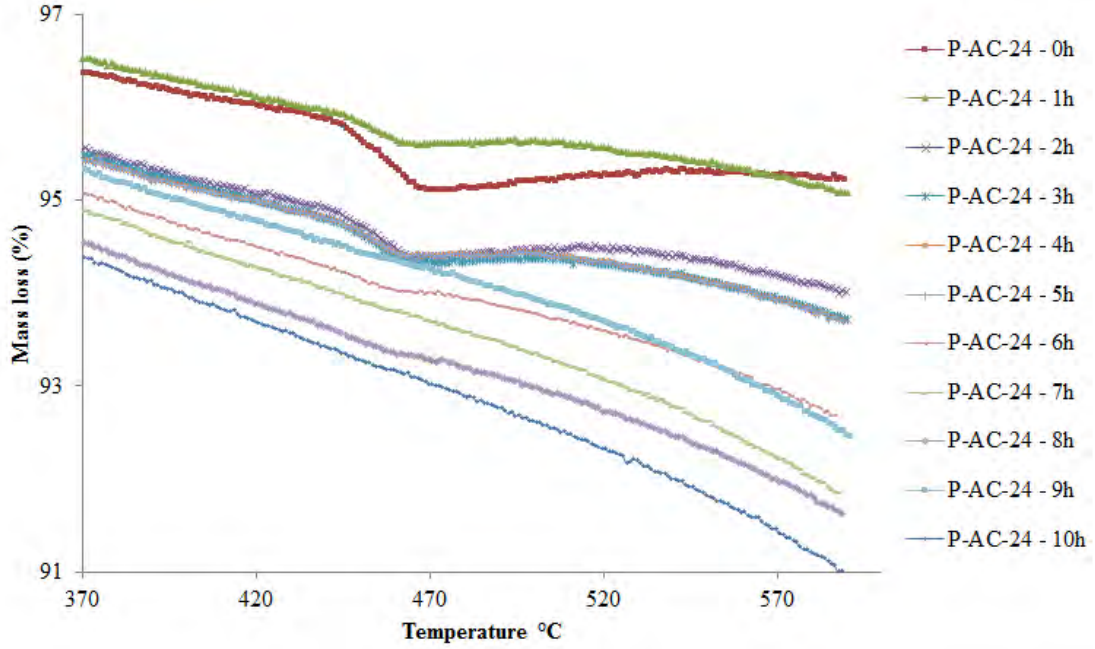

Figure 43 - XRD patterns of the four sets of curing regimes.

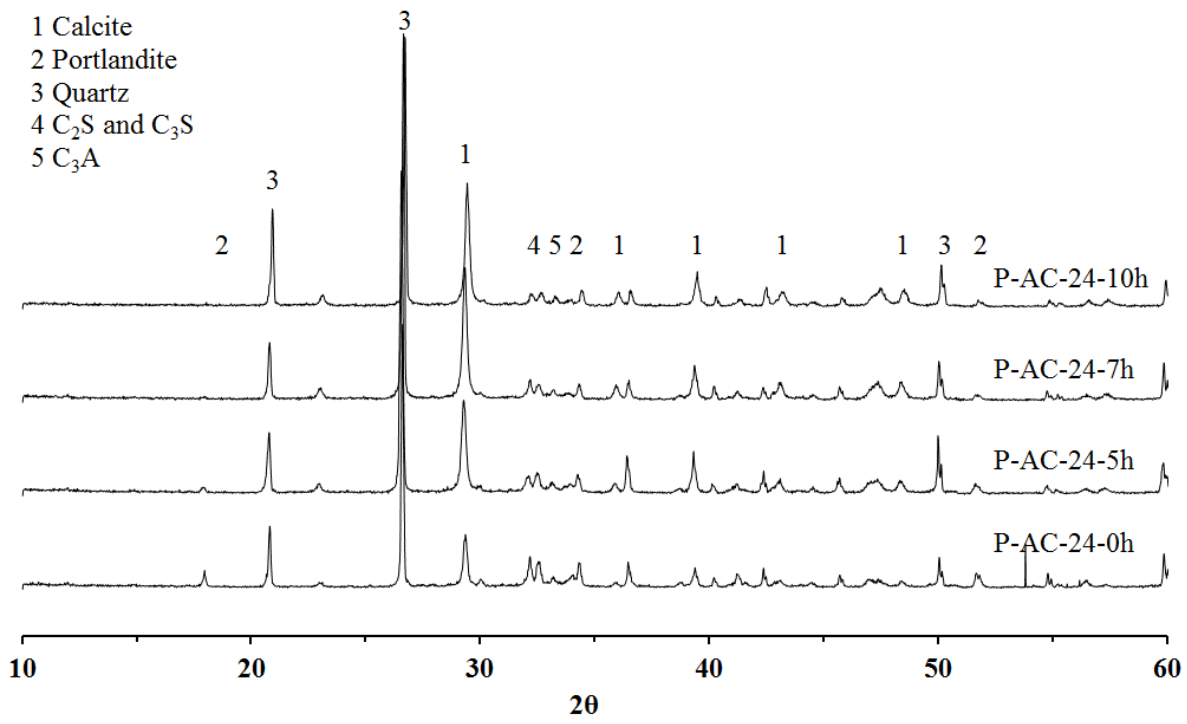

Source: authorships.

According with Taylor (1990), TG has often been used to determine CO_2, but is not suitable because the loss at 700-900°C is not only due to CO_2. The presence of calcite peaks is a proof that CO_2 is existing. Also, the $CaCO_3$ could occur in other forms (e.g. as vaterite and aragonite) (YLMÉN et al., 2009), but in this 10 h analysis of accelerated carbonated process, the XRD pattern (Figure 43) indicates that there is an absence of this last phases mentioned, and calcite is the only form of calcium carbonate identified.

The estimated amount of mass loss of calcium hydroxide $Ca(OH)_2$ and calcium carbonate ($CaCO_3$) is calculated following the procedure proposed by Borges et al. (2010) using the equations (14) and (15). This procedure considers increased molecular mass resulting from the carbonation process, as shown in Table 23 and would suggest an increase to the percentage of mass lost, confirmed in the thermogravimetric data (DTG) presented in Figure 40 Dehydroxylation, L1, occurs between 450 and 500°C, the mass loss in this range decreases as the carbonation exposure time increases, and decarbonation losses, L2, occurs between 600–750°C. The initial amount of $Ca(OH)_2$ may be directly calculated from Eq. (16). The corresponding amount of $CaCO_3$ resulting from the total $Ca(OH)_2$ that carbonated was

estimated using Eq. (17).

$$\%\mathrm{CH} = \mathrm{L1} \cdot \frac{74}{18} = 4.11 \cdot \mathrm{L1} \quad \text{(Eq. 14)}$$

$$\%\mathrm{CC} = \mathrm{L2} \cdot \frac{100}{44} = 2.27 \cdot \mathrm{L2} \quad \text{(Eq. 15)}$$

$$\%\mathrm{CH}_{\,\mathrm{Initial}} = \%\mathrm{CH} + (0.74 \cdot \%CC) \quad \text{(Eq. 16)}$$

$$\%\mathrm{CC} = 1.35 \cdot \%\mathrm{CH} \quad \text{(Eq. 17)}$$

On Table 23, after elaborating the estimative amount of the main phases as calcium hydroxide, the C-S-H gel and the calcium carbonated, the two groups mentioned previously prevalent, but with a difference, the first group (from P-AC-24-0h to P-AC-24-5h) presents the fast decrease of amount of CH and absence of C-S-H carbonation process. The second group (P-AC-24-6h to P-AC-24-10h) shows the slow rate of calcium hydroxide carbonation process and the occurrence of C-S-H carbonation process. The primary and secondary accelerate carbonation occurs in a couple of hours which still consider that occurs as simultaneously reaction.

Table 23 - The estimation of the extent of carbonation of C–S–H from TGA data, before and after supercritical carbonation treatment, non-aged and aged.

Curing Regime	**Uncarbonated composite**			**Curing Regime**	**Carbonated composite**				
	CH from TGA (%)	CC from TGA (%)	Calcula-tion of initial CH (%)		CH from TGA (%)	CC from TGA (%)	Amount carbonated of CH (%)	Expected CC from carbonating CH (%)	Carbonates formed by C–S–H (%)
P-AC-24-0h	4.32	6.81	9.35						
				P-AC-24-1h	2.05	8.17	7.3	9.85	-1.7
				P-AC-24-2h	1.76	9.26	7.58	10.24	-0.98
				P-AC-24-3h	1.73	9.19	7.63	10.3	-1.11
				P-AC-24-4h	1.73	12.05	7.63	10.3	-1.75
				P-AC-24-5h	1.11	14.18	8.25	11.13	3.05
				P-AC-24-6h	0.82	15.32	8.53	11.52	3.8
				P-AC-24-7h	0.57	20.49	8.78	11.85	8.65
				P-AC-24-8h	0.86	20.38	8.49	11.46	8.92
				P-AC-24-9h	0.86	18.77	8.49	11.46	7.31
				P-AC-24-10h	0.53	21.16	21.15	11.91	9.24

Source: authorships.

Between 7 h and 10 h of carbonation process, the Table 23 presents a little increase of the amount of CH and a decrease of the amount of the $CaCO_3$,. This could be attributed to the interchange of Ca^{2+} ions in the carbonation process, that after 7 h it is considered that occurs complete in the CH carbonation process, so from this point the primary carbonation process enter in a cycle don't allowed to reduce more the portlandite, nor did influence the increase of

the calcium carbonate. At 10 h of carbonation process the increase of the amount of calcium carbonate it is only attributed to the secondary carbonation process.

4.4.2. FTIR spectrometer analysis

In all of the samples, except for the P-AC-24-0 h, the carbonate is easily seen with DR-FTIR spectroscopy within 5 h, 7 h and 10 h of exposure to CO_2 atmospheres.

In a moist atmosphere the CO_2 reacts with calcium extracted from both the clinker and the calcium silica gel. Figure 44 shows the peaks at 879, 1088, 1425, 1804 and 2511 cm^{-1} can be observed in all of the spectra and were assigned to $CaCO_3$ for the condition P-AC-24-5 h, P-AC-24-7 h and P-AC-24-10 h. The formation of calcium carbonate is evident since 5 h of carbonation process with a maximum peak at 10 h carbonated condition. It is interesting to note that for the 10-h hydration sample there is also a dip at 3000 cm^{-1} and ~950-1,100 cm^{-1} corresponding to the peaks for C-S-H (YLMÉN et al.,2009). The band at ~1,650 cm^{-1}, together with the increased intensity in the OH-stretching region, indicates absorption of water for all hydration times.

The formation of $CaCO_3$ in cement is a complex process that can contain reactions at various particle surfaces. In the early stages the carbonates formed could be considered amorphous, since the crystallites have not yet developed a well-defined structure. The broadening of the band observed at 1,088 cm^{-1} indicates a less ordered structure because the peak is expected to be narrow if the phases are crystalline (YLMÉN et al., 2013).

At early edges the formation of $CaCO_3$ is consistent with the infrared spectra of synthesized amorphous calcium carbonate (LAM et al., 2007; ANDERSEN AND LJERKA BREČEVIĆ, 1991). At later stages a more crystalline product can be expected. Consequently, the characteristic vibration peaks in the region 1,300 − 1,700 cm^{-1} are characteristic of all carbonate species irrespective of the chemical and physical form (YLMÉN et al., 2013).

In a CO_2 rich atmosphere there is a noticeable presence of $Ca(OH)_2$, seen as a peak at 3,643 cm^{-1} in the condition P-AC-24-0 h. Also, asymmetric stretching of SO_4^2 at 910 cm^{-1} (MYNENI et al., 1998) was observed only in uncarbonated matrix, different of symmetric stretching at 1000 cm^{-1} occurring in P-AC-24-0 h. It indicates the decrease of SO_4^2 free ions when carbonation process occurs.

Figure 44 - FTIR patterns of Carbonated curing process along 10 h in fiber–cement specimens

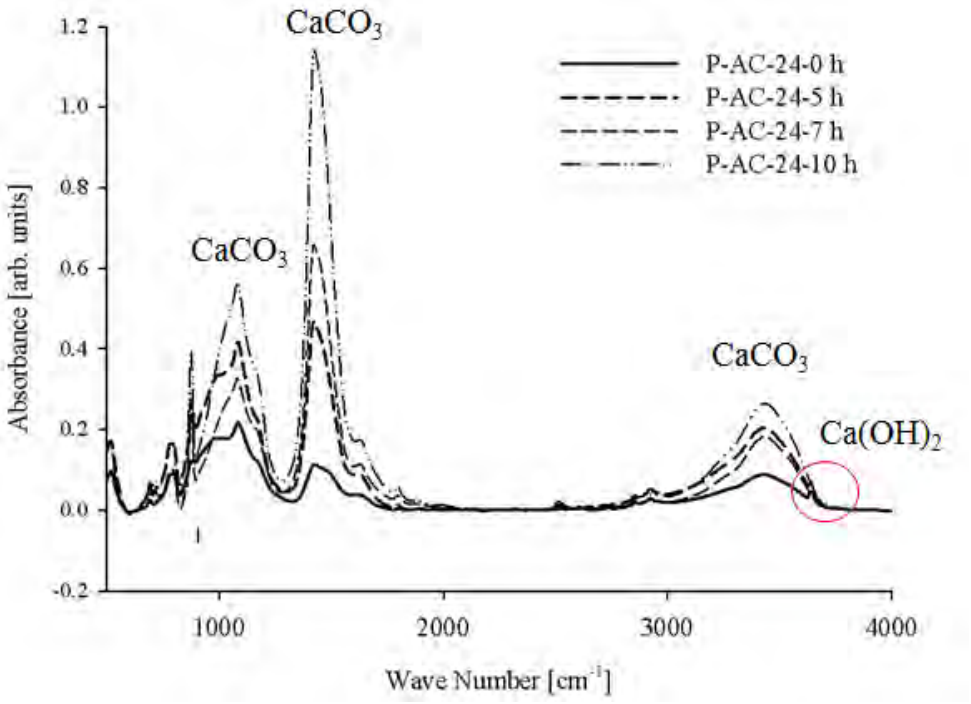

Source: authorships.

4.4.3. Microstructure of the composites SEM

Micrographs presents were obtained by a SEM in Back-Scattered Electron Image (BSEI) mode for the observation of the morphological features of cut and polished surfaces of composites subjected to a very early age carbonated composites, the condition P-AC-24-0 h, P-AC-24-5 h, P-AC-24-7 h and P-AC-24-10 h. The images have a magnification of 300 x and accelerating voltage of 15 kV. The SEM micrographs shown are typical images of the microstructure chosen from around six representative images for each composite treatment.

Figure 45 a depicts arrow 1 the initial porosity is observed in the matrix, which is influenced by the application of the slurry-dewatering and manual pressing in the composite at the fabrication process and the significant volume of fibers; that eases the penetration of CO_2 for enhanced the composite (TONOLI et al., 2010). The cement matrix (including around the fibers) become denser and compact along the 10 h of carbonation process (Fig. 45b, c, d).

The uncarbonated composite presents swelling in the fibers, due the water absorption, accompanied by volume expansion, from 24 h of initial hydration process of the matrix (arrow 2 in Figure 45a). After 5 h of carbonation process the cellulose fiber shrinkage, arrow 3 (Figure 45b,c,d) shows the interface fiber-matrix, it is notable how the accelerated carbonation process

improves the contact between cellulosic fibers and cement matrix, and possibly favoring the better adhesion between them (PIZZOL et al., 2014). However, arrow 4 (Figure 45 c,d) depicts cracks in the matrix that are observed in two of the carbonated conditions (P-AC-24-7h and P-AC-24-10h) and surrounding of some of the cellulose pulp. These cracks are indicative of a weak contact between cellulose fibers and matrix, the deficient fiber-matrix interface is linked to behavior of mechanical properties (SAVASTANO et al., 2003; SAVASTANO et al., 2005). These cracks could appear due the fiber swelling and shrinkage along the matrix hydration process. Another problem that appears in the samples under carbonated conditions (P-AC-24-7h and P-AC-24-10h) is indicated with Arrow 5; the early carbonation did not prevent the re-precipitation of hydration products inside the cellulose fibers as different alkaline solid phases into the fiber. This re-precipitation of solids into the fiber voids (both fiber cell wall and fiber lumen) induces the embrittlement of the cellulose fibers by the attack of released alkaline's ions (SANTOS et al., 2015; TONOLI et al., 2016).

Figure 45- BSEI SEM for fabricated composites. a.) P-AC-24-0 h. b.) P-AC-24-5 h. c.) P-AC-24-7 h. d.) P-AC-24-10 h

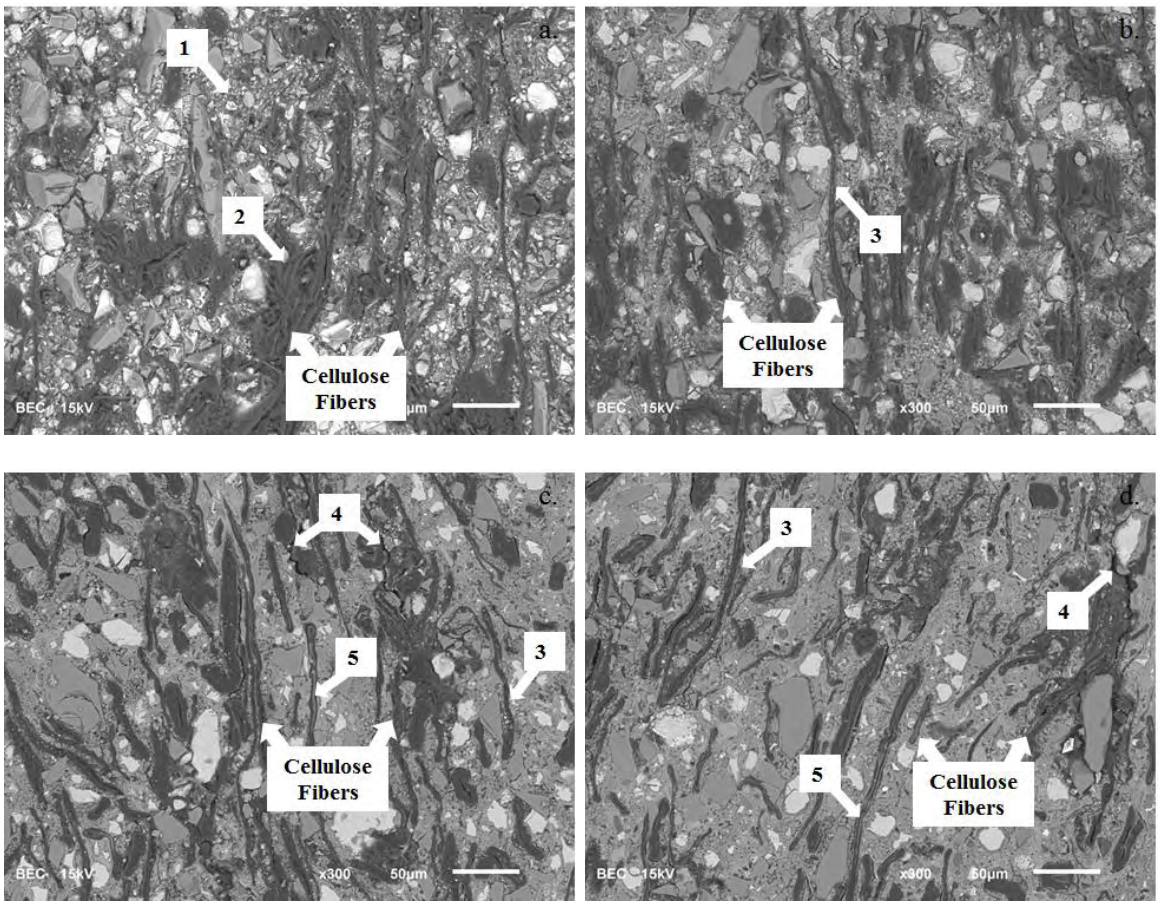

Source: authorships.

5. FINAL CONSIDERATIONS

5.1. Stage 2: Definition of optional parameters for supercritical carbonation process of vegetable Fiber-cement composites at a very early age

The main contributions for define parameters for supercritical carbonation process at very early age of vegetable Fiber-Cement Composites are:

- The results indicate that the bleached pulp reinforcement carbonated composites show average higher values of MOR, LOP, MOE, and SE that were 24%, 24%, 27% and 25%, relating the unbleached pulp reinforcement carbonated composites. This difference was attributed to the degree of crystallinity, the lignin content and hydrophobic of the vegetal fiber that could influence the improvement of the mechanical behavior of a cementitious composite subjected to carbonation. The SEM images showed that bleached cellulose pulp had better fibers-matrix adhesion than the unbleached cellulose pulp.
- The carbonation time of 2 h or 1 h resulted in no statistically significant effect on the specimen's bulk density, modulus of rupture, modulus of elasticity or specific energy. It would appear that for guaranteed improvements to the mechanical properties of composites, the accelerated supercritical carbonation process only requires 1 h.
- Thermal hydration duration of 24 h or 48 h resulted in no statistically significant effect on the physical and mechanical properties (bulk density, water adsorption, modulus of rupture, modulus of elasticity and specific energy) of the vegetable fiber-cement composites. During the thermal curing of samples, hydration occurs at a rapid rate; for both cases hydration results were similar, highlighted by the TG/DTA results which revealed similar percentages of calcium hydroxide and calcium carbonate for specimens with 24 h or 48 h of thermal curing.
- The results confirm what previous studies have concluded regarding the effectiveness of the carbonation curing process in decreasing the alkalinity and mitigating the degradation of cellulose fibers of natural fiber reinforced cement composites.

5.2. Stage 3: Comparative study between two kinds of mineral addition in cellulose pulp fiber-cement composites subjected to accelerated carbonation at very early age.

The main contributions for a comparative study between two kinds of mineral addition in cellulose pulp fiber-cement composites subjected to accelerated carbonation at very early age are:

- The effect of the mineral addition resulted in statistical significant effect on the mechanical properties (modulus of rupture, limit of proportionality and modulus of elasticity) of the unbleached Pinus vegetable fibre -cement composites with 24 h of initial curing and subject to carbonation process. The composite with addition of ground silica resulted in flexural test average statistically significant higher values of Limit of proportionality around 46% comparing with the limestone composite. This could be attribute to the interface interaction between the matrix and the mineral addition. On the other hand, the effect of the mineral addition resulted in no statistical significant effect on the physical properties (water absorption and bulk density). Which means both carbonated cementitious matrices, have the same densification and compaction
- The initial hydration duration of 10 h or 24 h resulted in no statistically significant effect on the physical and mechanical properties (bulk density, water adsorption, modulus of rupture, modulus of elasticity and specific energy under flexure) of the vegetable fiber-cement composites.
- The composite with silica addition consumes higher amount of calcium hydroxide (CH) in comparison with the composite with limestone addition, based on the CH residue detected in the XRD analysis: 3.5% and 11.5% respectively. This could be due the XRD patterns of quantification of the phases of each mineral addition and owing silica chemically stable at low temperatures.

5.3. Stage 4: Durability and hydration kinetics study in carbonated fiber-cement composites using silica as a mineral addition.

The main contributions of the of durability and hydration kinetics study in carbonated fiber-cement composites using silica as a mineral addition are:

• The use of silica as a mineral addition in cementitious composites subject to uncarbonated and very early age carbonated curing process both after 200 accelerated aging cycles presents

no reduction of mechanical performance in MOR, LOP and MOE, except the SE. This suggested that the use of silica in conjunction with unbleached pine fiber is an appropriate strategy to mitigate degradation of the composite, even if it is not present in an autoclaved condition. The SEM images show on both composites a good interfacial fiber-matrix bonding strength. Also, the XRD results, on both uncarbonated and carbonated composites, does not show the presence of ettringite formation which favorites decrease the degradation of pulp fiber into cement matrix. However, further studies for do not have a reduction in SE on the composites after accelerated aging cycles, still needed.

- The initial hydration duration of 10 h or 24 h resulted in no statistically significant effect on the physical and mechanical properties (bulk density, water adsorption, modulus of rupture, modulus of elasticity and specific energy under flexure) of the vegetable fiber-cement composites. During the curing of samples, hydration occurs at a normal rate; for both cases hydration results were similar, highlighted by the TG/DTG results which revealed similar percentages of calcium hydroxide and calcium carbonate for specimens with 10 h or 24 h of curing.

- In the TGA, for the peak at 800°C related to decarbonation of $CaCO_3$, uncarbonated composites before ageing and initial hydrated by 24 h presented loss of mass of about 4.15%, while the carbonated composites before ageing showed loss of mass around 23.6%. These results suggest the effectiveness of the treatment with accelerated carbonation for 10 h and the efficacy to measurement the increase of $CaCO_3$ after the curing process, due to the use of silica as neutral mineral addition on the composite.

- The XRD estimative amount of calcium carbonate in the carbonated composite presents an increase before and after accelerated aging from 34% to 41.1%. This increase could be attributed to the natural carbonation at the aging chamber and the cement hydration process.

5.4. Stage 5: Evolution of the hydration kinetics on unbleached cellulose pulp fiber-cement composites subjected to accelerated carbonation at very early age

The main contributions of the study of the evolution of the hydration kinetics on unbleached cellulose pulp fiber-cement composites subjected to accelerated carbonation at very early age are:

- Following 10 h of carbonation process in a fiber-cement composite that uses silica as mineral addition, DTA results shows that after 7 h of carbonation process it is considered a complete reduction of the amount of calcium hydroxide. This study suggested that the carbonation time with atmospheric CO_2 concentration (20 vol%) could be reduce from 10 h to 7 h.

- The carbonation kinetic hydration at very early edge on unbleached pines cellulose pulp fiber-cement composites using silica as mineral addition, identified the main phases in the X-ray diffraction patterns of the carbonated cementitious composites are: calcite ($CaCO_3$); portlandite (P); tricalcium aluminate (C_3A); belite (C_2S) and alite (C_3S).

- SEM shows how the accelerated carbonation process improves the contact between cellulosic fibers and cement matrix, and possibly favoring the better adhesion between them. However, along of carbonation process, some issues could be affected the effectiveness of the treatment on cellulose pulp fiber-cement composite, which is the apparition of cracks in the matrix and surrounding the fibers. These problems could be related to the parameters chosen for accelerated carbonation curing process that could be affecting the kinetic hydration of the matrix or due to the selection of the fiber.

6. CONCLUSIONS

- The use of unbleached or bleached cellulosic pulp for cementitious composites resulted in statistically significant effects on the mechanical properties of samples, including modulus of rupture, modulus of elasticity and specific energy. There is not statistically significant difference between 24 h and 48 h of initial thermal hydration, nor did between 2 h and 1 h of exposure time of CO_2 at the chamber for supercritical carbonation. The supercritical treatment research suggests that the optimal parameters for production of vegetable fiber-cement composites include the use of bleached cellulosic pulp, 24 h of thermal initial hydration and 1 h of supercritical carbonation. However, the implications for fiber-cement industry are a challenge upon, the CO_2 autoclave process could be done at laboratory scale but for applicate at real scale still needs to create an adequate infrastructure and establish the most proper process for being an applicate technology.
- The use of limestone or silica as a mineral addition for carbonated cementitious composites resulted in statistically significant effects on the mechanical properties of samples, including modulus of rupture, modulus of elasticity and limit of proportionality. There is not statistically significant difference between 10 h and 24 h of initial hydration. This stage suggests that the better parameters for production of carbonated vegetable fiber-cement composites include the use of ground silica as mineral addition, 24 h of sealed initial hydration and 10 h of accelerated carbonation in the environmental climate chamber at temperature of 45°C and relative humidity (RH) of 90%. The CO_2 content in the environmental climate chamber was monitored to 20 vol%.
- The use of silica as a mineral addition for carbonated cementitious composites after Accelerated Aging Cycles resulted in no statistically significant effects on the mechanical properties of samples, including modulus of rupture, modulus of elasticity and limit of proportionality. There is not statistically significant difference between 10 h and 24 h of initial hydration. This stage suggests that the better parameters for production of carbonated vegetable fiber-cement composites include the use of ground silica as mineral addition, 10 h of sealed initial hydration and 10 h of accelerated carbonation in the climate chamber at temperature of 45°C and relative humidity (RH) of 90%. The CO_2 content in the climate chamber was monitored to 20 vol%.
- The use of silica as a mineral addition for carbonated cementitious composites, allow to study at early edge the evolution of the hydration kinetics. This stage suggests that the

better parameters for production of vegetable fiber-cement composites include the use of ground silica as mineral addition, 10 h of sealed initial hydration and 7 h of accelerated carbonation in the climate chamber at a temperature of 45°C and relative humidity (RH) of 90%. The CO_2 content in the climate chamber was monitored to 20 vol%.

7. SUGESTIONS FOR FUTURE RESEARCH

- Study of the influence of low concentrations (e.g. 5%, 10%) of CO_2, on fiber-cement cementitious composites subject to accelerated carbonation process that use silica as mineral addition. This research is suggested due the current

- Study of the amorphous amount of calcium carbonated and calcium hydroxide through Synchrotron Light Source (LNLS) Rietveld analysis, in fiber-cement cementitious composites subject to accelerated carbonation process.

8. REFERENCES OR BIBLIOGRAPHY

ANDERSEN, F. A.; LJERKA BREČEVIĆ, L. Infrared spectra of amorphous and crystalline calcium carbonate. Acta Chemica Scandinavica. 1991, v. 45, p. 1018‑1024.

AGOPYAN, V. et al. Developments on vegetable fibre–cement based materials in São Paulo, Brazil: an overview. Cement & Concrete, v. 27, n. 5, p. 527–536, 2005.

ALMEIDA, A.E.F. et al. "Efeito de carbonatação acelerada em fibra de celulose kraft reforçado à base de cimento de materiais". Em Procedimento: 1º TMS-ABM Congresso Internacional de Materiais, Rio de Janeiro, Brasil.

ALMEIDA, A.E.F. et al. Improved durability of vegetable fiber reinforced cement composite subject to accelerated carbonation at early age. Cement & Concrete Composites. 2013, v. 42, p. 49–58.

ALVAREZ, D.; ABANADES, C. Determination of the critical product layer thickness in the reaction of CaO with CO2. Ind Eng Chem Res. 2005, v. 44, p. 5608-5615.

AMERICAN SOCIETY FOR TESTING AND MATERIALS – ASTM C150/C150M-11. Standard specification for Portland cement, 2011.

AMERICAN SOCIETY FOR TESTING AND MATERIALS – ASTM C948-81. Standard Test Method for Dry and Wet Bulk Density, Water Absorption, and Apparent Porosity of Thin Sections of Glass-Fiber Reinforced Concrete, ASTM International, West Conshohocken, PA, 2009.

ANDERSEN, F. A.; LJERKA BREČEVIĆ, L. (1991). Infrared spectra of amorphous and crystalline calcium carbonate. Acta Chemica Scandinavica, 1991, v. 45, p. 1018–1024.

ARDANUY, M.; CLARAMUNT, J.; TOLEDO FILHO, R.D. Cellulosic fiber reinforced cement-based composites: A review of recent research. Construction and Building Materials. 2015, v. 79, p. 115–128.

AULIN, C. Novel oil resistant cellulosic materials. 2009. 55 p. Ph.D. Dissertation. Royal Institute of Technology Department of Fibre and Polymer Technology. Stockholm.

AZWA, Z.N. et al. A review on the degradability of polymeric composites based on natural fibres. Materials & Design**.** 2013, v. 47, p. 424–442.

BAROGHEL-BOUNY, V. Water vapour sorption experiments on hardened cementitous materials. Part 1: Essential tool for analysis of hygral behaviour and its relation to pore structure. Cement and Concrete Research. 2007, v. 37(3), p. 414–37.

BARRETT, E.P.; JOYNER, L.G.; HALENDA, P.P. The determination of pore volume and area distributions in porous substances. I. Computations from nitrogen isotherms. J American Chemical Society. 1951, v. 73(1), p. 373–80.

BAZZONI, A. Study of early hydration mechanisms of cement by means of electron microscopy, Thèse EPFL n°6296, 2014 (http://infoscience.epfl.ch/record/200217/files/EPFL_TH6296.pdf).

BAZZONI, A. et al. The effect ofmagnesium and zinc ions on the hydration kinetics of C_3S, J. American Ceramic Society. 2014, v. 97, p. 3684–3693.

BENSTED, J. Some hydration investigations involving Portland cementeffect of calcium carbonate substitution of gypsum, World. Cement Technology. 1980, v. 11 (8), p. 395–406.

BENTUR, A; MINDESS, S. Fibre Reinforced Cementitious Composites. Second edition. Elsevier Applied Science, London and new York, 2007.

BIAGIOTTI, J.; PUGLIA, D.; KENNY, J.M. A review on natural fibre- based composites; part I. Structure, Processing and Properties of Vegetable Fibres. 2008, p. 37–41.

BJÖRNSTRÖM, J. Influence of nano-silica and organic admixtures on cement hydration: A mechanistic investigation. PhD thesis. Department of Chemistry, Göteborg University, Gothenburg, Sweden. 2005.

BLACK, L. et al. "Structural features of C-S-H(I) and its carbonation in air – A Raman spectroscopic study. Part II: Carbonated phases," Journal of the American Ceramics Society. 2007, v. 90, p. 908-917.

BORGES, P.H.R. et al. Carbonation of CH and C‑S‑H in composite cement pastes containing high amounts of BFS. Cem Concr Res. 2010, v. 40, p. 284‑92.

BROWN, P.W. et al. Analyses of the aqueous phase during early C_3S hydration. Cement and Concrete Research. 1984, v. 14, p. 257–262.

BRUNAUER, S.; EMMETT, P.; TELLER, E. Adsorption of gases in multimolecular layers. J American Chemical Society. 1938, v. 60 (2), p. 309–19.

BULLARD, J.W. et al. Mechanisms of cement hydration. Cement and Concrete Research. 2011, v. 41, p. 1208–23.

BULLARD, J.W.; FLATT, R.J. New insights into the effect of calcium hydroxide precipitation on the kinetics of tricalcium silicate hydration, J. American Ceramic Society. 2010, v. 93, p. 1894–1903.

CASPI, EL'AD N. et al. On the structure of aragonite. Acta Crystallographica Section B, 2005, v. 61, p. 129-132.

CHANG, C.-F.; CHEN, J.-W. The experimental investigation of concrete carbonation depth. Cement and Concrete Research. 2006, v. 36, p. 1760–1767.

CHEN, J.J.; THOMAS, J.J.; JENNINGS, H.M. Decalcification shrinkage of cement paste. Cement and Concrete Research. 2006, v. 36, p. 801–9.

CHEN, Y. et al. Effect of beating on recycled properties of unbleached eucalyptus cellulose fiber, Carbohydrate Polymer. 2012, v. 87, p. 730‑736.

CHRISTOPHE, C. La carbonatation. Le Magazine Béton[s]. 2006, v. 2, p. 53–54.

COLLETT, F. et al. Porous structure and water vapour sorption of hemp-based materials. Construction and Building Materials. 2008, v. 22 (6), p. 1271–80

COOKE, A.M. Durability of autoclaved cellulose fiber cement composites. In: Proceedings: 7th inorganic-bonded wood and fiber conference; 2000. p. 2–37.

CORREIA, V.C. Produção de celulose nanofibrilada a partir de polpa organossolve de bambu para nanoreforço de compósitos cimentícios. 2015. 170 p. Ph.D. Dissertation. Universidade de São Paulo Faculdade de Zootecnia e Engenharia de Alimentos, Pirassununga.

CORREIA, V.C. et al. Potential of bamboo organosolv pulp as a reinforcing element in fiber–cement materials Construction and Building Materials. 2014, v. 72, p. 65-71.

CORREIA, V.C. et al. Grinding process for the production of nanofibrillated cellulose based on unbleached and bleached bamboo organosolv pulp. 2016, v. 23, p. 2971–2987.

COSTOYA, M.M. Effect of particle size on the hydration kinetics and microstructural development of tricalcium silicate, PhD dissertation, École Polytechnique Fédérale de Lausanne, Lausanne, Switzerland, 2008.

COUTTS, R.S.P; KIGHTLY, P. Bonding in wood fibre cement composites. Journal Material Science. 1984, v. 19, p. 3355–9.

COUTTS, R.S.P.; NI, Y. Autoclaved bamboo pulp fibre reinforced. Cement and Concrete Composites. 1995, v. 17, p. 99–106.

COUTTS, R.S.P. A review of Australian research into natural fibre cement composites. Cement and Concrete Composites. 2005, v. 27, p. 518-526.

DAI, D.; FAN, M. Wood fibres as reinforcements in natural fibre composites: structure, properties, processing and applications. Natural Fibre Composites Materials, Processes and Applications. 2014, p. 3–65.

DE LA TORRE, Á. G. et al. The superstructure of C_3S from synchrotron and neutron powder diffraction and its role in quantitative phase analyses, Cement and Concrete Research, 2002, v. 32 (9), p. 1347-1356.

DELGADO, A. H., PAROLI, R. M., & BEAUDOIN, J. J. Comparison of IR techniques for the characterization of construction cement minerals and hydrated products. Applied Spectroscopy,1996, v. 50(8), p. 970–976.

DENCE, C.W.; REEVE, D.W. Pulp Bleaching. Principles and Practices; TAPPI Press: Atlanta, GA, 1996.

DEVITO, R.A. Estudos físicos e mecânicos de telhas de cimento de escoria de alto-forno reforçado com fibras celulósicas residuais. 2003. 156 p. Master Dissertation de mestrado, Universidade de São Paulo, São Carlos.

DIAS, C. M. R.; SAVASTANO JR., H.; JOHN, V.M. Exploring the potential of functionally graded materials concept for the development of fiber cement. Construction And Building Materials, 2010, v.24, n.2, p.140-146.

DU MANOIR, J.R.; AND DUBELSTEN, P. "Pulp bleaching process comprising oxygen delignification and xylanase enzyme treatment." U.S. Patent No. 5,179,021. 12 Jan. 1993.

EUROPEAN COMMITTEE FOR STANDARDIZATION. EN 494, Fiber–cement profiled sheets and fittings for roofing – Products specification and test methods BSI – British Standards Institution; 1994.

FARAHI, E.; PURNELL, P.; SHORT, N.R. Supercritical carbonation of calcareous composites: influence of curing. Cement and Concrete Composites. 2013, v. 43, p. 48–53.

FELDMAN, R.F.; RAMACHANDRAN, V.S.; SEREDA, P.J. Influence of $CaCO_3$ on the hydration of 3CaOd Al_2O_3. J. American Ceramic Society. 1965, v. 48 (1), p. 25–30.

FERNÁNDEZ-BERTOS, M. et al. A review of accelerated carbonation technology in the treatment of cement-based materials and sequestration of CO_2. J Hazardous Materials. 2004, v. 112 (3), p. 193–205.

FERNANDEZ LOPEZ, R. Calcined clayey soils as a potential replacement for cement in developing countries. 2009. 153 p. Ph.D. Dissertation. EPFL No 4302, Lausanne, Switzerland.

FOURNIER, R.O.; JACK J. ROWE, J.J. The solubility of amorphous silica in water at high temperature and high pressures. American Mineralogist. 1977, v. 62, p. 1052-1056.

FULLER, W.B.; THOMPSON, S.E., The Laws of Proportioning Concrete, American Society of Civil Engineers, Vol.33, 1907, pp.223-298.

GARCIA-GONZALEZ, C.A. et al. Modification of composition and microstructure of Portland cement pastes as a result of natural and supercritical carbonate procedures. Indutrial Engineering Chemistry Research. 2006, v. 45 (14), p. 4985–92.

GARCÍA-GONZÁLEZ, C.A. et al. New insights on the use of supercritical carbon dioxide for the accelerated carbonation of cement pastes. Journal Supercritical Fluids 2008, v. 43 (3), p. 500–9.

GROVES, G.W. et al. Progressive changes in the structure of hardened C3S cement pastes due to carbonation, J. American Ceramic Society. 1991, v. 74 (11), p. 2891–2896.

GUTTERIDGE, W.A.; DALZIEL, J.A. Filler cement: the effect of the secondary component on the hydration of Portland cement: part I. A fine non-hydraulic filler, Cement and Concrete Research. 1990, v. 20 (5), p. 778–782.

GUTTERIDGE, W.A.; DALZIEL, J.A. Filler cement: the effect of the secondary component on the hydration of Portland cement: part II: fine hydraulic binders, Cement and Concrete Research. 1990, v. 20 (6), p. 853–861.

HAGYMASSY, J.J.; BRUNAUER, S.; MIKHAIL, R.S. Pore structure analysis by water vapour adsorption I. t-curves for water vapour. Journal of Colloid and Interface Science. 1969, v. 29, p. 485–91.

HASHIMOTO, H. et al. Journal. Solid State Chemistry. 1980, v. 33, p. 181.

HAWKINS, P.; TENNIS, P.; DETWILER, R. The Use of Limestone in Portland Cement: a State-of-the-Art Review, Portland Cement Association, Skokie, Illinois, USA, 2003.

HENDERSON, D.M.; GUTOWSKY, H.S. A nuclear magnetic resonance determination of the hydrogen positions in $Ca(OH)_2$. American Mineralogist, 1962, v. 47, 1231 - 1251.

HILLS, J. P. The mechanism of the thermal decomposition of calcium carbonate. Research Fellow in Process Metallurgy, Department of Metallurgy, Imperial College, London Chemical Engineering Science, Pergamon Press. Printed in Great Britain. 1968, v. 23, pp. 297-320.

HOUST, Y. F. The role of moisture in the carbonation of cementitious materials. Internationale Zeitschrift für Bauinstandsetzen. 1996, v. 1, P. 49–66.

HUNNICUTT, W.A. Characterization of Calcium–Silicate–Hydrate and Calcium- Alumino-Silicate-Hydrate, University of Illinois, Urbana-Champaign, 2013.

HYVERT, N. et al. Dependency of C–S–H carbonation rate on CO_2 pressure to explain transition from accelerated tests to natural carbonation. Cement and Concrete Research. 2010, v. 40, p. 1582–1589.

INTERNATIONAL UNION OF PURE AND APPLIED CHEMISTRY, (IUAPC) 4. Reporting physisorption data for gas/solid systems with special reference to the determination of surface area and porosity. International Union of Pure and Applied Chemistry. 1985. p. 603–19.

JAWAID, M.; ABDUL KHALIL, H.P.S. Cellulosic/synthetic fibre reinforced polymer hybrid composites: a review. Carbohydrate Polymers, 2011, v. 86, p. 1–18.

JENNINGS, H.M. et al. Characterization and modeling of pores and surfaces in cement paste: correlations to processing and properties. J Advance Concrete Technology. 2008, v. 6(4), p. 5–29.

LAM, R.S.K. et al. Synthesis-dependant structural variations in amorphous calcium carbonate. CrystEngComm, 2007, v. 9, p. 1226‑1236.

LANGFORD, J.I.; WILSON, A.J.C. Scherrer after sixty years: A survey and some new results in the determination of crystallite size. 1978, v. 11 (2), p. 102-113.

LAVOINE, N. et al. Microfibrillated cellulose – Its barrier properties and applications in cellulosic materials: A review. Carbohydrate Polymers, 2012, v. 90, p. 735-764.

LENGOWSKI, E.C. et al. Cellulose acquirement evaluation methods with different degrees of crystallinity. Scientia Forestalis, Piracicaba. 2013; v. 41 (98), p. 185-194.

LIWU, M.; PANESAR, D. Effects of accelerated carbonation on the microstructure of Portland cement pastes containing reactive MgO. Cement and Concrete Research. 2012, v. 42, p. 769–777.

LIWU, M.; PANESAR, D. Microstructure of Reactive Magnesia Cement Pastes Subjected to High Carbon Dioxide Concentration. Journal of the Chinese Ceramic Society. 2014, V.42, No. 2 (Early Researcher Award MEDI)

LOTHENBACH, B. et al. Influence of limestone on the hydration of Portland cements. Cement and Concrete Research. 2008, v. 38, p. 848–860.

LOTHENBACH, B.; SCRIVENER, K.L.; HOOTON, R.D. Supplementary cementitious materials Supplementary cementitious materials. Cement and Concrete Research. 2011, v. 41, p. 1244–1256.

DU MANOIR, J.R.; AND DUBELSTEN, P. "Pulp bleaching process comprising oxygen delignification and xylanase enzyme treatment." U.S. Patent No. 5,179,021. 12 Jan. 1993.

MARCHAND, J.; SAMSON, E.; MALTAIS, Y. Modeling microstructural alterations of concrete subjected to external sulfate attack. In: Marchand J, Skalny J, editors. Materials science of concrete special volume: Sulfate Attack Mechanisms. 1999. p. 211–58.

MARTINEZ-CORREA, H.A. et al. Extracts from pitanga (Eugenia uniflora L.) leaves: influence of extraction process on antioxidant properties and yield of phenolic compounds. J Supercrit Fluids. 2011, v. 55, p. 998–1006.

MATSCHEI, T.; GLASSER, F. P. Temperature dependence, 0 to 40 °C, of the mineralogy of Portland cement paste in the presence of calcium carbonate. Cement and Concrete Research, 2010, v. 40, p. 763–777.

MATSUSHITA, F.; AONO, Y.; SHIBATA, S. Calcium silicate structure and carbonation shrinkage of a tobermorite-based material. Cement and Concrete Research. 2004, v. 34, p. 1251–7.

MEJIA B., J.E. et al. Evaluation of cellulosic pulps treated by hornification as reinforcement of cementitious composites. Constr Build Mater 2015; 100: 83–90.

MELO FILHO, J.A.; SILVA, F.A.; TOLEDO FILHO, R.D. Degradation kinetics and aging mechanisms on sisal fiber cement composite systems. Cement and Concrete Composites 2013, v. 40, p. 30‑9.

MCINTOSH, R.M.; SHARP, J.H.; WILBURN, F.W. The thermal decomposition of dolomite, School of Materials, Division of Ceramics, Glasses and Polymers, University of Sheffield, Sheffield SlO 2TZ, Gt. Britain, Received 26 January 1990.

MO, L.; PANESAR, D.K. Microstructure of Reactive Magnesia Cement Pastes Subjected to High Carbon Dioxide Concentration. Journal of the Chinese Ceramic Society. 2014, v.42, No. 2.

MOHR, B.J., NANKO, H., KURTIS, K.E. Durability of Kraft pulp fiber-cement composites to wet/dry cycling. Cement and Concrete Composites, 2005, v. 27 (4), p. 435– 448.

MOHR, B.J.; BIERNACKI, J.J.; KURTIS, K.E. Microstructural and chemical effects of wet/dry cycling on pulp fiber–cement composites. Cement and Concrete Research. 2006, v. 36, p. 1240–1251.

MOHR, B.J.; BIERNACKI, J.J.; KURTIS, K.E. Supplementary cementitious materials for mitigating degradation of kraft pulp fiber-cement composites, Cement and Concrete Research. 2007, v. 37, p. 1531–1543.

MORANDEAU, A.; THIÉRY, M.; DANGLA, P. Investigation of the carbonation mechanism of CH and C–S–H in terms of kinetics, microstructure changes and moisture properties. Cement and Concrete Research. 2014, v. 56, p. 153–170.

MORTON, J.H.; COOKE, T.; AKERS, S.A.S. Performance of slash pine fibers in fiber cement products. Construction and Building Materials. 2010, v. 24, p. 165–170.

MURAT, M. Hydration reaction and hardening of calcined clays and related minerals: I. Preliminary investigation on metakaolin, Cement Concrete Research. 1983, v. 13(2), p. 259–266.

MYNENI, S.C.B. et al. Vibrational spectroscopy of functional group chemistry and arsenate coordination in ettringite. Geochimica et Cosmochimica, 1998, Acta 62, p. 349–3514

NEWTON, R.C.; MANNING, C.E. Hydration state and activity of aqueous silica inH2O CO_2 fluids at high pressure and temperature. American Mineralogist. 2009, v. 94, p. 1287–1290.

PACHECO-TORGAL, F.; JALALI, S. Cementitious building materials reinforced with vegetable fibres: a review. Construction and Building Materials. 2011, v. 25, p. 575–581.

PANESAR, D.K. AND FRANCIS, J. Influence of limestone and slag on the pore structure of cement paste based on mercury intrusion porosimetry and water vapour sorption. Construction and Building Materials. 2014, v.52, p. 52-58.

PERA, J.; HUSSON, S.; GUILHOT, B. Influence of finely ground limestone on cement hydration, Cement and Concrete Composites. 1999, v. 21 (2), p. 99–105.

PEREIRA, C.L. Aproveitamento do resíduo do coco verde para produção de compósitos destinados à construção rural., 2012. 137 p. Ph.D. Dissertation. Universidade de São Paulo Faculdade de Zootecnia e Engenharia de Alimentos, Pirassununga.

PETER, M.A. et al. Competition of several carbonation reactions in concrete: A parametric study. Cement and Concrete Research. 2008, v. 12, p. 1385–1393.

PHAM, S.T.; PRINCE, W. Effects of Carbonation on the Microstructure of Cement Materials: Influence of Measuring Methods and of Types of Cement. International Journal of Concrete Structures and Materials. 2014, v. 8, p. 327.

PIZZOL, V. D. Carbonatação acelerada: nova tecnologia de cura para fibrocimento sem amianto. 60 p. Dissertação (Mestrado) – Universidade Federal de Lavras, Lavras, 2013.

PIZZOL, V. D. et al. Effect of accelerated carbonation on the microstructure and physical properties of hybrid fiber-cement composites. Minerals Engineering. 2014, v. 59, p. 101-106.

PICANÇO, M.S.; GHAVAMI, K. Comportamento à compressão de argamassas reforçadas com fibras vegetais da Amazônia / Behavior of cement mortar reinforced with Amazonian fibers subjected to compression. Rem: Revista Escola de Minas. 2008, v. 61(1); p. 13-18; 2008-03.

PITARELO, P.A. Produçao de etanol celulósico a partir do bagaço de cana pré-tratado por explosão a vapor. 2013. 162 f. Tese (Doutorado) – Universidade Federal do Paraná, Paraná, 2013.

RAMACHANDRAN, V.S. Kinetics of hydration of tricalciumsilicate in presence of calcium chloride by thermal methods, Thermochim Acta 2. 1971, p. 41–55.

RAMACHANDRAN, V.S.; BEAUDOIN, J.J. Handbook of Analytical Techniques in Concrete Science and Technology, William Andrew Publishing/Noyes, 2001.

RARICK, R.L. et al. Deterioration of the nitrogen BET surface area of dried cement paste with storage time. Advanced Cement Based Materials. 1996, v. 3, n. 2, p. 72–5.

ROJAS, M.F.; CABRERA J. The effect of temperature on the hydration rate and stability of the hydration phases of metakaolin-lime-water systems. Cement Concrete Research. 2002, v. 32, p. 133–8.

ROMA, L.C.; MARTELLO, L.S.; SAVASTANO, H. Evaluation of mechanical, physical and thermal performance of cement-based tiles reinforced with vegetable fibers. Construction and Building Materials. 2008, v. 22, p. 668–74.

ROSTAMI, V.; SHAO, Y.; BOYD, A.J. Durability of concrete pipes subjected to combined steam and carbonation curing. Construction and Building Materials. 2012, v. 25, p. 3345–3355.

ROSTAMI, V.; SHAO, Y.; BOYD, A.J.; HE, Z. Microstructure of cement paste subject to early carbonation curing. Cement and Concrete Research. 2012, v. 42, p. 186–193.

SAHA, P.; MANNA, S.; SEN, R.; ROY, D.; ADHIKARI, B.; Durability of lignocellusic fibers treated with vegetable oil-phenolic resine. Carbohydr Polym. 2012, v. 87 (2), p. 1628-1636.

SANTOS, S.F. et al. Supercritical carbonation treatment on extruded fibre–cement reinforced with vegetable fibres. Cement & Concrete Composites. 2015, v 56, p. 84–94.

SATYANARAYANA, K.G.; ARIZAGA, G.G.C.; WYPYCH, F. Biodegradable composites based on lignocellulosic fibers—An overview. Progress in Polymer Science, 2009, v, 34, p. 982–1021.

SAVASTANO, JR. H.; AGOPYAN, V. Transition Zone Studies of Vegetable Fibre-Cement Paste Composites. Cement and Concrete Composites, Kidlington, 1999, v. 21, n. 1, p. 49-57.

SAVASTANO, JR. H.; WARDEN, P. G.; COUTTS, R. S. P. Brazilian waste fibers as reinforcement for cement-based composites. Cement & Concrete Composites, 2000 v. 22, p. 379–84.

SAVASTANO JR, H. WARDEN P.G., COUTTS R.S.P. Potential of alternative fiber cements as building materials for developing areas. Cement & Concrete Composites. 2003, v (6), p. 585‑592.

SAVASTANO JR, H.; WARDEN, P. G.; COUTTS, R. S. P. Microstructure and mechanical properties of waste fibre–cement composites. Cement and Concrete Composites, Barking, 2005, v. 27, n. 5, p. 583-592.

SAVASTANO JR., H.; SANTOS, S. F. Produtos de fibrocimento. In: Geraldo Cechella Isaía. (Org.). Materiais de construção civil e princípios de ciência e engenharia de materiais. 1 ed. São Paulo: IBRACON, 2007, v. 2, p. 983-1005.

SCRIVENER, K.L; NONAT, A. Hydration of cementitious materials, present and future, Cement and Concrete Research. 2011, v. 41, p. 651–665.

SCRIVENER, K.L.; JUILLAND, P.; MONTEIRO, P.J.M. Advances in understanding hydration of Portland cement. Cement and Concrete Research. 2015, v. 78, p. 38–56

SHA, W.; O'NEILL, E.A.; GUO, Z. Differential scanning calorimetry study of ordinary Portland cement. Cement and Concrete Research. 1999, v. 29, p. 1487–1489.

SHAABAN, A.F. Determination of the kinetic parameters of the rection between SO_2 and CaO using the thermogravimetric technique. Thermochim Acta. 1991, v. 180, p. 9-21.

SHALWAN, A.; YOUSIF, B.F. Mechanical and tribological behaviour of polymeric composites based on natural fibres. Materials And Design. 2013, v. 48, p. 14–24.

SHARMA, R.L.; PANDEY, S.P. Influence of mineral additives on the hydration characteristics of ordinary Portland cement, Cement and Concrete Research. 1999, v. 29, p. 1525–1529.

SHI, C.; WU, Y. CO_2 curing of concrete blocks – research toward greener production. Concrete International. 2009, v. 31 (2), p. 39–44.

SILVA, P.S. GLASSER, F.P. Hydration of cements based on metakaolin: Thermochemistry, Advances in Cement Research. 1990, v. 3(12), p. 167–177.

SILVA, A.C. (2002). Estudo da durabilidade de compósitos reforçados com fibras de celulose. 128 f. Dissertação (Mestrado) – Escola Politécnica da Universidade de São Paulo. Departamento de Engenharia de Construção Civil, São Paulo, 2002.

SINGH, L.P. et al. Beneficial role of nanosilica in cement based materials – a review, Construction and Building Materials. 2013, v. 47, p. 1069–1077.

SITEPU, H.; O'COONOR B.H.; LI, D. Comparative evaluation of the March and generalized spherical harmonic preferred orientation models using X-ray diffraction data for molybdite and calcite powders. Journal of Applied Crystallography, 2005, v. 38, p. 158-167.

SISOMPHON, K.; LUTZ, F. Carbonation rates of concretes containing high volume of pozzolanic materials, Cement and Concrete Research. 2007, v. 37 (2007) 1647–1653.

SJÖSTRÖM, E. Wood Chemistry. Fundamentals and Applications, 2nd ed; Academic Press: New Tork, 1993.

SKOOG, D.A.; WEST, D.M.; HOLLER, F.J. *Analytical Chemistry an Introduction*. 6 ed., 1994, cap.6, p. 96-117.

STARK, J. Optimierte Bindemittelsysteme für die Betonindustrie, Beton. 2004, v. 54 (10), p. 486–490.

STURCOVA, A.; DAVIES, G.R.; EICHHORN, S.J. Elastic modulus and stress-transfer properties of tunicate cellulose whiskers, Biomacromolecules. 2005, v. 6, p. 1055‑1061.

SULAPHA, P. et al. Carbonation of concrete containing mineral admixtures, Journal of Materials in Civil Engineering. 2003, v. 15, p. 134–143.

TAHA, A.S. SERRY, M.A. EL-DIDAMONY, H. Hydration characteristics of metakaolin–lime–gypsum, Thermochim Acta. 1985, v. 90, p. 287– 296.

TAYLOR, H.F.W. Cement Chemistry. Emeritus Professor of chemistry, University of Aberdeen, Academic Press, London 1990.

TFR1-Test for the determination of modulus of rupture and limit of proportionality of thin libre reinforced cement sections. Materials and Structures. 1984; v. 17 (102).

THIERY, M. et al. Investigation of the carbonation front shape on cementitious materials: effects of the chemical kinetics. Cement and Concrete Research. 2007, v. 37(3), p. 1047–58.

THOMAS, J.J.; JENNINGS, H.M.; ALLEN, A.J. The surface area of hardened cement paste as measured by various techniques. Concrete Science and Engineering 1999, v.1, p. 45–64.

THOMAS, J.J. et al. Modeling and simulation of cement hydration kinetics and microstructure development, Cement and Concrete Research. 2011, v 411 (12), p. 1257–1278, (this issue).

THOMAS, S. et al. Natural Fibres: Structure, Properties and Applications. In: Kalia, S.; Kaith, B. S.; Kaur, I. (eds). Cellulose fibers: Bio and nano-Polymer Composites (Green Chemistry and Technology). New York: Springer. New York, 2011, p. 24-63.

TONOLI, G.H.D. et al. Cellulose modified fibres in cement based composites. Composites Part A: Applied Science and Manufacturing, Kidlinton. 2009, v. 40, n. 12, p. 2046-2053.

TONOLI, G.H.D. et al. Effect of accelerated carbonation on cementitious roofing tiles reinforced with lignocellulosic fibre. Construction and Building Materials. 2010, v. 24 (2), p. 193–201.

TONOLI, G.H.D. et al. Surface properties of eucalyptus pulp fibres as reinforcement of cement-based composites, Holzforschung, 2010, v. 64, p. 595–601.

TONOLI, G.H.D.; Santos, S.F.; Teixeira, R.S.; Pereira-da-Silva, M.A.; Rocco Lahr, F.A. Effects of Eucalyptus Pulp Refining on the Performance and Durability of Fibre–Cement Composites. Journal of Tropical Forest Science. 2013. v. 25, n. 3, p. 400–409.

Tonoli, G.H.D. et al. Rationalizing the impact of aging on fiber–matrix interface and stability of cement-based composites submitted to carbonation at early ages. Journal of Materials Science. 2016, v. 51, p. 7929–7943.

TSURUMI, T. et al. Crystal structure and hydration of belite. Ceramic transactions. 1994, v. 40, p. 19-25.

WEI, J.; MEYER, C. Degradation mechanisms of natural fiber in the matrix of cement composites. Cement and Concrete Research. 2015, v. 73, p. 1-16.

YLMÉN, R et al. Early hydration and setting of Portland cement monitored by IR, SEM and Vicat Techniques. Cement and Concrete Research. 2009, v. 39, p. 433–439.

YLMÉN, R; JÄGLID, U. Carbonation of Portland Cement Studied by Diffuse Reflection Fourier Transform Infrared Spectroscopy. International Journal of Concrete Structures and Materials. 2013, v. 7, n. 2, p.119–125.

YU, P. et al. Structure of calcium silicate hydrate (C‐S‐H): near-, mid-, and far-infrared spectroscopy. Journal of American Ceramic Society, 1999, v. 82(3), p. 742‐748.